INVESTIGATION ON BURR CONTROL DURING THE DRILLING OF DUCTILE MATERIALS

INVESTIGATION ON BURR CONTROL DURING THE DRILLING OF

DUCTILE MATERIALS

By

AHMED SWEED, B. ENG.

A Thesis

Submitted to the School of Graduate Studies

in Partial Fulfilment of the Requirements

for the Degree

Master of Applied Science,

McMaster University, Hamilton, Ontario

MASTER OF APPLIED SCIENCE (2021)　　　　　　　　McMaster University

(Mechanical Engineering)　　　　　　　　　　　　　Hamilton, Ontario

TITLE:　　　　　　　**INVESTIGATION ON BURR CONTROL DURING THE**

　　　　　　　　　　DRILLING OF DUCTILE MATERIALS

AUTHOR:　　　　Ahmed Sweed

　　　　　　　　　B. ENG. (Mechanical Engineering)

　　　　　　　　　McMaster University, Hamilton, Ontario

SUPERVISOR:　　Dr. Stephen C. Veldhuis

　　　　　　　　　Department of Mechanical Engineering

　　　　　　　　　McMaster University

NUMBER OF PAGES: xiv, 104

Abstract

Burrs are rough protrusions that form along the edge of a component during processing and are commonly produced during machining. Generally, the presence and severity of a burr directly impacts the final part quality. Thus, burrs need to be removed in subsequent processes to avoid injury when handling a part and/or negatively impacting the part's functionality. The size, shape, and nature of the attachment of the burr to the cutting edge are highly dependent on the material, tooling, and process parameters used during machining.

This research aimed to develop two new approaches to minimize and/or eliminate burr formation during the drilling of ductile materials. The first new method outlined in this thesis relates to injecting materials in different forms at high pressures under the workpiece on the side from which the drilling tool exits to support the drilling thrust force and thereby minimize exit burr formation. The second method introduced a novel technique for designing and testing highly effective step drills based on the workpiece material and cutting parameters, using commercial drills. Testing the two approaches showed promising results for producing comparatively smaller exit burrs.

<u>Acknowledgements</u>

To my lovely daughters, Sandy & Selina

Table of Contents

List of Figures

<u>List of Tables</u>

List of all Abbreviations and Symbols

HSS   — High-speed steel

F_{th} — Drilling thrust forces

M   — Drilling torque

F_r — Drilling radial forces

BUE   — Built-up edge

DBCC — Drilling burr control charts

CO_2 — Carbon dioxide

HPC   — High-pressure coolant

a   — Burr height measured at one section

a_m — Mean burr height for all measurements

SD   — Standard deviation of the burr height

SEM   — Standard error of the mean of the burr height

F_i — Supporting force (force under the drilled hole exit)

P_i — Injecting pressure

A_i — Area of the drilled hole

ℓ — Step size of a step drill

D_1 — Step diameter of a step drill / First drill diameter

D_2 — Final diameter of a step drill / Second drill diameter

θ_1 — Point angle of a drill / Step drill

θ_2 — Step angle of a step drill

r_β — Drill edge radius

<u>Declaration of Academic Achievement</u>

I, Ahmed Sweed, hereby declare that the thesis entitled "INVESTIGATION ON BURR CONTROL DURING THE DRILLING OF DUCTILE MATERIALS" is my own work and that I am the sole author of this thesis.

Chapter 1. Introduction

1.1. Background

Out of all the machining processes, drilling is considered the most commonly used process in the industry. Almost 36% of machining hours are consumed by hole-making [1]. In drilling, a drilling tool has two or more cutting edges that rotate and feed into the workpiece to create holes. Many factors such as cutting parameters, drill geometry, and workpiece materials affect the quality of the produced hole.

Burrs are unwanted extra materials that remain after different machining processes, such as drilling, turning, and milling, affecting the product's quality and functionality. There are various post-processes for removing burrs, but they are costly, and rarely completely remove the burrs. Ideally the deburring operation is avoided as the costs related to burr removal can account for 15-20% of the total machining cost for automotive components and can reach 30% for ultra-precision parts in the aerospace industry [2]. Kalpakjian and Schmid estimated the cost for only manually deburring using files and scrapers to be 10% of the total manufacturing cost of the part [3]. The tremendous cost of removing burrs makes it an essential topic for industry and research, so studying the fundamentals of burr formation mechanisms in drilling is crucial to introduce solutions for preventing or minimizing burrs and to provide procedures for producing high-end quality parts.

1.2. Motivation

Due to the importance of producing high-quality holes in the industry and the high costs related to deburring, along with safety concerns from handling and assembling parts with burrs, many efforts have been made to minimize and control burr formation in drilling. However, the extensive effort spent to study the burr formation mechanisms and parameters that affect burr formation, minimizing and controlling burrs in drilling is still challenging. This research aims to improve the drilled hole quality by introducing two new approaches for minimizing exit burr height in drilling.

1.3. Research Objectives

The work introduced in this thesis is divided into two approaches. The main research objectives for this thesis work are presented below.

1. Understanding the fundamentals of burr formation mechanisms in the drilling of ductile materials.

2. Development of a novel approach that uses pressurized materials at the drill hole exit to control burrs.

3. Development of a systematic approach for burr control through step drill design.

1.4. Methodology

Figure 1 summarizes all tests that were performed in approach 1, as well as all the resources that were used for the analysis. Likewise, Figure 2 represents the steps and equipment that were used to conduct the study of approach 2.

1.4.1. Approach 1
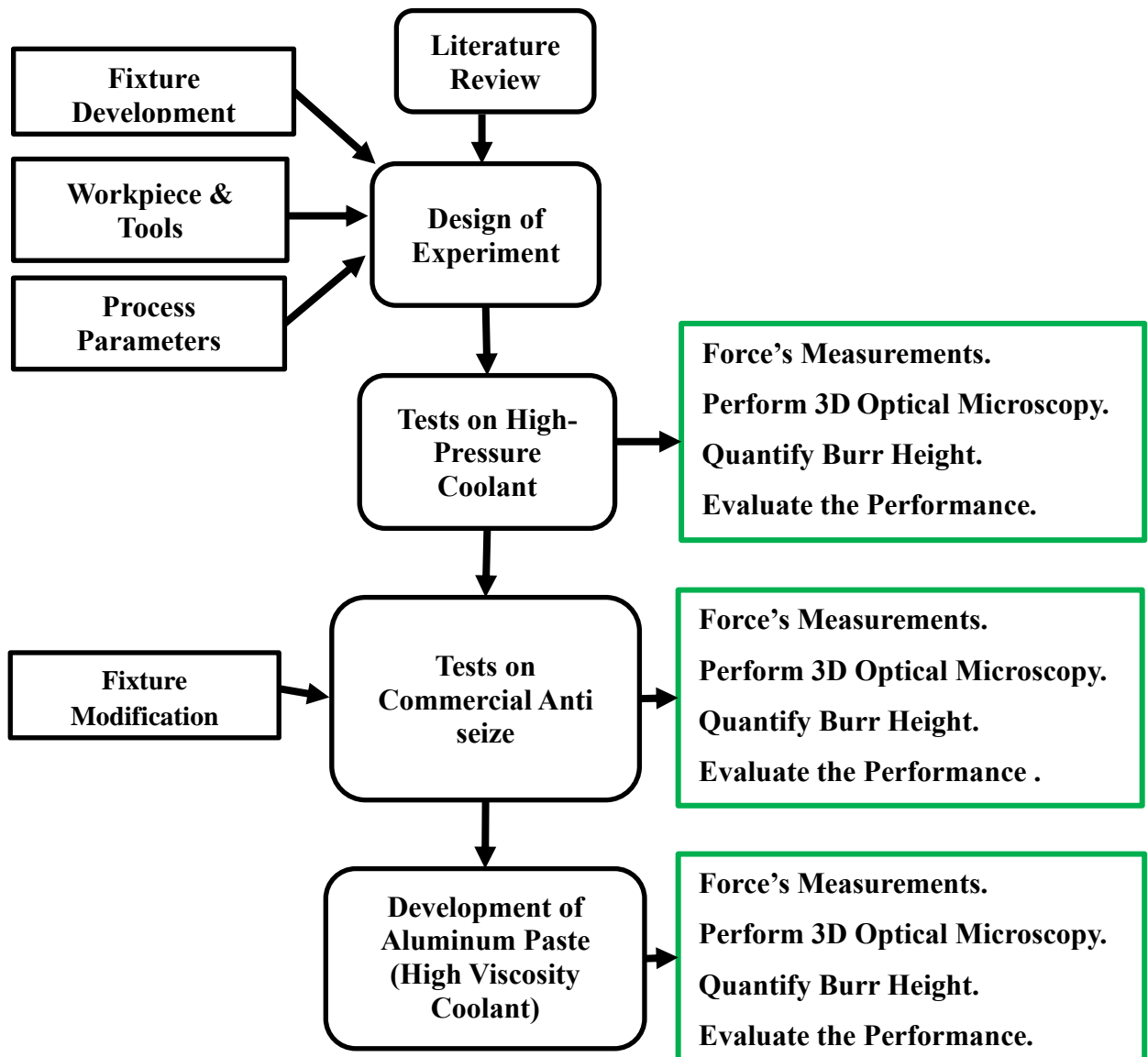
Figure 1: Research methodology (Approach 1)

1.4.2. Approach 2

```
┌──────────────────┐          ┌──────────────┐
│      Tools       │          │  Literature  │
│  (Off-the-shelf) │          │    Review    │
└──────────────────┘          └──────────────┘
                                     │
                                     ▼
┌──────────────────┐          ┌──────────────┐
│    Workpiece     │──────────│  Design of   │
│    (Industry)    │          │  Experiment  │
└──────────────────┘          └──────────────┘

┌──────────────────┐
│ Process parameters│
│    (Industry)    │
└──────────────────┘
```

| Tests on Effect of Step Size, and Step Profile on Burr Height | → | Benchmark Tools. Burr Formation High speed Videos. Perform 3D Optical Microscopy. Quantify Burr Height. |

Design & Make the Step Drill

| Test & Validate the Step Drill | → | Burr Formation High Speed Videos. Perform 3D Optical Microscopy. Quantify Burr Height. Compare Burr Height with the Benchmark |

Figure 2: Research methodology (Approach 2)

1.5. Thesis Outline

This thesis is organized into five chapters as follows:

CHAPTER 1: Introduction — This chapter presents a brief background and discusses the motivation for this thesis. The experimental methodology is presented along with the main research objectives.

CHAPTER 2: Literature review — This chapter presents a detailed overview of the drilling operation, burr formation mechanisms, the effect of machining parameters in this process on burr formation, a review of different burr control techniques, and the burr measurement methodologies.

CHAPTER 3: Approach 1—A detailed description of the first proposed idea and design and the experimental setup for the machining tests is provided along with necessary information about the process parameters, workpiece, and cutting tools. In addition, the results of the study are discussed.

CHAPTER 4: Approach 2—A detailed description of the second proposed idea is provided in addition to the experimental setup for the machining tests and information about the process parameters, workpiece, and cutting tools. Results and discussion were also included in this chapter.

CHAPTER 5: This chapter provides a summary of all the findings of this research and recommends future research work to improve the discussed ideas.

APPENDIX A: High-speed video images of the burr formation sequence for all tests explained in approach 2 are included.

Chapter 2. Literature Review

2.1. The Drilling Operation

2.1.1. Drill Geometry

Drill geometry has an essential role in drilling as it can directly affect the tool life and drilling quality. Although there are various drill designs, the standard-point twist drill is still the most common tool used across many different applications. Figure 3 shows the main features and parameters that affect the drilling performance, such as the drill diameter, helix angle, point angle, and chisel edge.
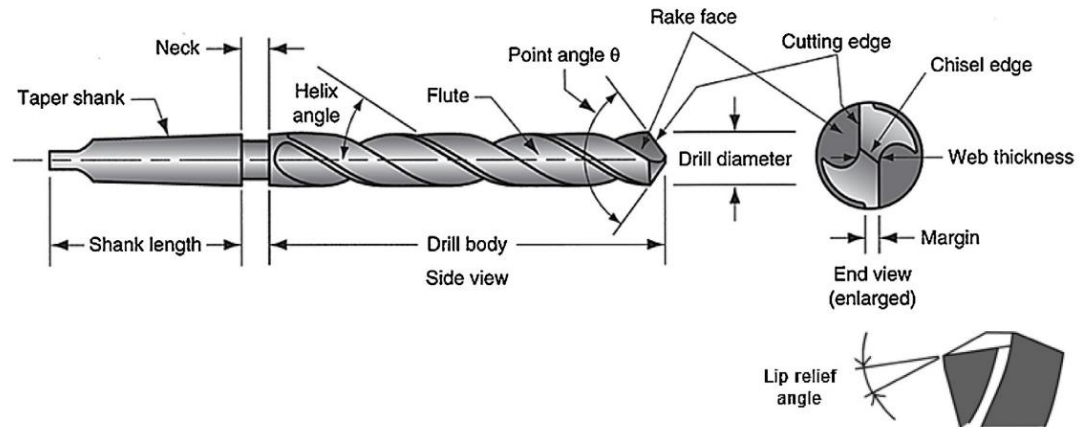
Figure 3: Geometry of Twist drill (Used with permission [4])

Depending on the application, the previously mentioned features can change to meet the job requirements. Figure 4 illustrates common drill point shapes for different purposes; for example, the twist drill shown in shape A has a shorter chisel edge than the standard drills, and this is preferred when lower feed forces are required. Similarly, shape B has a corrected rake angle to provide more stability and better chip formation.

The split point tools have reduced an additional 6% of the chisel edge for a more positive rake angle [5].

shape A	shape B
web-thinned chisel edge	web-thinned chisel edge with corrected major cutting edge
shape C	shape D
split point	web-thinned chisel edge with beveled corners
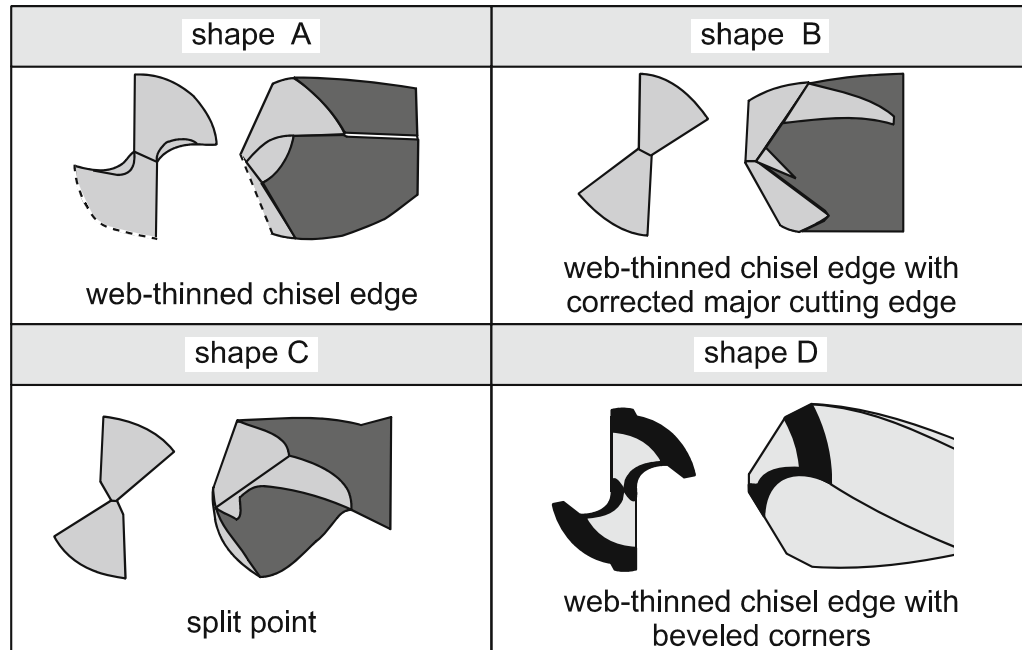
Figure 4 Common drill-point shapes (Used with permission [5]), according to [6].

2.1.2. Drill Material

In metal cutting, there has been a lot of effort put into developing new tool grades. Nevertheless, the two most common materials used for twist drill manufacturing are high-speed steels (HSS) and carbides. Coatings are often used to protect the drill from high cutting temperatures, reduce friction and enhance wear resistance to effectively increase tool life.

2.1.3. Forces in Drilling

There are three force components in drilling. Only two essential forces need to be measured, the thrust force (F_{th}), which is perpendicular to the workpiece surface, and the torque M which determines the spindle power requirements to rotate the drill. The radial force (F_r) is balanced on both cutting blades [7],[8], as shown in Figure 5.
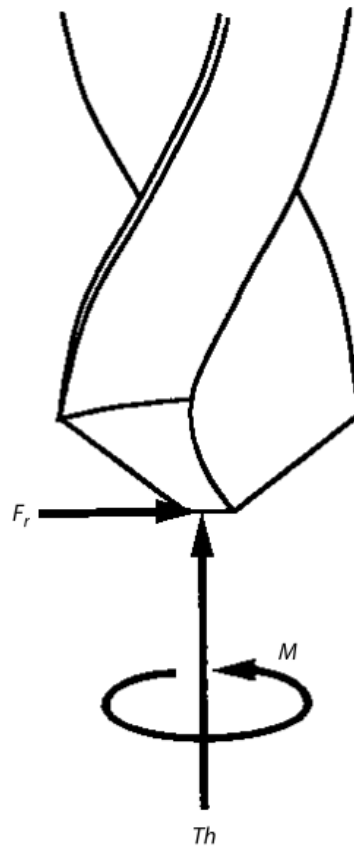
Figure 5: Forces in drilling (Used with permission [7])

2.1.4. Wear in Drilling

Tool wear is a normal result of all machining processes; it occurs due to the high friction between the cutting tool and the workpiece, resulting in high temperatures and stresses on the tool surface. Figure 6 shows the typical wear location on a twist drill

during the drilling process. This wear occurs due to different wear mechanisms. Abrasive wear can happen when the cutting edge meets hard particles in the workpiece material during cutting. These particles gradually remove small pieces of the cutting tool. Adhesive wear is also expected in drilling, especially when cutting soft materials such as aluminum; it takes place when chips adhere to the tool surface and grow gradually, causing BUE [9]. Tool wear is undesired in drilling, and extensive effort is expended on minimizing and controlling it because it can affect dimensional accuracy, increase the cutting forces and tool temperature, and thus increase the machining costs.
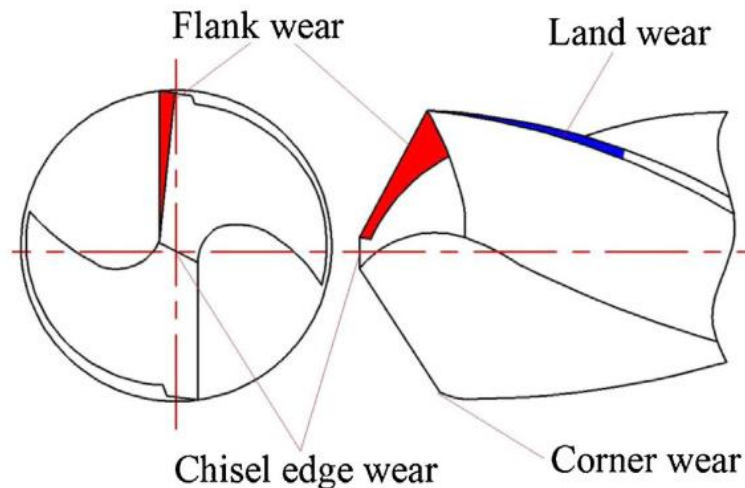
Figure 6: Tool wear forms in drilling(Used with permission [10])

2.2. Burrs in Drilling

2.2.1. Burr Types

In machining, burrs can be divided into four main types: Poisson burrs, rollover burrs, tear burrs, and cut-off burrs, as shown in Figure 7.
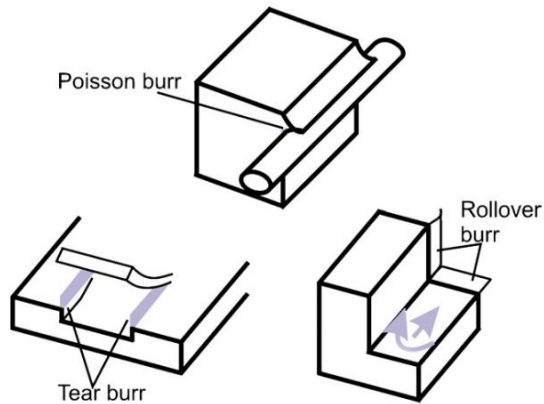
Figure 7: Illustration of burr types (Used with permission [11]), according to [12]

The Poisson burr, also known as the side burr, occurs due to the material's tendency to plunge under compression. The Poisson burr often occurs during turning processes and is a function of the effective edge radius, pressure, and material properties, as shown in Figure 8 [12], [13].
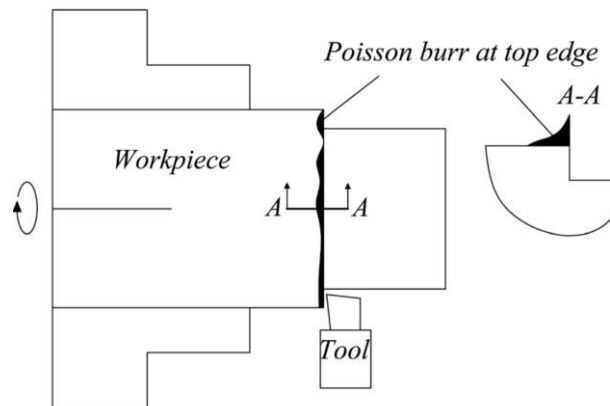
Figure 8: Schematic illustration of the Poisson burr formed in turning (Used with permission [14])

The rollover burr is a large burr that occurs at the cutting tool exit when the chip bends rather than is sheared. The rollover burr is a function of the depth of cut, the shear and rake angles, and the workpiece material properties.

Tear burrs occur as a result of material tearing rather than shearing. They are common in punching operations, side milling, and drilling operations. The cut-off burrs can be easily observed in saw cuts and automatic screw machine parts when the workpiece gets separated from the raw material before finishing the cutting process. It could be avoided by supporting the piece being cut until the end of the process [12].

In drilling, burrs can be classified into entrance burrs and exit burrs based on their location. Entrance burrs form at the hole entrance when the drill engages with the workpiece due to tearing, a bending action followed by clean shearing, or lateral extrusion. At the burr exit, two different types of burrs are expected based on the drill situation. When the drill is very sharp, a Poisson burr occurs due to the rubbing at the margins of the drill. However, when the drill is worn out, the uncut chip curls at the hole exit, causing a rollover burr [13].

The literature identifies five types of burr shapes in drilling, as shown in Figure 9. The first two images on the top left of Figure 9 are Type I and Type II, consecutively, which are uniform burrs without drill caps but with different burr sizes. Type 3 is a uniform burr with a cap, and Type 4 is a crown burr. The crown burr is relatively larger than the previously mentioned types and has an uneven height distribution around the hole. The transient burr was observed during the drilling of AISI 4118 and appeared after the uniform burr in the transient stage to becoming a crown burr [15], [16]. In this study, uniform burrs with and without drill caps were observed, as described in the following chapters.
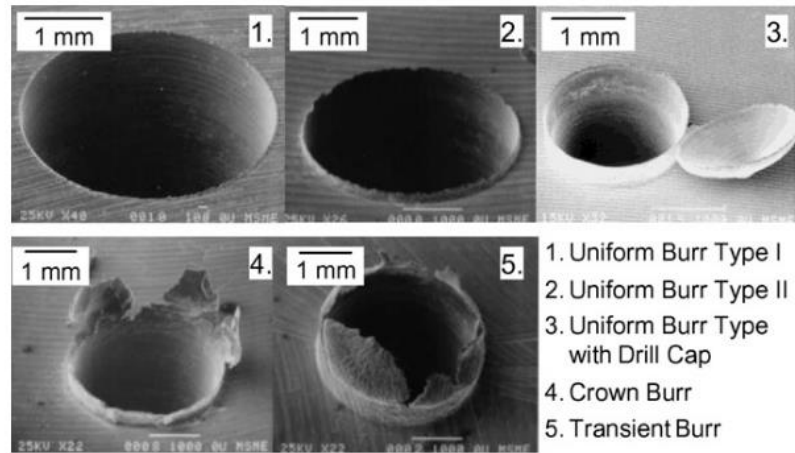
Figure 9: Drilling burr types (Used with permission [11]).

2.2.2. Burr Mechanisms

In machining, burrs form through eight main stages depending on the workpiece material's ductility, as shown in Figure 10. The first five stages are typical for all materials, and starting from step six, the mechanism changes based on the workpiece material. Stage one is continuous cutting, where the cutting tool cuts the workpiece and generates flow-type chips in the case of ductile materials or crack-type chips when cutting brittle materials. In stage two, the pre-initiation, the cutting edge moves towards the exit surface and the elastic deformation zone touches the workpiece edge. The plastic deformation zone in the area around the primary shear zone also extends toward the workpiece edge. When the tool comes closer to the workpiece edge, stage three begins, and a plastic deformation zone starts to form at the workpiece edge. Also, the plastic deformation extends more. In stage four, a large deformation occurs at the workpiece edge, creating a pivoting point in which the cutting forces may decrease

because of the catastrophic deformation. At stage five, the two previously mentioned plastic deformation zones extend and connect, forming a negative shear zone [17].

For ductile materials, the crack starts to initiate in stage 6-i at the cutting tool tip in the primary shear zone in the same direction as the machined surface. This occurs because the ductile materials have a critical fracture strain larger than the strain in the negative shear zone. In stage 7-i, the tool generates crack growth in the direction of the cutting line, along the primary shear zone, also deforming the workpiece edge. At the final stage (8-i), the crack propagates more until it reaches the workpiece edge and separates the chip, resulting in a positive burr [17].

The crack also initiates at the tool tip in brittle materials but in the direction of the negative shear zone towards the pivoting point. This occurs because brittle materials have a critical fracture strain lower than the strain in the negative shear zone, as shown in stage 6-ii. In stage 7-ii, the crack propagates in the direction of the negative shear zone and may change from the shear mode to the opening mode. Also, the workpiece edge slightly deforms because of the crack propagation. At the end stage, the crack reaches the pivoting point and separates the chip above the negative shear line, causing a negative burr [17].
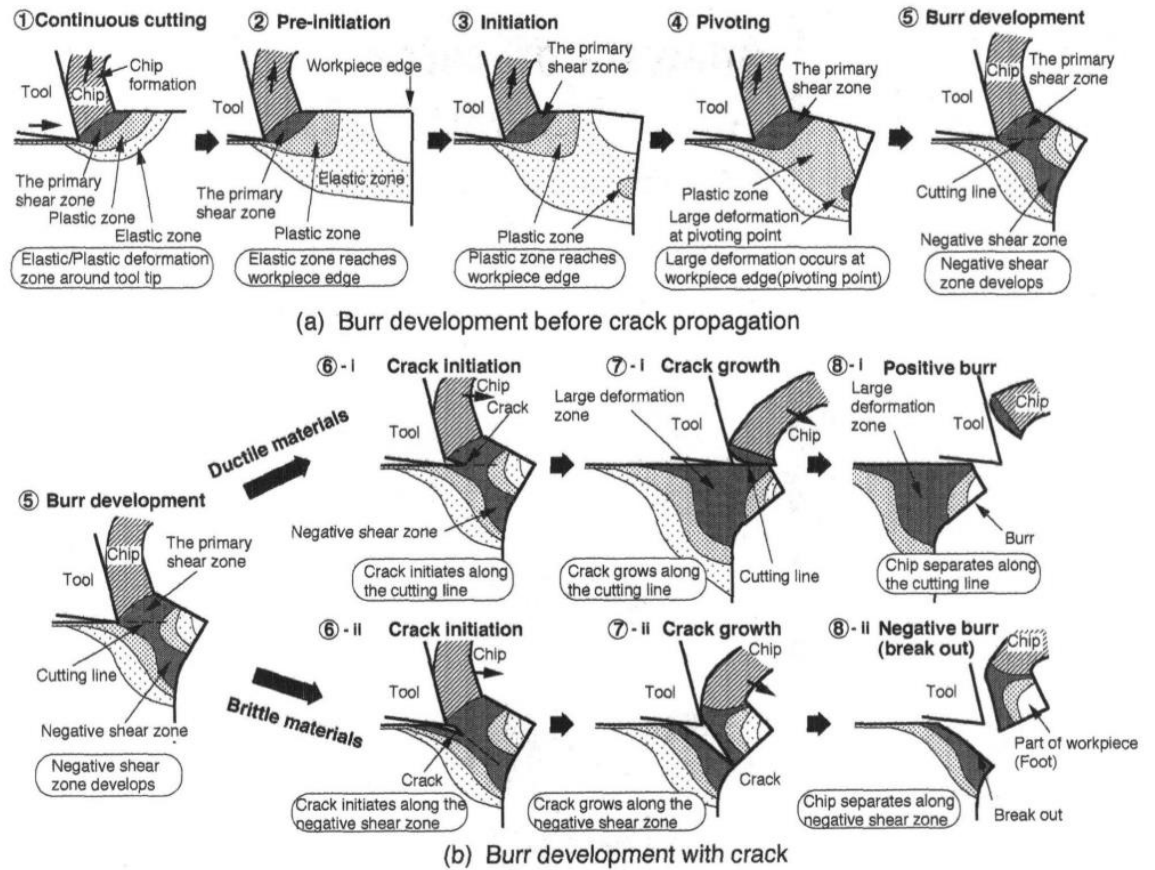
Figure 10: Schematic illustration of the burr formation process (Used with permission [17])

2.2.3. Cutting Parameters' Influence on Burrs

Cutting parameters, such as feed rates and cutting speed, have a notable relationship to the produced burrs [2]. A thorough effort was made to study how machining parameters affect burr formation in drilling.

Pande et al. investigated the effect of feed rate, workpiece hardness, and hole size on burr height to identify the optimal conditions to minimize it [18]. It was found that feed rates influence the resulting burrs. Burr height was significant at slow feed rates, then started to reduce at intermediate feed rates and rise again at fast feed rates.

Abdelhafeez et al. studied the effect of feed rate and cutting speed on burr size during the drilling of Ti-6Al-4V titanium, Al7010-T7451, and Al2024-T351 aluminum alloys. The study reported that the smallest burr size was found at an intermediate feed rate and high cutting speed. Feed rate has the most significant impact on the exit burr height; feed rates lower than the tool edge radius produce large burrs due to the ploughing effect, and higher feed rates also form large burrs because of the higher thrust forces [19] [18].

Stein and Dornfeld studied the effect of tool wear, cutting speed, and feed rate on burr height during the drilling of stainless steel 304L using a small drill diameter of 0.91 mm. The study concluded that drill wear tremendously increases the burr height. Also, burr height is high at low feed rates due to the ploughing action, then shortens as the feed rate increases until it reaches 12 µm/rev, after which the burr height grows with more feed rate increases due to an increase in the thrust force. Moreover, accelerating spindle speed was found to raise the burr height [20].

Costa et al. reported that burr height increases as a function of tool wear at both slow and fast cutting speeds. Burr height increases exponentially after the tool has reached 64% wear at the slower cutting speed and 82% at the faster cutting speed [21].

Coolant plays an essential role in reducing burrs in drilling. The high temperatures during dry cutting increase the material ductility and lead to higher burr heights. However, cooling down the workpiece using coolants can cause more brittle material behaviour and leads to smaller burrs [22].

2.2.4. Influence of Workpiece Material on Burrs

The workpiece material plays an essential role in the resulting burr size. The ductility and strain hardening exponent make burr shape differ between materials. Extremely ductile materials, such as high nickel alloys and low carbon steels, generally form large burrs since they have more capacity for plastic deformation. On the contrary, brittle materials with an elongation range of 0.5-3% often produce no visible burrs. Likewise, materials with a high strain hardening exponent, such as stainless steels, can develop noticeable burrs compared to low strain hardening materials. Tool wear can indirectly influence burr size by elevating the workpiece temperature and subsequently increase the ductility and produce large burrs [13], [16].

Material hardness can also affect burr size; materials with high hardness values can make a larger burr since the thrust force is higher. The optimum hardness range that produces a small exit-burr height is 130-140 BHN. Materials with high ductility, such as copper and aluminum, make larger burr sizes. Also, very hard materials like ferrous metals produce larger burrs due to the higher thrust forces [18].

2.2.5. Impact of Tool Geometry on Burrs

Gillespie et al. conducted a study to understand the effect of different helix angles on the height and thickness of exit burrs. A high helix angle was found to produce smaller entrance and exit burr heights and thinner burrs than a low helix angle. Increasing the helix angle increases the effective rake angle and thus leads to lower thrust forces and smaller burrs [23], [16].

Neugebauer et al. studied the effect of using different drill diameters on the exit burr height. The study found that burr height increases proportionally with the drill diameter[23], [24].

Kim and Dornfeld studied the effect of changing the drill diameter, point angle, and web thickness ratio on the exit burr size for two different materials, AISI 304L stainless steel, and AISI 4118 low alloy steel. The study reported that doubling the drill diameter from 4 mm to 8 mm caused a 10% increase in burr height. Moreover, burr size enlarges as the drill point angle widens. By increasing the point angle, the effective rake angle decrease, causing the thrust force and the burr size to increase accordingly. In addition, increasing the web thickness ratio extends the non-efficient cutting length, leading to greater thrust force and burr size [16].

2.2.6. Influence of Coatings on Burrs.

In drilling, cutting temperature plays a significant role in controlling the burr size. By lowering the temperature, ductility reduces, leading to smaller burrs [13], [16]. Reducing the friction between the cutting tool and the chip can reduce heat generation and cutting forces.

Rivero et al. studied the effect of using low-friction coatings, such as tungsten carbide / carbon (WC/C), on the produced burr size during the dry drilling of aluminum 7075-T6. The study reported that a Balinit Hardlube coating, a multilayer of TiAlN and low-friction coating WC/C, produced smaller burr sizes than an uncoated drill at all feed rates tested [25].

Huang et al. investigated different coatings and cutting parameters on the burr height in the drilling of aluminum 6061. The study revealed that the CrN coated drill produced the smallest burr height at moderate cutting speeds and feed rates [26].

2.2.7. Influence of Exit Surface Profile on Burrs

One important factor that affects burr formation in drilling is the tool/workpiece orientation. As seen in Figure 11, the exit surface angle can vary depending on the workpiece's exit surface profile. By increasing the exit surface angle, the pivoting point that triggers the plastic bending of the burr moves closer to the drilled hole at the bottom side, producing a smaller burr [27]. Min et al. predicted the likelihood of burr location and burr height distribution based on the combined effect of the interaction angle and the effective exit surface angle [28]. The influence of the spindle speed, feed rate, and exit surface angle were investigated during the drilling of Al7075. The study revealed that the minimum burr height was observed with a low exit surface angle, slow feed rate, and fast spindle speed. Additionally, the burrs occurred around the hole periphery only in a specific region between 110° and 357° [29].

$$\alpha = 30^o \qquad \alpha = 15^o \qquad \alpha = 0^o$$
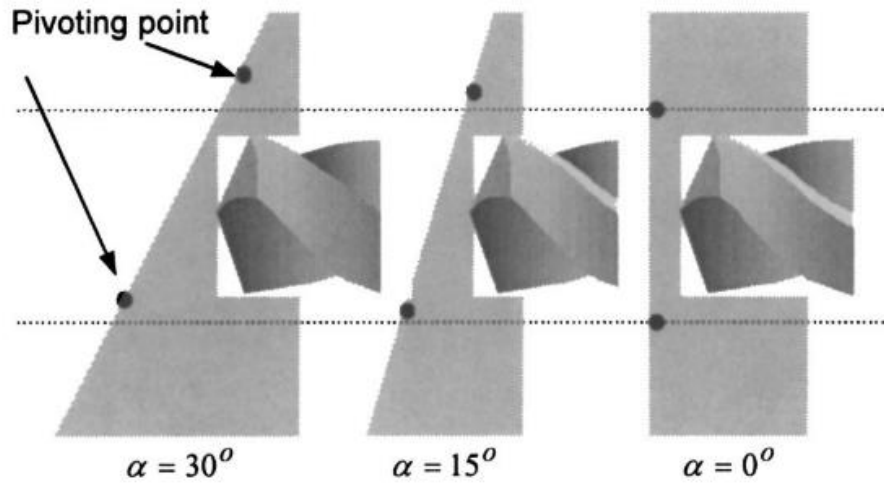
Figure 11: Variation of the pivoting point (Used with permission [28])

2.3. Burr Measurement

Accurate and precise burr measurement is vital in order for researchers and engineers to enable burr detection and control. There are several methods for burr measurements. Figure 12 classifies the typical measuring methods into four main categories: destructive measurement methods, mechanical measurements methods, optical measurements methods, and electrical measurement methods [11]. In this section, the methodology of each technique is explained in addition to its advantages and disadvantages.
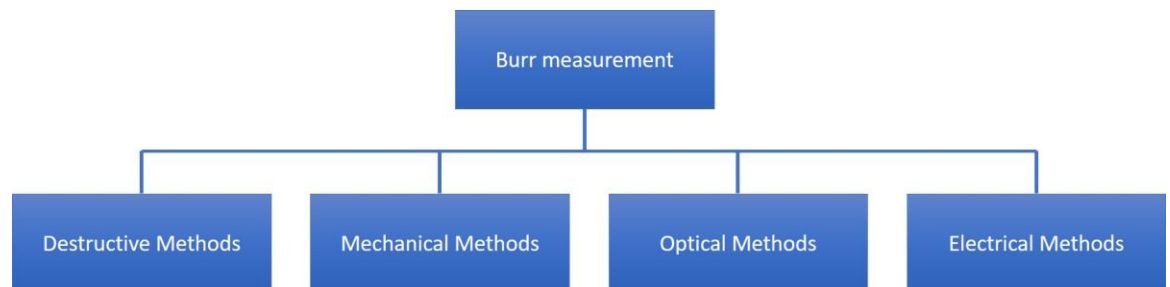
Figure 12: Burr measurement methods

A metallographic cross-section sample of the burr was prepared by sectioning the edge, as shown in Figure 13. The advantage of this method is that it allows all the burr dimensions and hardness to be measured accurately but it does require that the part be destroyed [11], [30], [31].
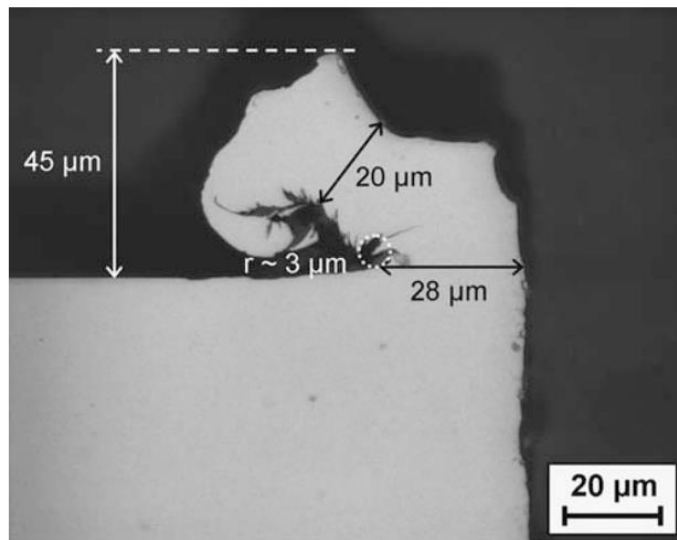
Figure 13: Cross-section of a burr (Used with permission [32]**)**

In mechanical methods, a stylus is used to measure the burr profile, as seen in Figure 14. In this method, advanced calculations are needed to compensate for the shape effect of the tracer point of the stylus and get more accurate measurements of the burr. Moreover, this method can only measure the burr height and is limited to the workpiece material stiffness since the burr could be deformed due to the contact force of the stylus [11], [31].
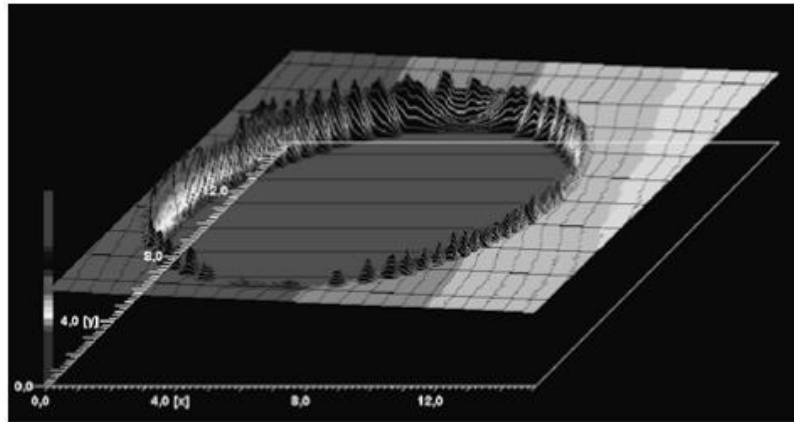
Figure 14: Burr analysis applying stylus method (Used with permission [31]**)**

Optical systems are commonly used for burr measurements, such as optical microscopes and camera systems[31]. In this dissertation, a 3D optical microscope was used to measure burr height precisely. More details are explained in section 3.2.3.

2.4. Burr Control

2.4.1. Deburring Techniques

Deburring is the process of removing burrs from a machined part to improve its quality. According to a study performed in the German automotive and machine tool industry, deburring-related costs can increase part cost by about 15% because of workforce costs, 2% due to rejected parts, and 4% because of machine breakdown [11], [33]. Deburring operations can be categorized into four main groups. They are mechanical deburring, thermal deburring, chemical deburring, and electrical deburring [13], as shown in Figure 15.
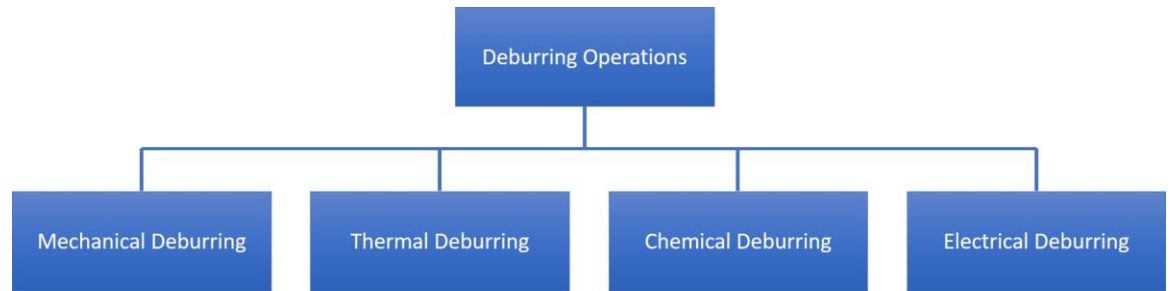
Figure 15: Deburring operations according to [13]

Within these four categories, there are several techniques for deburring, such as brushing, electrochemical deburring, and thermal energy methods. Electrochemical deburring is a quick method for deburring hard-to-reach burrs, which can dissolve burrs in 5-10 seconds using a specially designed tool to concentrate dissolving solutions at an applied electricity [13]. According to Gillespie, thermal deburring is considered the fastest method for deburring many parts in a fraction of a second. This occurs by generating a high-temperature shock wave enough for burning and evaporating the burr [13].

2.4.2. Burr Minimization Techniques

Due to the high cost of deburring, many innovative ideas were developed to produce high-quality machined parts with acceptable burr sizes. In this section, some techniques and their impact on burr minimization are explained.

As described previously in section 2.2.3, process parameters significantly impact the resulting exit burr in drilling. Drilling burr control charts (DBCC) is a tool built from a large amount of experimental data on the exit burr size at various cutting speeds and feeds for different materials [2], [15]. An expert system could be established using

the burr control charts to anticipate the burr type and size at selected speeds, feeds, and tool diameters.

Biermann et al. introduced an innovative cooling technique for burr minimization during the turning of Austenitic-Ferritic duplex stainless steel. This material has a high fracture toughness, which produces a comparatively sizeable positive burr [17]. In this research, carbon dioxide (CO_2) based in-process cooling was used, resulting in a significant reduction in the workpiece temperature. The accelerated cooling of the workpiece lowered its formability, resulting in a smaller burr. Also, the kinetic energy generated by the cold blast of CO_2 caused the burr to deform and break [34], as shown in Figure 16. The same idea was tested with the face milling of EN AW-6060 aluminum by precooling the workpiece with dry ice in addition to using two CO_2 nozzles for in-process cooling. The results showed a burr volume reduction of about 30-40% compared to dry machining. This technique was also tested with the drilling of 34CrNiMo6 steel and AlMgSi1 aluminum at different feed rates. In contrast with the favourable results of the previous turning and milling tests, drilling using CO_2 showed no significant difference in burr height compared with using coolant [22].
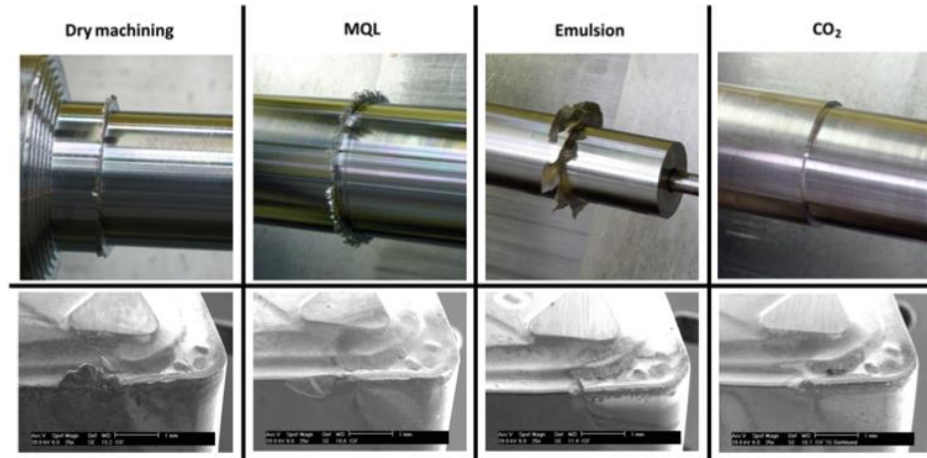
Figure 16: Influence of the cooling concept on burr formation and tool wear in turning stainless steel (Used with permission [34]**)**

Orbital milling is a common technique for burr and drilling cap control in the aerospace industry. It was first introduced to the aerospace industry by a company called Novator. In this technique, a special end mill with a diameter smaller than the required hole diameter is fed inside the workpiece in a spiral motion, resulting in lower thrust forces and high-quality holes with a short burr height [35], as illustrated in Figure 17. Extensive research was performed to study the effect of the cutting parameters and tool geometry on the produced burrs and drill caps during the orbital drilling of primed glad aluminum 2024 [36]. The study reported that high-quality holes can be achieved with slower feed rates. Also, fast axial feed rates can successfully remove the drilled cap.
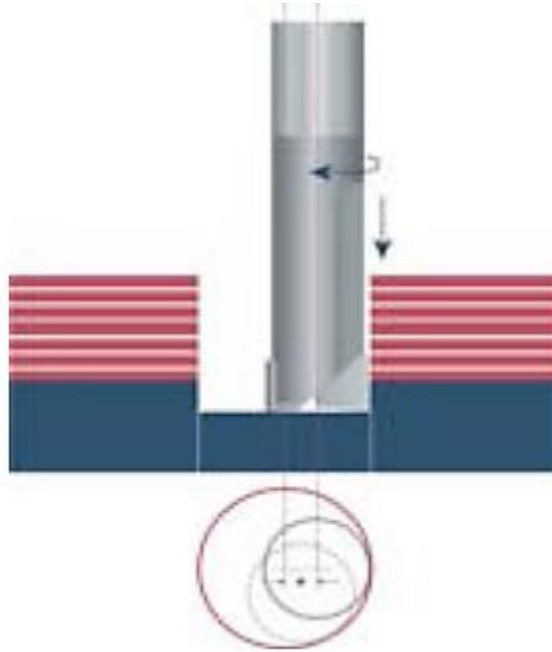
Figure 17: Orbital milling principle (Used with permission [35]**)**

Drilling stacked materials, or, as it is sometimes called, drilling with backup support, is also a common method in burr control that has been used in the aerospace industry. In this technique, a supporting plate is used under the drilled hole to minimize the exit burr formation. Kundu et al. investigated the effect of using backup support under different cutting conditions during the drilling of aluminum alloy flats. The study revealed that using backup support at a slow feed rate, along with a moderate cutting speed and water cooling, reduced the burr height by 33% [37]. Another study was conducted to investigate the influence of the drill geometry, coatings, cutting parameters, clamp type, and distance on the resultant interfacial burrs. It was found that the drill point angle, clamp distance, and clamp type had the most significant impact on the interfacial burr. Additionally, it was concluded that the minimum interfacial burr size was obtained using a step drill with a 118° point angle [38]. Tian et al. studied the

correlation between the feed rate, thrust force, interlayer gap, and interlayer burr. They found that the thrust force increased when a higher feed rate was used, which expanded the interlayer gap and increased the interlayer burr. Based on this correlation, a preload pressing force was tested as a trial to reduce the interlayer gap and the consequent interlayer burr. The results showed a reduction in the interlayer burr height as the pressing force increased, and when the pressing force exceeded 247.5 N, the interlayer burr was controlled significantly [39].

Ultrasonic assisted (UA) vibration was also shown to have an impact on reducing burr size. In UA drilling, a high-frequency vibration in the feed direction was added through the tool or the workpiece. The effect of UA drilling on burr formation was investigated by Takeyama et al., who found that using ultrasonic vibration significantly reduced the thrust force and the burr size [40]. Chang et al. studied burr size using different vibration frequencies, vibration amplitudes, and cutting parameters while drilling aluminum AL1100-0. The results showed a reduction in burr height at a high vibration frequency of 20 kHz and a high peak to peak vibration magnitude of 4 microns. The authors related the decrease in burr height using UA drilling to the thrust force. The UA drilling produced segmented chips as opposed to the long chips created in conventional drilling, which reduced the thrust force and burr height [41].

Chapter 3. Approach 1: Burr Control Using Pressurized Materials

This chapter explains a new technique for exit burr control during the drilling of aluminum 6061-T6. The main objectives of this study are summarized as follows:

❖ Develop a new effective burr minimization and control technique by injecting different materials at high pressures under the workpiece at the drill exit side.

❖ Develop a new injecting material that could be used for this technique.

❖ Study the correlation between different injecting material mixtures and burr height.

❖ Study the correlation between the injecting pressure, thrust force, and burr height.

3.1. Experimental Procedures

This section explains all the experimental procedures, including the idea, fixture design, injecting material development, and experimental setup.

3.1.1. Idea Overview.

The idea was to develop a new technique for burr minimization and eliminate drilled cap formation during the drilling of ductile materials. The new method involves injecting a material at high pressures under the exit side of the workpiece where the drilling tool emerges, as shown in Figure 18. This material counterbalances the drilling thrust force and supports the workpiece at the exit side, leading to a lower burr size and no drilled cap. The injecting materials tested in this dissertation were in a liquid or paste form, as explained in the next section.
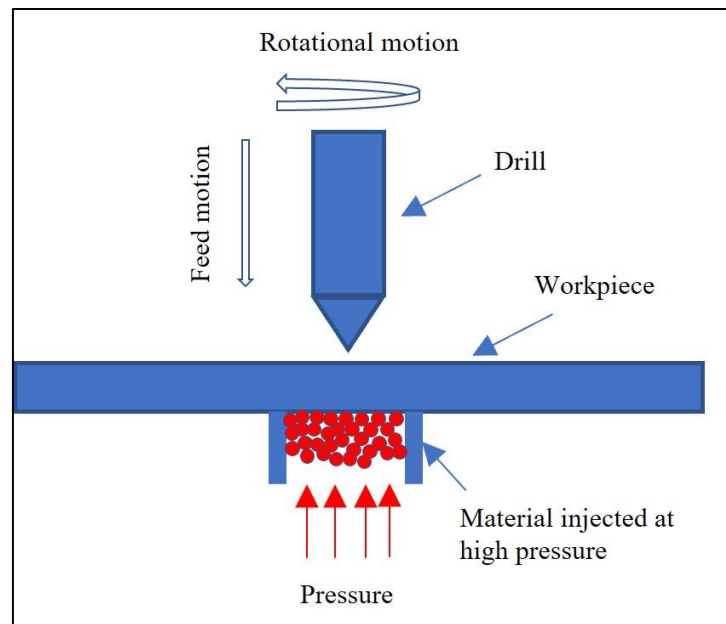
Figure 18: Idea explanation

3.1.2. Idea & Design Development.

In order to implement the idea, a considerable amount of time and effort was spent on developing a fixture for the experimental work. The main goal of the new design is to deliver materials underneath the drilled hole at different pressures. The first design was created to provide a high-pressure coolant at the burr exit side. As shown in Figure 19, the design consists of a holding block and two holding clamps made of medium carbon steel AISI 1045. Internal runners were drilled inside the holding block to deliver the high-pressure coolant precisely under the workpiece hole exit. Also, four counterbored holes were made in a square pattern with a 70 mm hole-center to hole-center length to clamp the block on the top of a table dynamometer for force measurements. The inlet hole of the holding block has a 3/8- 18 NPT thread to connect with the HPC hose for coolant delivery. The two holding clamps were

designed to provide enough clamping force on the top of the workpiece using two M12*1.75 bolts.
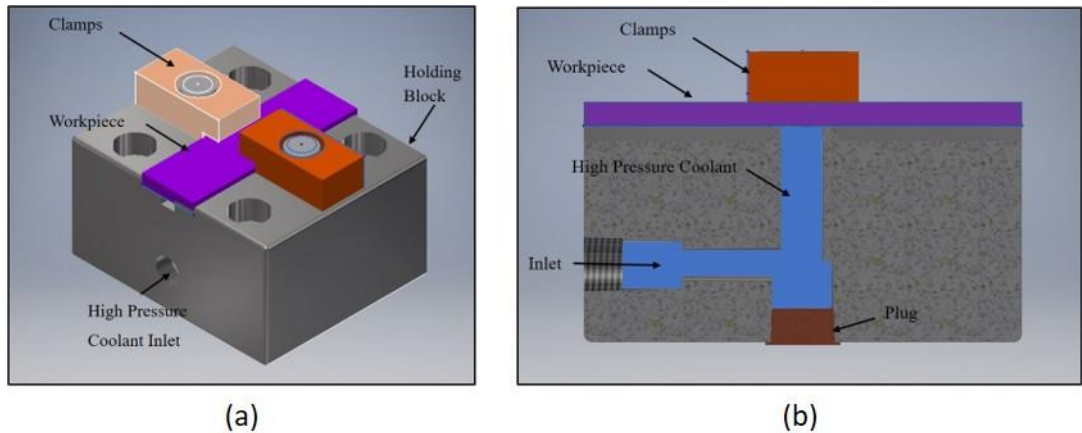
Figure 19: (a) 3D view of the fixture design, (b) Cross-section

Then the design was modified to deliver materials in a paste form by adding an injecting unit to the design, as shown in Figure 20. The injecting unit has two main functions. The first function is storing and providing the paste material under the drill hole exit at different pressures through the holding block channels. The second is to transfer the pressure from the hydraulic oil/pressuring system to the injecting material. The injecting unit is an AISI 1045 steel tube with an outer diameter of 1.5 inches and a wall thickness of 0.25 inches. The cylinder has two ends; the right end is connected to the outlet hose of a foot pedal intensifier (details about the pressurizing system are explained in section 3.2.2), and the left end is connected to the block through a 1 x 3/8 NPT thread. Inside this unit, there is a pusher to separate the hydraulic oil from the intensifier and paste stored in the injecting chamber, and to transfer the pressure from the inlet side to the outlet side, as shown in Figure 20(b).
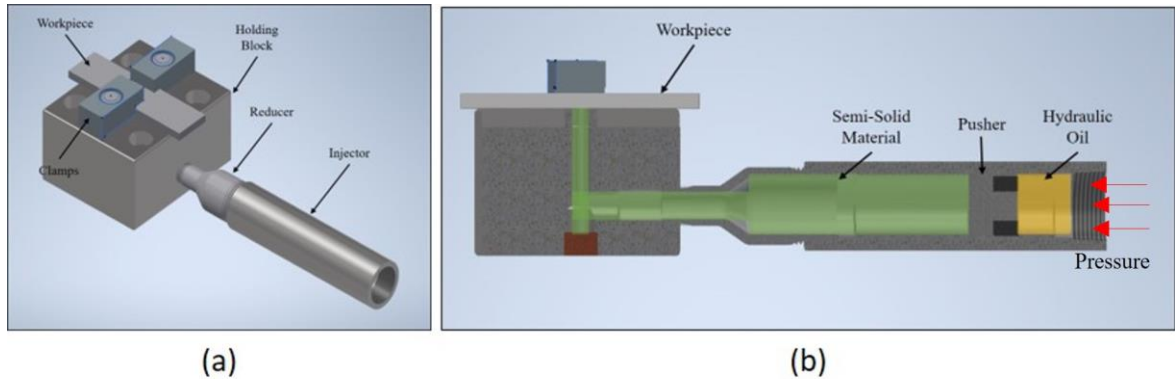
Figure 20: (a) 3D view of the modified design, (b) Cross-section of the design

3.1.3. Workpiece Properties

In this study, Aluminum 6061-T6 flats with 6*1*0.25 inches were used (see Figure 21). The chemical composition and mechanical properties of the alloy used are illustrated in Table 1 and Table 2 [42]. Aluminum alloys are used widely in engineering applications due to their relatively high strength-to-weight ratios compared to other metals, such as steel. This unique property makes aluminum a good choice for applications that require lightweight and strong materials, applications such as automotive and aerospace components [43]. Despite the excellent machinability of aluminum alloys, their relatively higher ductility stimulates large burr and drilled cap production. Therefore, burr control when machining this material is challenging.
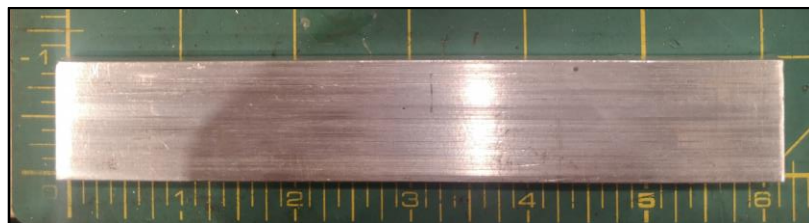
Figure 21: Workpiece

Table 1—Chemical composition of Aluminum 6061-T6 [42]

					Chemical Composition					
Element	Si	Fe	Cu	Mn	Mg	Cr	Zn	Ti	Other	Al
Weight%	0.4-0.8	~0.7	0.15-0.4	~0.15	0.8-1.2	0.04-0.35	~0.25	~0.15	~0.15	rem

Table 2—Mechanical properties of Aluminum 6061-T6 [42]

	Mechanical Properties		
Yield Strength (0.2% offset) (MPa)	Ultimate Tensile Strength (MPa)	Hardness (Rockwell E)	Elongation (%) in 50 mm
240	260	90	10

3.1.4. Tooling Selection

The twist drill used for this test was a 7 mm diameter uncoated carbide OSG drill with a straight shank. Table 3 presents detailed information about the drill. The twist drill was selected to have a low helix angle, which has been shown to produce a larger burr than a high helix angle drill [16], [23]. The intention with this choice was to maximize the exit burr formation to study the effect of the new technique on burr size in a challenging environment. Before the experiment, all the twist drills were examined under a 2D optical microscope (Keyence) for any cutting edge defects, such as microchipping. The drill was scanned using a 3D optical microscope (Alicona), as shown in Figure 22, to perform a microgeometry analysis of the cutting edge, if needed. In order to avoid the effects of drill wear, a new drill was used for each test.

Table 3— Specifications of the drill

Drill	
Type:	Metric, no coolant through
Material:	Uncoated Carbide
Diameter:	7.0 mm
Point angle:	135 °
Flutes:	2
Flute length:	40 mm
Helix angle	12°
Make:	OSG
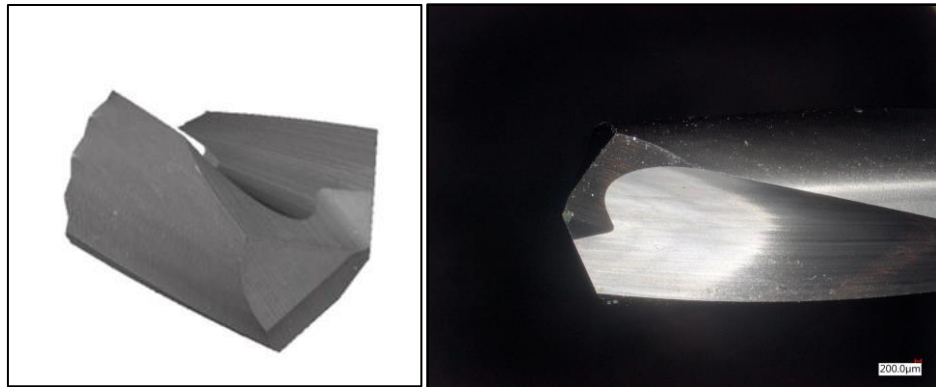
Figure 22: 3D scan of the 7mm OSG drill

3.1.5. Process Parameters

A fast feed rate has been found to significantly affect burr size. It directly increases the thrust force, creating more plastic deformation and enlarging the resultant burr [18]–[20]. In order to test the injection technique in a challenging environment, the cutting parameters were selected to produce a large exit burr. A high feed rate was chosen to maximize the exit burr size. In addition, dry machining was selected because it keeps the cutting temperature high ahead of the drilling tool, which may cause material softening, increase the material ductility in the cutting zone, and produce a larger burr [37]. Table 4 explains the cutting parameters and the drilling geometry used in this experiment.

Table 4—Process parameters of the drilling test

Parameters	Drilling
Hole diameter, mm	7.0
Hole depth, mm	6.25
Spindle speed, RPM	6000
Feed, mm/min	2000
Feed rate, mm/rev	0.33
Coolant	No coolant

3.1.6. Injecting Material Development

The development of the injecting/supporting material used in this study went through four phases, as shown in Figure 23. In Phase 1, the first series of tests were performed using a high-pressure coolant. A ChipBlaster high-pressure pump was used. This pump can deliver coolant at a maximum flow rate of 8 GPM and a maximum pressure of 1000 psi. The pump also has a pressure control valve to control the output pressure and pressure gauges to measure the pressure in the system. The coolant used in this test was a semi-synthetic coolant at a concentration of 8-10% according to the refractometer index.
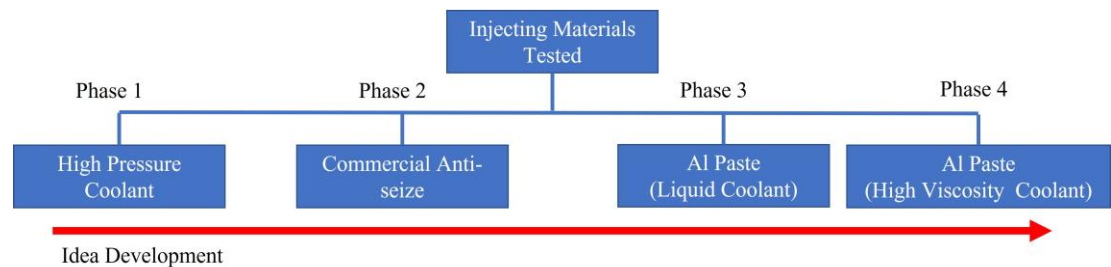
Figure 23: Injecting-material development

Phase 2 was the turning point from injecting material in a liquid form to injecting it as a paste. In this phase, a Permatex® Silver Grade commercial anti-seize was injected at the drilled hole exit. The anti-seize used was a blend of aluminum, copper, and graphite microparticles mixed in a grease medium. The testing of this anti-seize was done to understand the effect of injecting material in a paste form at high pressures on the exit burr size. Although the results from phase 2 were promising, as explained in section 3.3.1, it is not recommended to use anti-seize inside a CNC machine as it

may contaminate the inner machine components and the cooling system, causing many issues.

In phase 3, a unique aluminum paste was developed for this application based on the performance of the anti-seize from phase 2. The material was a mixture of aluminum microparticles and CommCool™ HD semi-synthetic coolant, as shown in Figure 24. The advantage of this material is that it can easily be mixed with the machine coolant without causing damage to the machine components. The material was injected into the holding block at 7000 psi. As a result of injecting the material at this high pressure, severe leakage was observed in different locations in the holding block, especially underneath the workpiece.

Figure 24: Aluminum paste (Al powder + liquid coolant)

Because of the failure that occurred in phase 3, a new form of coolant oil was developed to provide the mixture with high viscosity, avoid leakage, and enhance the mixture's stability at high pressures. The unique coolant was composed of 10% Viscool 6120 base oil, 85% water, and 5% Acusol 820 viscosity modifier. The additives were

mixed for 30 min to become uniform and viscous enough for the test, as shown in Figure 25. This form of coolant was later mixed with aluminum powder at different ratios to create an aluminum paste that can provide solid like behaviour when compressed at high pressures.

Figure 25: High viscosity coolant

The Aluminum powder used in phases 3 & 4 was bought from Sculpture Supply Canada. Its particle size was examined under an optical microscope at a high magnification of 500X, as shown in Figure 26. Fifteen images were analyzed, and the measurement results showed that the material follows a normal distribution, as shown in Figure 27, with a mean size of 48.8 microns and a standard deviation of 16.7 microns.
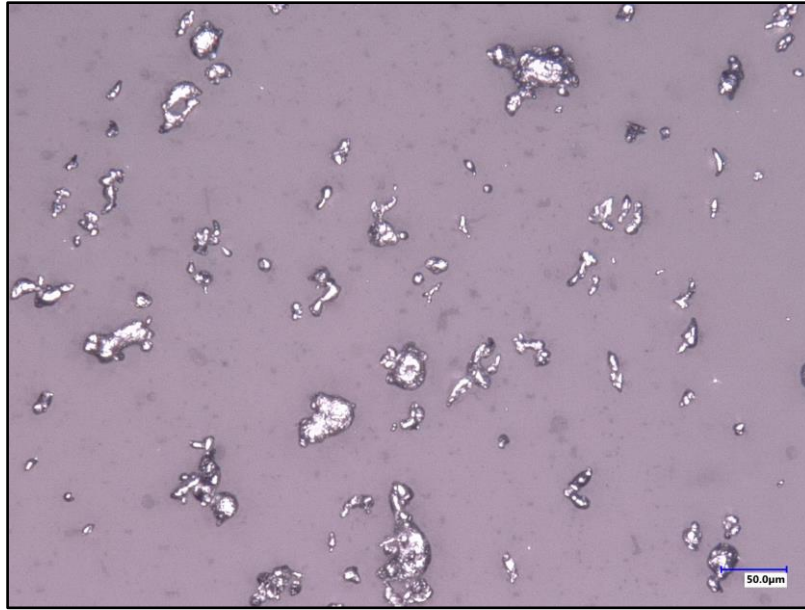
Figure 26: Optical image of aluminum powder at 500X magnification
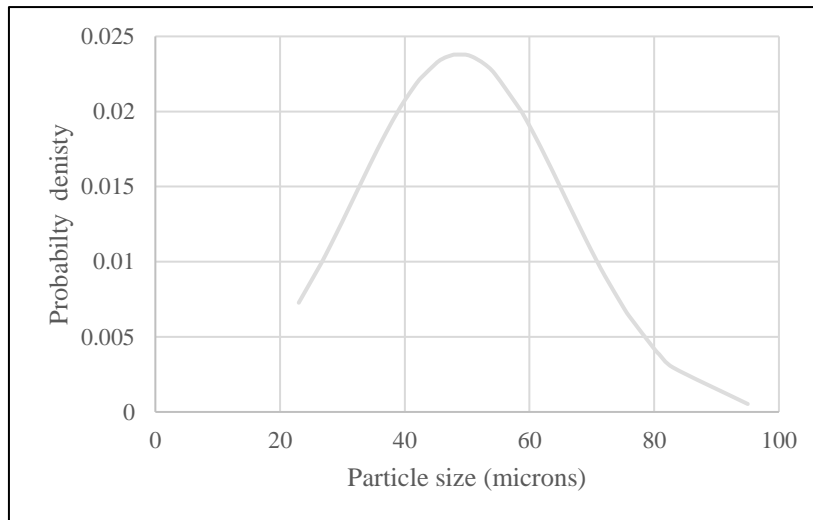
Figure 27: Aluminum powder, particle size distribution

3.1.7. Testing Plan

This experiment centered around two main objectives: firstly, to find the mixture with the minimum Al powder to coolant ratio necessary to obtain the shortest possible burr height, and secondly, to test this mixture at different pressures to understand the correlation between the applied pressure, thrust force, and produced burr. A testing plan was prepared to test different Al powder/coolant ratios, as seen in Table 5. The table shows the weight of both the aluminum powder and coolant as well as each substance's percentage of the mixture's total weight for each test. The first test was performed without using any injecting material in order to use its results as a benchmark and compare them with the results of the other tests. Each test was repeated three times using a new drill to achieve better data accuracy.

Table 5—Testing plan 1

Test #	Injected Material	Pressure (psi)	Al Powder wt (g)	Coolant wt (g)	Powder wt (%)	Coolant wt (%)
1(Benchmark)	No material	0	0	0	0	0
2	HPC	1000				
3	Anti-seize	7000				
4	Al paste	7000	22	90	20%	80%
5	Al paste	7000	60	90	40%	60%
6	Al paste	7000	90	90	50%	50%
7	Al paste	7000	135	90	60%	40%

A MITO portable scale was used during the experiment to weigh the Al powder/coolant mixtures precisely, as shown in Figure 28. This scale has a high precision of 0.1 g, a maximum weight range of 3000 g, and an error range of ±0.1%.

(a)   (b)
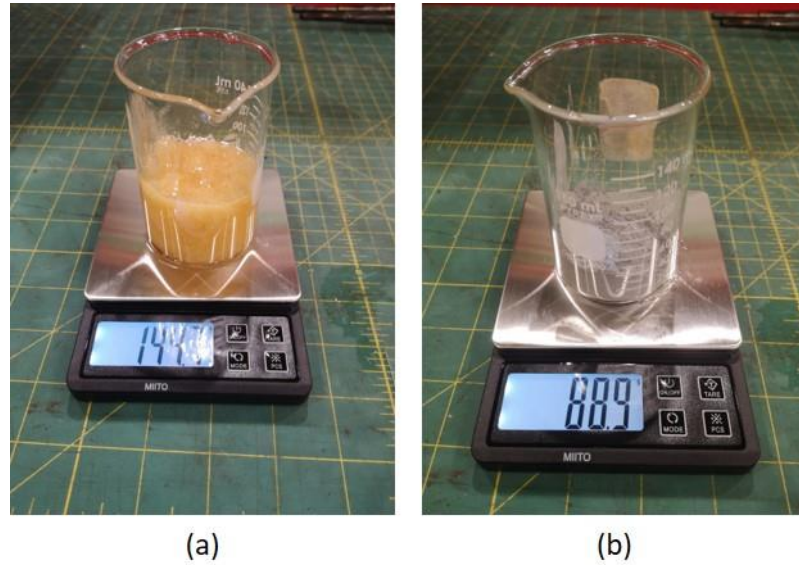
Figure 28: Mixture weighing and preparation, (a) High viscosity coolant, (b) Aluminum Powder

The second series of experiments was performed using the optimum Al paste mixture identified during testing plan one at different injecting pressures. Table 6 describes the aluminum mixture used in the test with applied pressure values.

Table 6—Testing plan 2

Test #	Injected Material	Pressure (psi)	Al Powder wt (g)	Coolant wt (g)	Powder wt (%)	Coolant wt (%)
1	Al paste	7000	60	90	40%	60%
2	Al paste	5000	60	90	40%	60%
3	Al paste	4000	60	90	40%	60%
4	Al paste	3000	60	90	40%	60%

3.1.8. Experimental Setup

The drilling experiments were performed on a Matsura RA IIIF, a three-axis vertical CNC milling center with a spindle power of 10 hp and a maximum spindle RPM of 8000. Figure 29 shows the setup used during the test. The machining tests were executed under dry conditions with a feed of 2000 mm/min and a spindle speed of 6000 RPM, as described in Table 4.
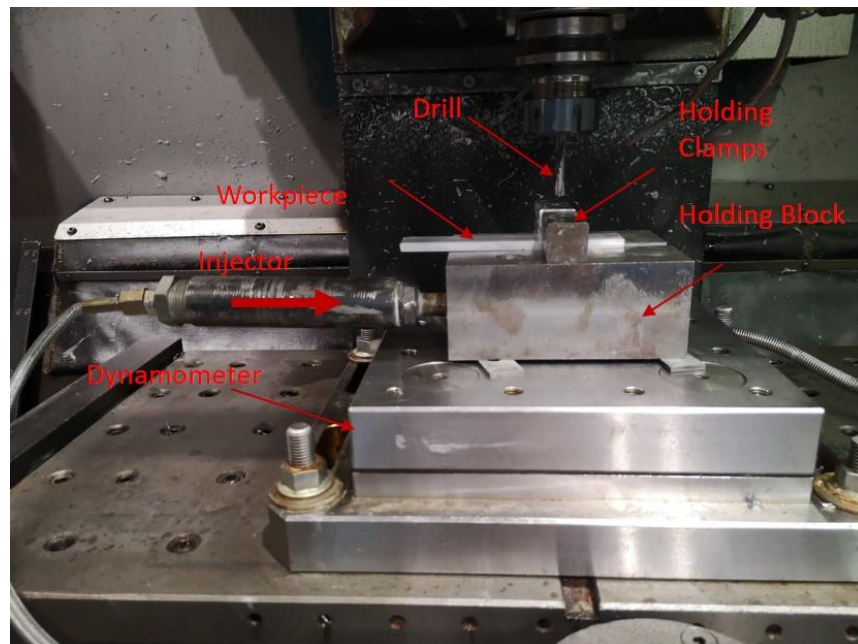
Figure 29: Experimental setup for drilling tests in a vertical CNC machine

3.2. Measurements

3.2.1. Drilling Forces

In this study, thrust force was measured using a Kistler 9255B table dynamometer. The dynamometer has four 3-component force sensors that measure forces in X, Y, and

Z directions, as shown in Figure 30. Drilling thrust force is measured in the Z direction, with a measurement range from -20 to 40 kN.
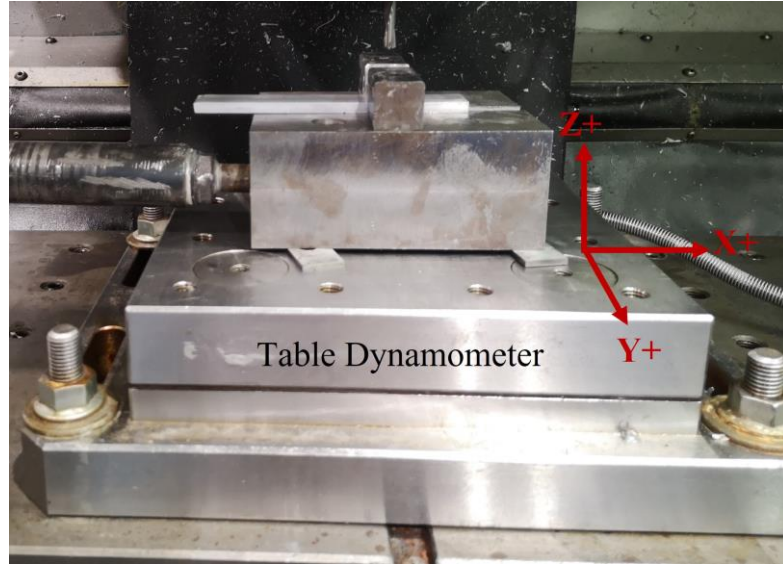
Figure 30: Dynamometer forces coordinating system

The dynamometer was connected to a Kistler 5167A81 eight-channel amplifier through a 1689B5 Kistler cable. The amplifier has a powerful data acquisition card that amplifies the output signal and delivers digitalized measurement values directly to Kistler dynoware software version 2825A-03 for visualization and signal analysis, as illustrated in Figure 31. In accordance with the manufacturer's recommendations, thrust force was measured at the center of the dynamometer for the most accurate results. The forces were collected at a sampling rate of 1000 Hz.
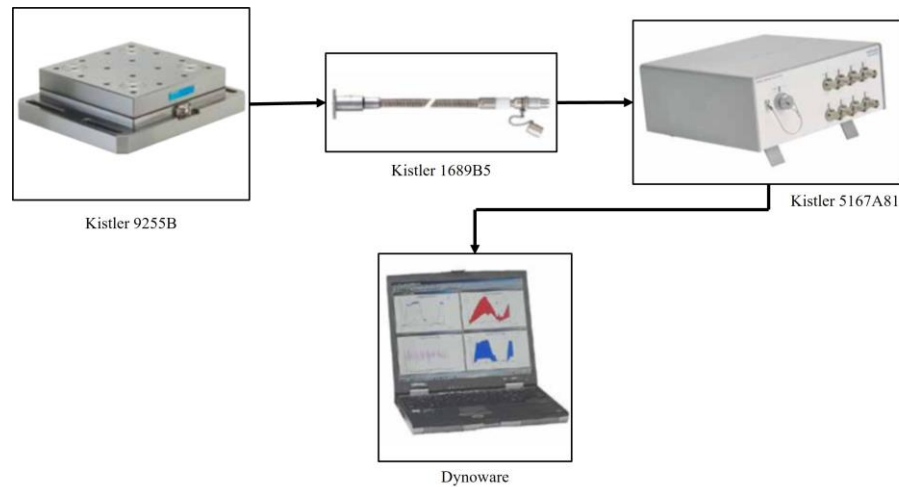
Figure 31: Illustration of force measuring components according to [44]

While each hole was drilled, thrust force was measured, mainly to understand the average thrust force at the hole exit, and these values were used to study the minimum injecting pressure needed to minimize the drilled exit burr.

3.2.2. Pressure

To perform the tests, an adequate pressurizing system was required. Figure 32 shows the main components of the system used in this work. The system consists of the following:

1. An air pressure regulator with a maximum output pressure of 125 psi, whose primary function is to control the air pressure that flows into the intensifier. This regulator controls the maximum output pressure in the system.

2. An air inlet nozzle, which allows the air to flow into the intensifier.
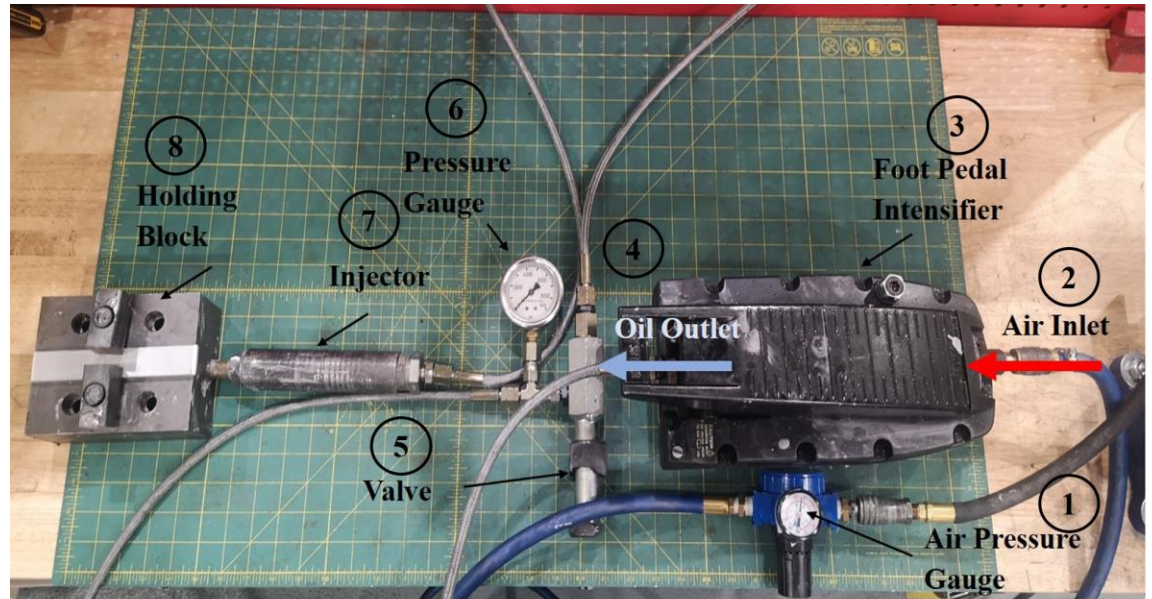
Figure 32: Pressuring system

3. A SWIFTSURE foot pedal intensifier. This intensifier has a hydraulic oil tank inside and uses an inlet air pressure ranging from 40 to 75 psi. It intensifies the inlet air pressure with an intensification ratio of 1:100 and can provide oil at a maximum pressure of 7500 psi.

4. An oil outlet nozzle, from which hydraulic oil exits the intensifier at high pressures.

5. A hydraulic pressure control valve to control the oil pressure in the system.

6. A pressure gauge with a measuring range of 0-9000 psi to precisely measure the oil pressure.

7. A material injector to transfer the pressure from the hydraulic oil to the injecting material.

8. A holding block, which holds the aluminum workpiece on the top, receives the injecting material from the injector at the required pressure, and directs it to underneath the hole exit.

3.2.3. Burr Size

According to the ISO 13715 standards, burr size (a) is the value measured from the burr tip perpendicular to the surface from which the burr is protruding [45], as shown in Figure 33. In this dissertation, the burr size value (a) was used to compare the results under different conditions.
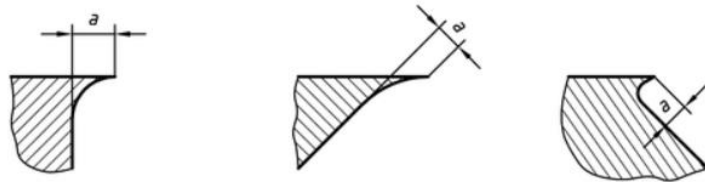
Figure 33: Burr size ((Used with permission [45])

The burr size of the exit burr was measured after each test using an Alicona Infinite Focus G5 optical microscope, as shown in Figure 34. This microscope can generate 3D images of the burr using focus variation technology with a lateral resolution of 400 nm and a vertical resolution down to 10 nm. The microscope also has an integrated software package to allow the user to analyze the captured images and perform different measurements.
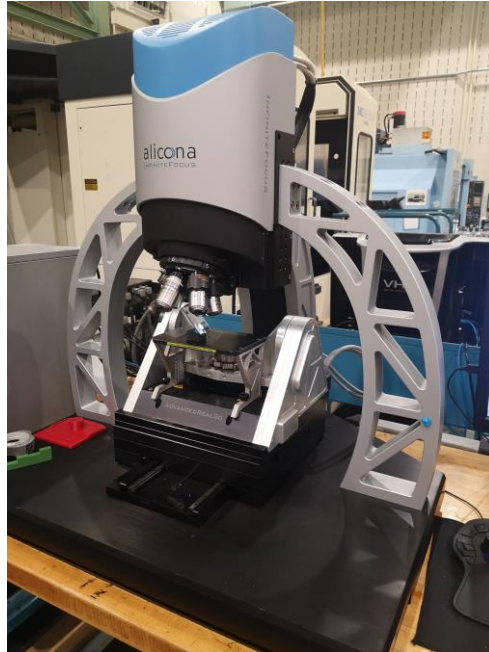
Figure 34: Alicona 3D optical microscope

All burr samples were scanned at 10X magnification at an approximately 45°
inclination. For each sample, images of the burrs were captured from at least five
sections to identify and measure the maximum burr size of each section, as shown in
Figure 35. The average burr size in all sections, as well as the standard error of the
mean, were calculated and reported for each test using Eq 1 and Eq 3.

$$a_m = \frac{\sum a}{n} \qquad\qquad \text{Eq 1}$$

$$SD = \frac{\sqrt{\sum (a - a_m)^2}}{n - 1} \qquad\qquad \text{Eq 2}$$

$$SEM = \frac{SD}{\sqrt{n}} \qquad\qquad \text{Eq 3}$$

Where,

a_m = mean burr size for each test

a = measure burr size for each section

n = number of measurements

SD = standard deviation

SEM = standard error of the mean

In addition to burr measurements, a Keyence 2D optical microscope was used in this study to capture high-resolution images of the burr to visually compare them side by side.
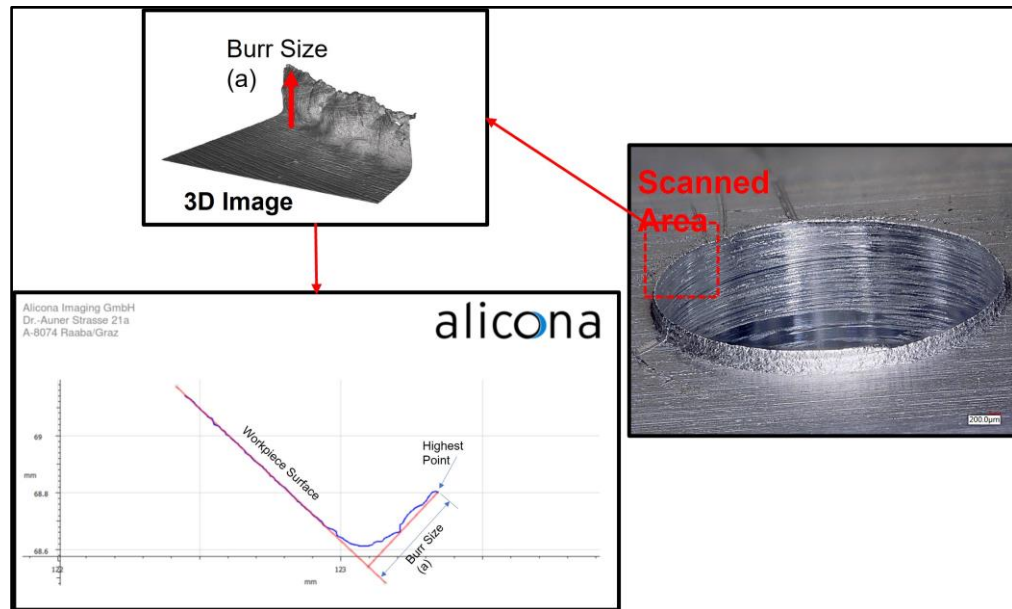
Figure 35: Burr measuring using a 3D microscope (Alicona)

3.3. Results

3.3.1. Burr Size:

The chart in Figure 36 shows the exit burr sizes that resulted from using different injecting materials. As seen, using a high-pressure coolant at 1000 psi as an injecting material had almost no effect on the burr size. It's also notable that the anti-seize produced a minimal burr compared to the regular drilling with no supporting material (benchmark). However, the newly developed aluminum paste with an aluminum content of 20% created a burr size similar to the benchmark. The paste started showing a significant reduction in burr size when it had 40% aluminum content, and Al content increases beyond 40% showed no further related burr size improvement. Figure 37 shows optical images of the exit burr under different conditions.
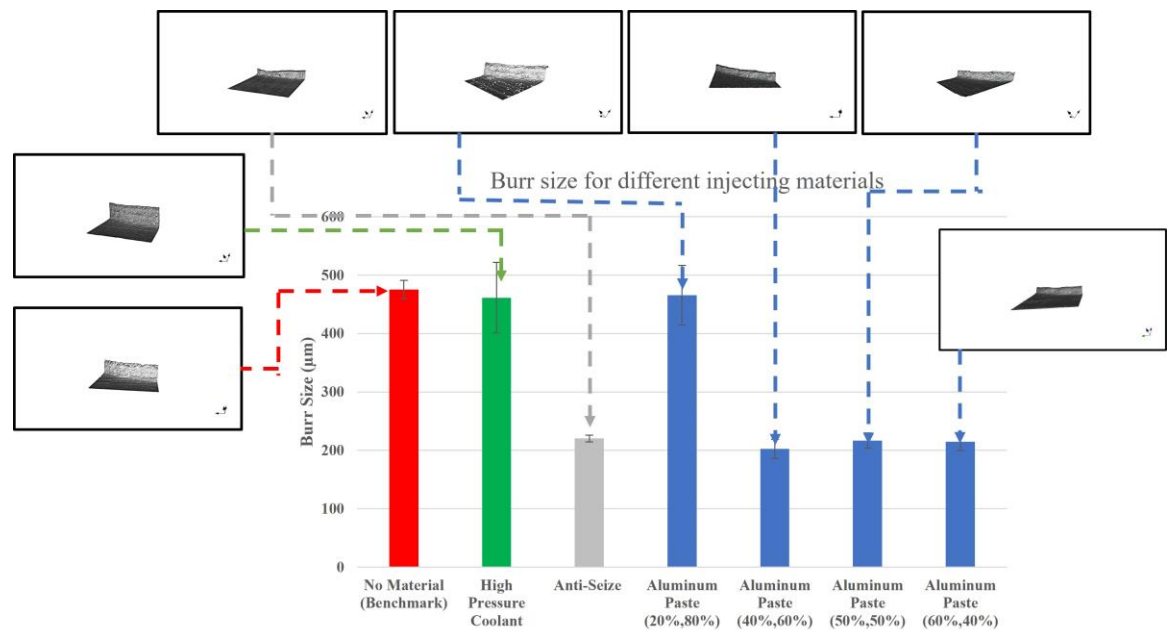
Figure 36: Burr size for different injecting materials
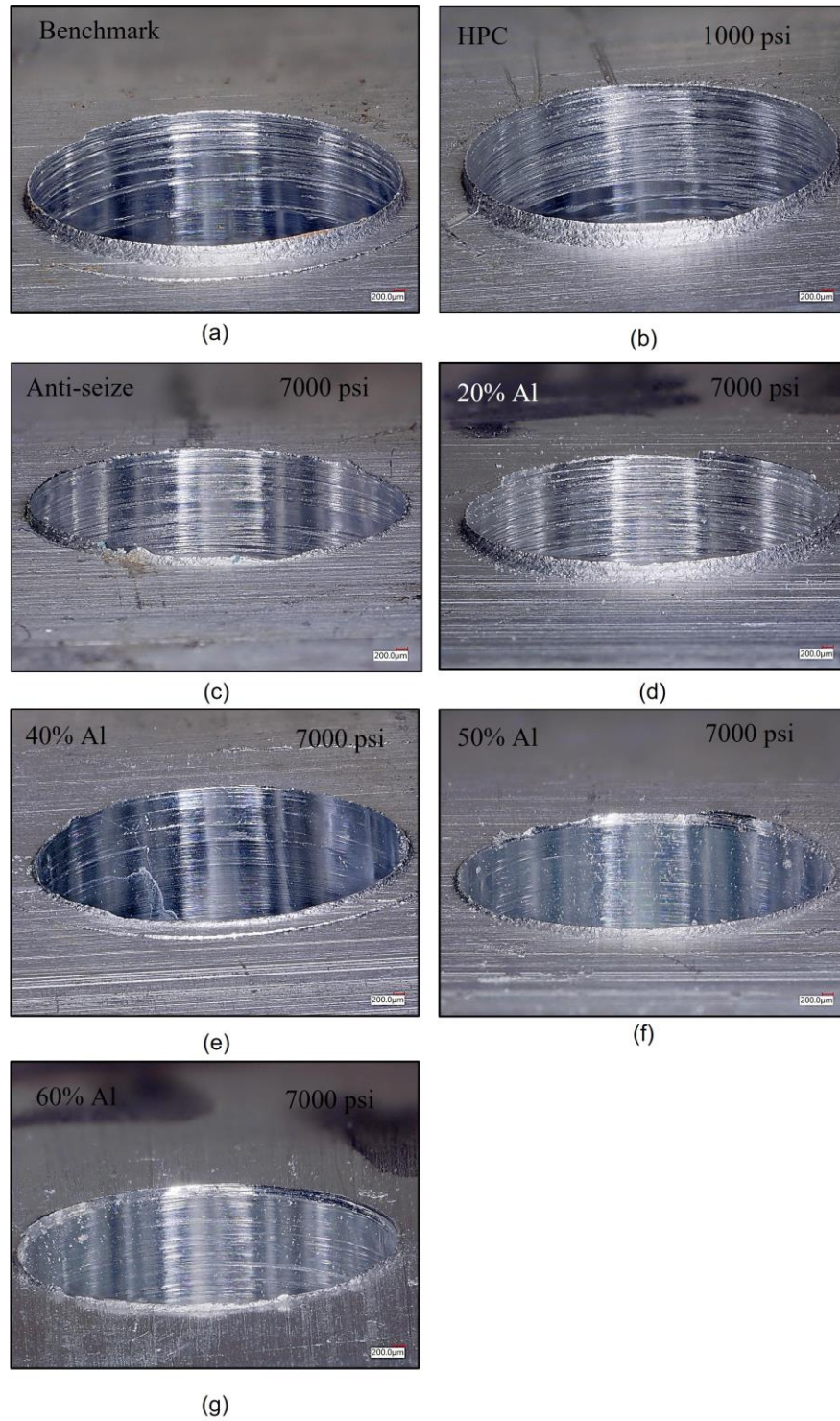
Figure 37: (a) Optical image of burr for benchmark at 50x, (b) High-pressure coolant at 1000 psi, (c) Anti-seize at 7000 psi, (d) 20% Al paste at 7000 psi, (e) 40% Al paste at 7000 psi, (f) 50% Al paste at 7000 psi, (g) 60% Al paste at 7000 psi.

3.3.2. Thrust Force

Thrust forces were measured during all the experiments. Figure 38 illustrates the typical thrust force graph as a function of time in the drilling operation. The graph has three main stages. In the first stage, the cutting lips are steadily engaging with the workpiece. After that is the steady drilling region, in which the cutting edges are fully engaged with the workpiece and the twist drill steadily cuts in the feed direction. At the drill exit, as a result of the high plastic deformation, fracture occurs, and the drill exits the workpiece. Using the graph, the thrust force was determined from the steady drilling region by calculating the moving average of approximately 0.11 seconds. Thrust force values for all tests were similar at about 431 N. This value was used to determine the correlation between the thrust forces, the applied pressure under the hole exits, and the burr height.
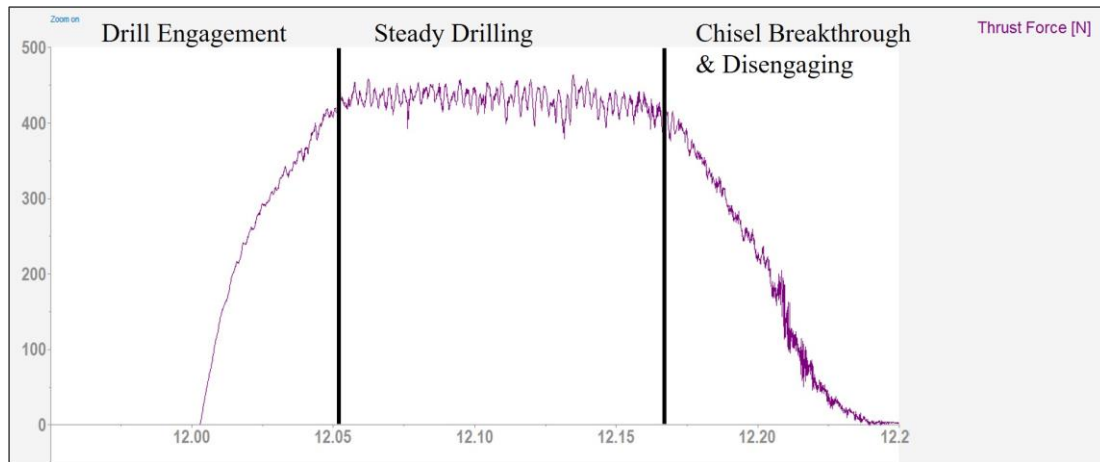
Figure 38: Thrust force graph for drilling a hole

3.3.3. Pressure

Another set of experiments was performed using aluminum paste with a mixture of 40% Al microparticles and 60% high viscosity coolant. The mixture was tested under different injecting pressures, and the results are shown in Figure 39. The figure illustrates that the smallest burr height achieved was 202.6 microns at a pressure of 7000 psi. a slight increase in burr height by reducing the pressure to reach 239.3 microns at a pressure of 4000 psi. When the injecting pressure drops down to 3000 psi, the burr height significantly increased to 529.6 microns, reaching a similar level to the condition without any supporting material (the benchmark). This confirms that the minimum effective pressure for producing a small burr is somewhere between 4000 psi and 3000 psi. However,
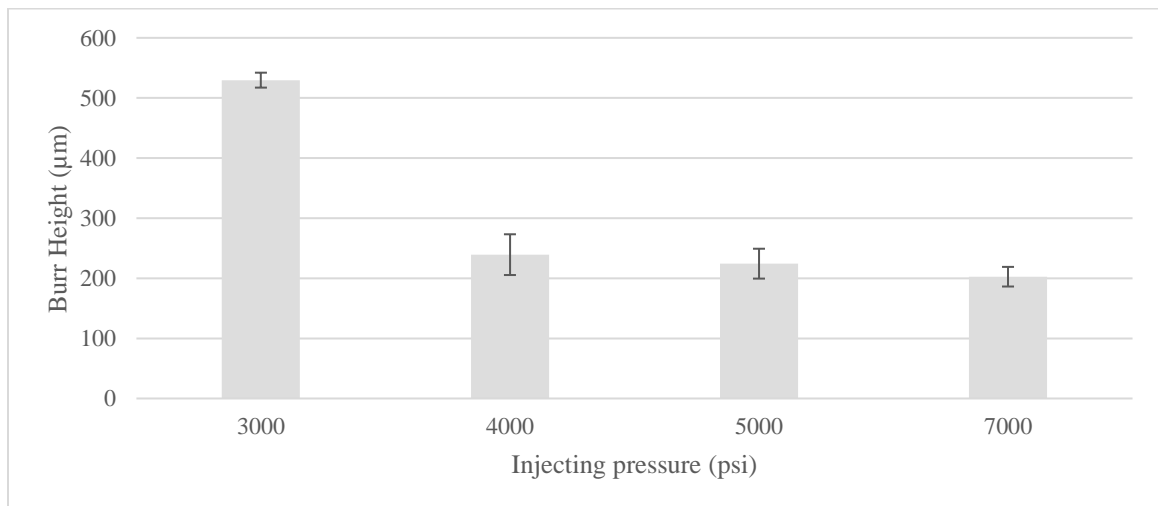
Figure 39: Burr height at different injecting pressure

In order to understand the relation between the thrust force from the drilling action and the injecting/supporting force under the hole exit, forces under the exit hole side were calculated using Eq 4

$$F_i = P_i A_i \qquad\qquad \text{Eq 4}$$

Where,

F_i = supporting force (force under the drilled hole exit)

P_i = injecting pressure

A_i = area of the drilled hole

Figure 40 illustrates the relationship between the calculated force under the hole exit and the produced burr size. The figure shows a significant improvement in burr size when the supporting force reaches 1061 N, approximately two and a half times the thrust force value (see Figure 41). Moreover, a slight reduction in burr size was observed by increasing the supporting force to more than 1061 N.
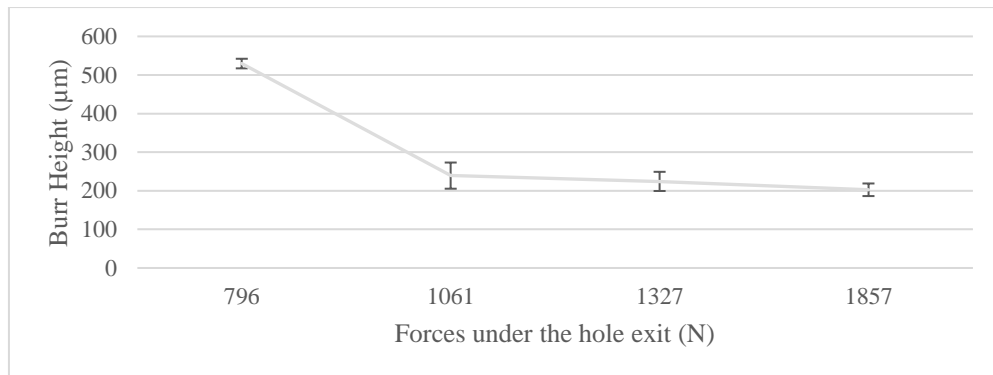
Figure 40: Burr heights at different injecting forces
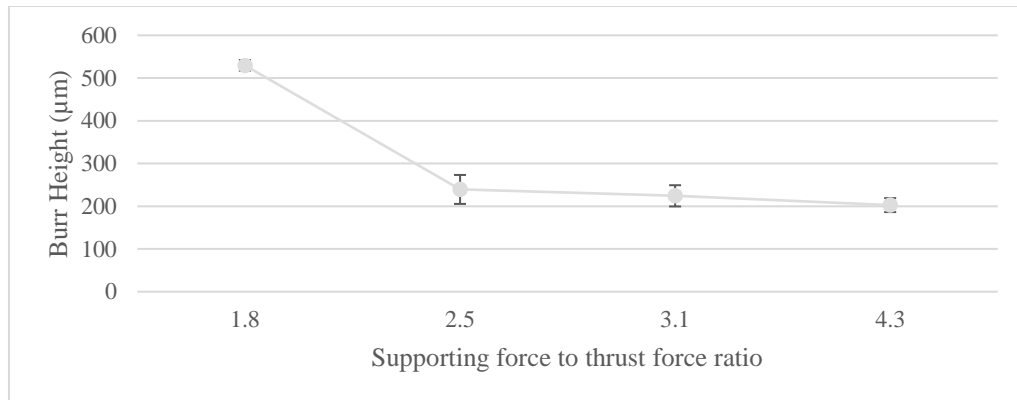
Figure 41: Burr height relation with calculated injecting to thrust force ratios

3.4. Discussion

Injecting aluminum paste at high pressures showed a significant reduction in burr height compared to conventional drilling. Moreover, no drilled cap was observed when using the new approach in contrast with conventional drilling, which produced a drilled cap in all experiments. During the conventional drilling of ductile materials, when the twist drill is near the hole exit, the material under the chisel edge starts to yield. The thrust force plastically deforms the material in front of the drill into a cone shape. With continuous drilling, fracture occurs at the hole perimeter, creating a uniform burr with or without a drilled cap [39], as seen in the high-speed images in Figure 42.
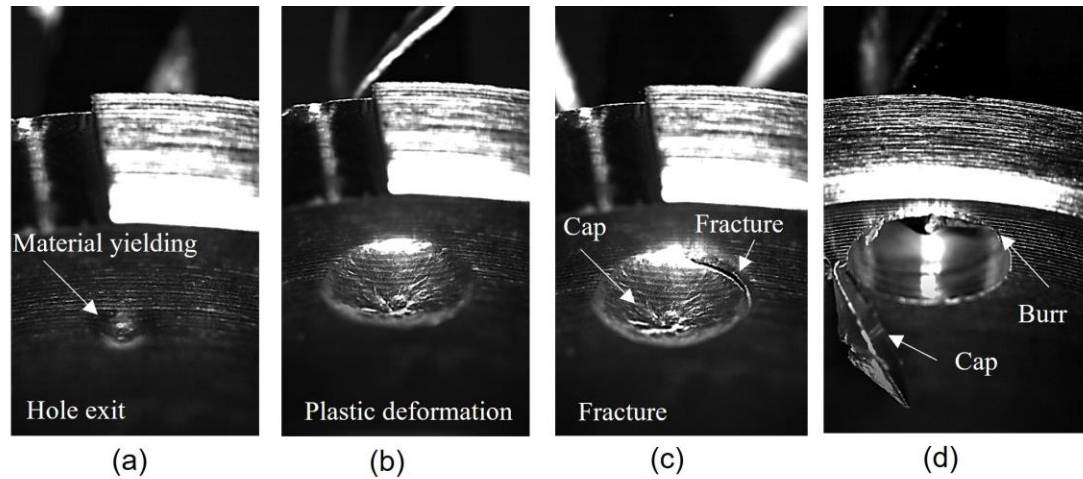
Figure 42: High-speed camera images of drilling exit burr formation (a) burr initiation, (b) material plastic deformation, (c) fracture, (d) burr and drilled cap at the end.

The reason for this improvement could be related to the burr formation mechanics. Figure 43 illustrates the expected steps for burr formation using the new approach. Figure 43 (a) shows that the twist drill gradually cuts the workpiece material in the feed direction. Before the drill approaches the hole exit, the material under the drill center-point starts to yield. At this moment, with enough injecting pressure, the aluminum paste creates a dam-like effect which supports the exit burr and prevents the burr from moving freely in the feed rate direction propelled by the thrust force, as shown in Figure 43 (b). As a result, the fracture occurs at the center of the drill, causing the aluminum paste to flow against the feed direction through the drill flutes under the applied pressure. The material flow and supporting pressure help keep the workpiece material balanced and prevent it from bending at the hole periphery under the thrust force (see Figure 43 (c)). While the twist drill proceeds towards the exit, the fracture in the hole center grows. Accordingly, the flow rate of the supporting material increases, and the

injecting pressure drops significantly until it reaches zero. Eventually, when the balancing force becomes lower than the thrust force, the thrust force starts to yield the workpiece material, causing a small burr to occur, as illustrated in Figure 43(d).

Reducing the injection pressure from 7000 psi to 4000 psi showed a slight increase in burr height from 203 microns to 239 microns which represents an increase of 17%. Reducing the injection pressure further from 4000 psi to 3000 psi increased the burr height significantly from 239 microns to 530 microns representing a 121% increase in burr height. The sudden increase in burr height was attributed to the lack of functional support provided by the lower pressure. By dropping the pressure to 3000 psi, the injecting pressure is no longer sufficient to create the dam-like effect needed to support the back of the drilled hole resulting in the formation of a large burr.

The minimum effective injection pressure needs to generate a support force that is greater than the thrust force associated with drilling. In this study, the injection/supporting force was two and a half times the thrust force to compensate for the pressure drop and the material flow that occurs due to the initial fracture at the hole center. The time required for the pressure to drop from its maximum value to become non-effective may impact the produced burr. More time may delay the deformation of workpiece material, thus reducing the burr size. In addition, providing constant pressure and continuously injecting the supporting material may serve to provide better support thus helping to reduce burr height further.

(a) Steady drilling

No initial yielding

Pressure

(b) Material yield

Dam effect

Yield balancing

Pressure

(c) Drill breakthrough

Material flow under pressure

Pressure decrease

(d) Burr Formation

Small Burr

No pressure/no flow
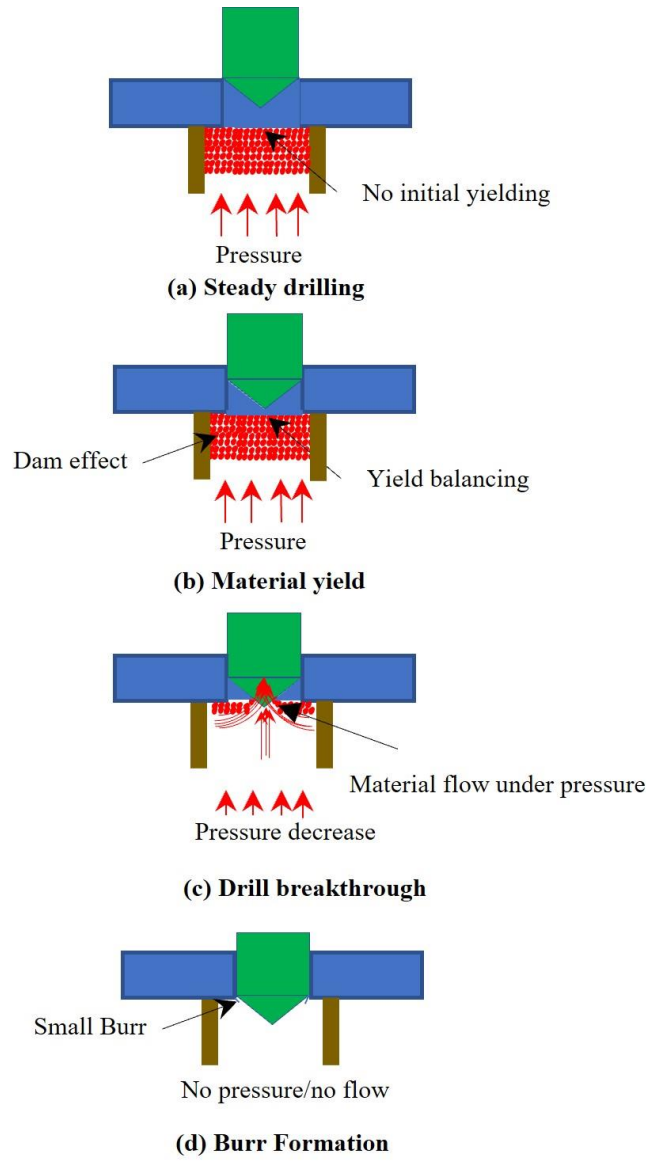
Figure 43: Burr formation mechanism using Al paste injection.

3.5. Conclusions

A novel approach for burr minimization and drilled cap elimination was developed and studied on the drilling of aluminum 6061-T6. The study included injecting a newly developed aluminum paste at high pressures under the drilled hole exit. The results showed a significant reduction in burr size when injecting aluminum paste with 40% Al content at 7000 psi. The reduction in burr size was approximately 57% compared to the benchmark, and there was no drilled cap. Different injecting pressures were also tested, and the minimum effective pressure to produce smaller burrs was found to be about 4000 psi. Moreover, the supporting force under the drilled hole exit was calculated. The minimum supporting force that significantly improves burr size was 1061 N, approximately two and half times the thrust force.

Chapter 4. Burr Control Using Step Drills

In this chapter, a new approach for designing and testing application-based step drills will be explained. The main objectives of this research can be summarized as the following:

❖ Understand the fundamentals of step drills and their performance in burr control.

❖ Develop a new experimental procedure for designing and testing highly effective step drills for a specific application.

❖ Conduct a preliminary study to understand the correlation between step size, step profile, and burr height.

❖ Use the optimum step size, and step profile from the preliminary results to design a new step drill.

❖ Test the step drill and compare its performance with the preliminary results and the benchmark.

4.1. Experimental Procedures.

In this section, a detailed description of the experimental procedures will be covered.

4.1.1. Idea Overview.

Drill geometry and design play an essential role in the produced hole quality. The tool market has a large variety of different drill designs to accommodate market needs. However, each drilling process has unique requirements based on the workpiece

material, cutting parameters, and cooling method. Step drills are common tools that have been used for burr control in industrial applications/products. When designing a step drill, it is important to consider how different parameters control its performance. The two primary parameters that affect the produced burr size are step size and step profile [46], [47]. Step profile can be in chamfer or radial shapes, as shown in Figure 44. In chamfer steps, the step angle θ_2 affects the step drill performance and needs to be studied. The performance of radial steps is affected by the step radius.
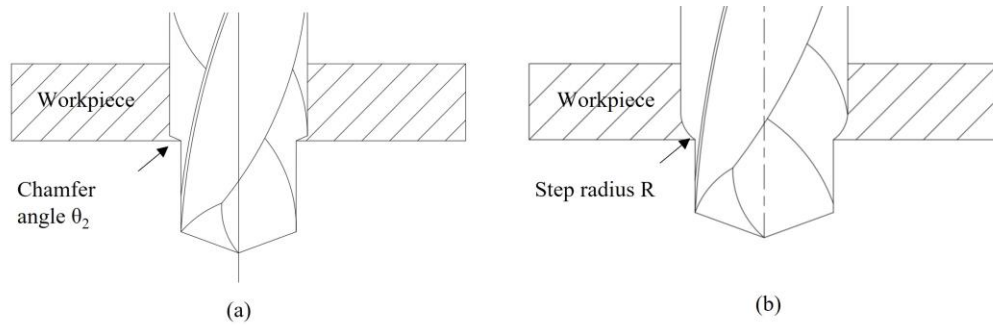
Figure 44: Step profile (a) chamfer step, (b) radial step

Figure 45 illustrates the main features of the step drill. D_1 is the first diameter responsible for drilling the first hole; D_2 is the second diameter and is located on the upper part of the tool for cutting the hole to its final diameter, and θ_2 is the step angle. The step size (ℓ) can be calculated using Eq 5.

$$l = \frac{D_2 - D_1}{2} \qquad \text{Eq 5}$$
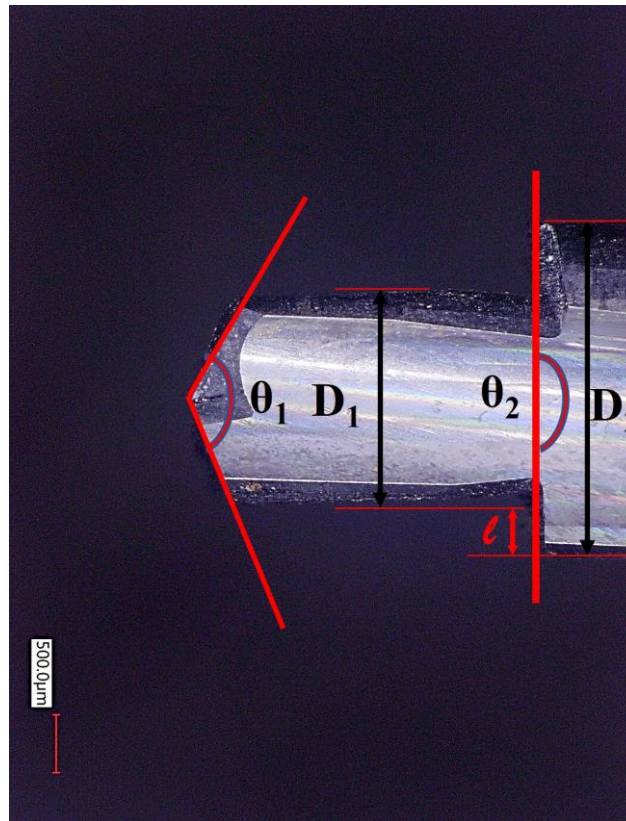
Figure 45: Schematic of a step drill

Due to the many parameters that affect exit burrs in drilling, such as the tool geometry, workpiece material properties, cutting parameters, and exit surface profile, step drill performance differs from one process to another. In industry, improving the hole quality by optimizing the process parameters or the workpiece material often has limitations. These limitations are usually due to the machine capabilities or the final product specifications. Thus, optimizing the drill geometry to improve the exit burr size is considered the most practical way to improve the hole quality. Testing and validating different step drill designs for a specific process by varying the step size, and step profile can take a long time as it includes designing the tools, grinding them, testing them, and validating them.

The idea proposed in this dissertation is a novel approach for designing and testing process-based step drills. The new method includes using off-the-shelf drills to precisely simulate the step drill and determine the optimum step size, and step profile to minimize burr and eliminate the drilled cap. In this methodology, we used two off-the-shelf drills to mimic the cutting action of a step drill. The first drill simulates the small diameter D_1 at the front side of the step drill. The second drill's diameter represents the large/final diameter D_2 on the upper portion of the step drill, and the point angle of the second drill represents the step angle θ_2 in the case of a chamfer step profile, as shown in Figure 46. The second drill also can have a radial corner with radius R to simulate the radial step profile. In this way, the time and cost required to design the step drills was reduced to a few days instead of months. It is more important that the process-based step drill design can achieve very high efficiency in burr control.
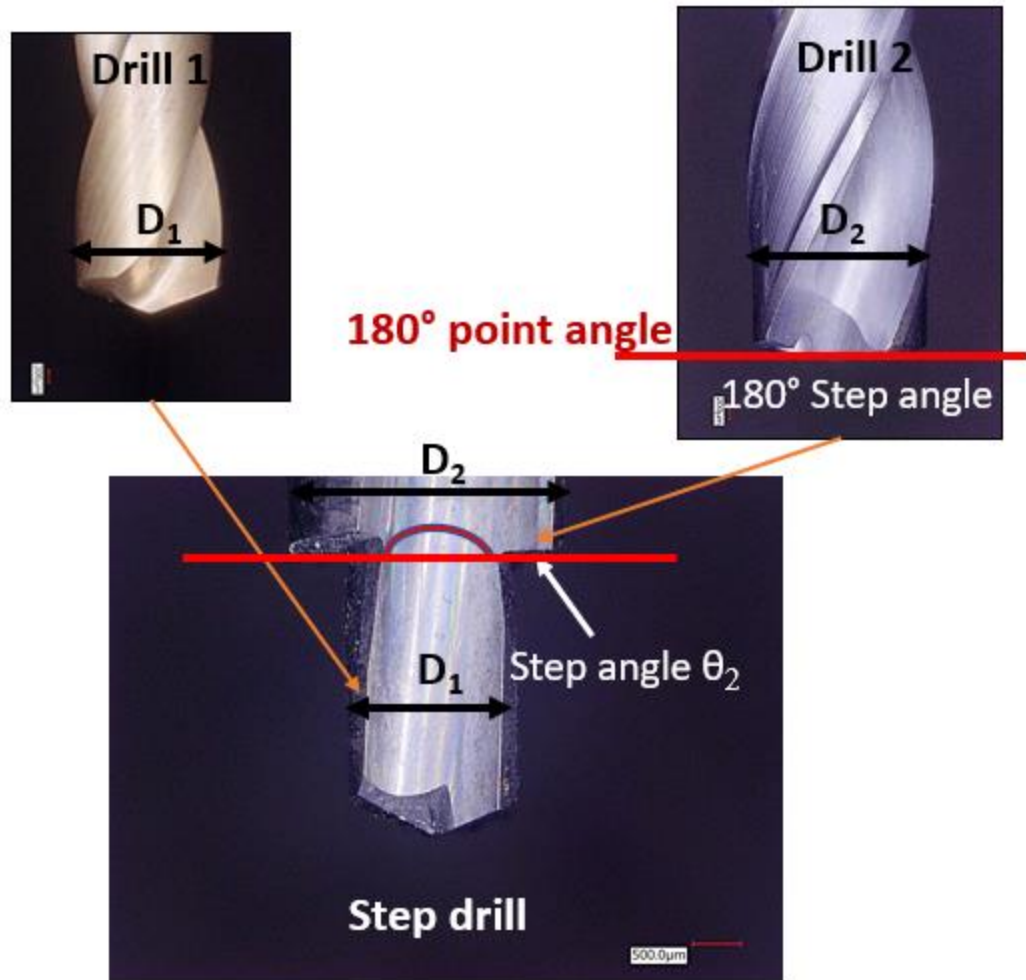
Figure 46: Idea explanation

4.1.2. Workpiece Preparations

For the experimental work, a cast aluminum component was studied that included oil holes. Oil holes needed to be drilled from the outer diameter all the way to the inner region. During the quality inspection of the oil holes, a large burr and a drilled cap were found attached to the exit surface. These burrs can interfere with the part's functionality and may lead to catastrophic failures.

The parts were machined using an OKUMA 2 axes CNC lathe to smooth the surface and remove any defects generated from preparing the part on the waterjet machine, as shown in Figure 47.

Figure 47: Workpiece preparation after water jetting, and turning the outer surface

4.1.3. Tooling Selection

As previously described, two significant factors affect the step drill's performance: step size and step profile. The main goal of this study was to understand the effect of changing these parameters step size and step profile on the produced burr and improve the burr by selecting the optimum step geometry and using it to design a step drill. Table 7 represents the four drills used to drill the first hole diameter D_1. The twist drills were selected to be identical in geometry with only differences in diameters. Table 8 illustrates the three drills used for drilling the second hole diameter D_2. These drills all had the same diameter as was required for the final hole size. However, drill #5 and drill #6 had different point angles to simulate the effect of a chamfer step with varying

angles. Drill #7 was selected to have rounded corners so that the impact of using a radial step profile on the exit burr size can be assessed.

Table 7—Tools used to drill the first hole D_1 with different diameters

	Drill #1	Drill #2	Drill #3	Drill #4
Type:	Metric	Metric	Metric	Metric
Coolant	Through coolant	Through coolant	Through coolant	Through coolant
Material:	TiAlN coated carbide	TiAlN coated carbide	TiAlN coated carbide	TiAlN coated carbide
Diameter:	6.7 mm	6.4 mm	6.1 mm	5.8 mm
Point Angle:	140 °	140 °	140 °	140 °
Flutes:	2	2	2	2
Flute length:	24 mm	24 mm	24 mm	24 mm
Make:	Kennametal	Kennametal	Kennametal	Kennametal

Table 8— Tools used to drill the second hole D_2.

	Drill #5	Drill #6	Drill #7
Type:	Metric	Metric	Metric
Coolant	Through coolant	Through coolant	Through coolant
Material:	Coated Carbide	Coated carbide	Coated Carbide
Diameter:	7.0 mm	7.0 mm	7.0 mm
Point Angle:	180 °	130 °	143 °
Flutes:	2	3	2
Corner radius	0	0	1.4 mm
Flute length:	24 mm	24 mm	24 mm
Make:	Kennametal	Kennametal	Kennametal

Based on the preliminary results from testing the off-the-shelf drills, a step drill was designed. Table 9 illustrates the features that were tested in this study as selected for the final step drill.

Table 9: Step drill main features

Step drill	
Type:	Metric
Material:	Uncoated solid carbide
Point angle θ_1 :	140
Small diameter D_1:	6.4 mm
Large diameter D_2:	7.0 mm
Step size ℓ :	0.3 mm
Step profile	Rounded step with 1.4 mm radius
Flutes:	2
Flute length:	23 mm
Helix angle:	25°
Make:	Berks

4.1.4. Process Parameters

Process parameters were selected to replicate commonly used machining parameters. Table 10 describes the cutting parameters used during the experiments. All drills used for drilling the first hole had identical geometry aside from the drill diameter. Thus, the cutting parameters used for drilling the first hole were similar for all the drills. As seen in Table 8, both drill #5 and drill #7 had two cutting flutes. However, drill #6 had three cutting flutes. In order to keep the chip load per flute the same for all the three drills while drilling the second hole, the spindle speed was adjusted to be 4000 RPM for only drill #6 instead of 6000 RPM like for drill #5 and drill #7.

Table 10—Process parameters of the drilling test

Parameters	Drilling hole 1 (D_1)	Drilling hole 2 (D_2)
Hole diameter, mm	Varies	7
Hole Depth, mm	5	5
Spindle speed, RPM	6000	6000, 4000
Feed rate, mm/min	2298	2298
Feed rate per flute, mm/rev/flute	0.192	0.192
Coolant	No coolant	No coolant

4.1.5. Testing Plan

A series of tests were performed to study the step size and step profile, as shown in Table 11. Each test was performed using two different drills with three repetitions. Changing the diameter of the first drill (D_1) produced different step sizes. Since the point angle of the second drill (θ_1) is equal to the step angle (θ_2), altering the point angle also changed the step angle for the chamfer steps. Drill #7 with a 1.4 mm corner radius was also tested to simulate the radial step profile with 1.4 mm R. Each test was repeated three times, and a visual inspection of the exit burr was performed to detect drill caps.

Table 11 —Array of tests

Test #	D_1 (mm)	D_2 (mm)	Point Angle (°)	Factor A Step Size ℓ (mm)	Factor B Step Profile	Speed RPM	Feed (mm/ min)	D2 Flutes #	Feedrate/ flute (mm/rev)
1	6.70	7	180	0.15	180	6000	2298	2	0.192
2	6.70	7	143	0.15	1.4 Radius	6000	2298	2	0.192
3	6.70	7	130	0.15	130	4000	2298	3	0.192
4	6.40	7	180	0.3	180	6000	2298	2	0.192
5	6.40	7	143	0.3	1.4 Radius	6000	2298	2	0.192
6	6.40	7	130	0.3	130	4000	2298	3	0.192
7	6.10	7	180	0.45	180	6000	2298	2	0.192
8	6.10	7	143	0.45	1.4 Radius	6000	2298	2	0.192
9	6.10	7	130	0.45	130	4000	2298	3	0.192
10	5.80	7	180	0.6	180	6000	2298	2	0.192
11	5.80	7	143	0.6	1.4 Radius	6000	2298	2	0.192
12	5.80	7	130	0.6	130	4000	2298	3	0.192
13(Benchmark)		7	180			6000	2298	2	0.192
14(Benchmark)		7	143			6000	2298	2	0.192
15(Benchmark)		7	130			6000	2298	2	0.192

4.1.6. Experimental Setup

All the experiments were done on a Matsura FX-5, a 3-axis vertical milling center with a maximum spindle speed of 27000 RPM and a maximum spindle power of 10 hp.

The CNC machine was run by a FANUC series 15i-M controlling unit. A Photron FASTCAM SA-Z high-speed camera was used during the experiments to capture slow-motion videos of the exit burr formation for all tests. The camera was positioned at an angle to capture the exit burr formation inside the bore shaft, as shown in Figure 48.
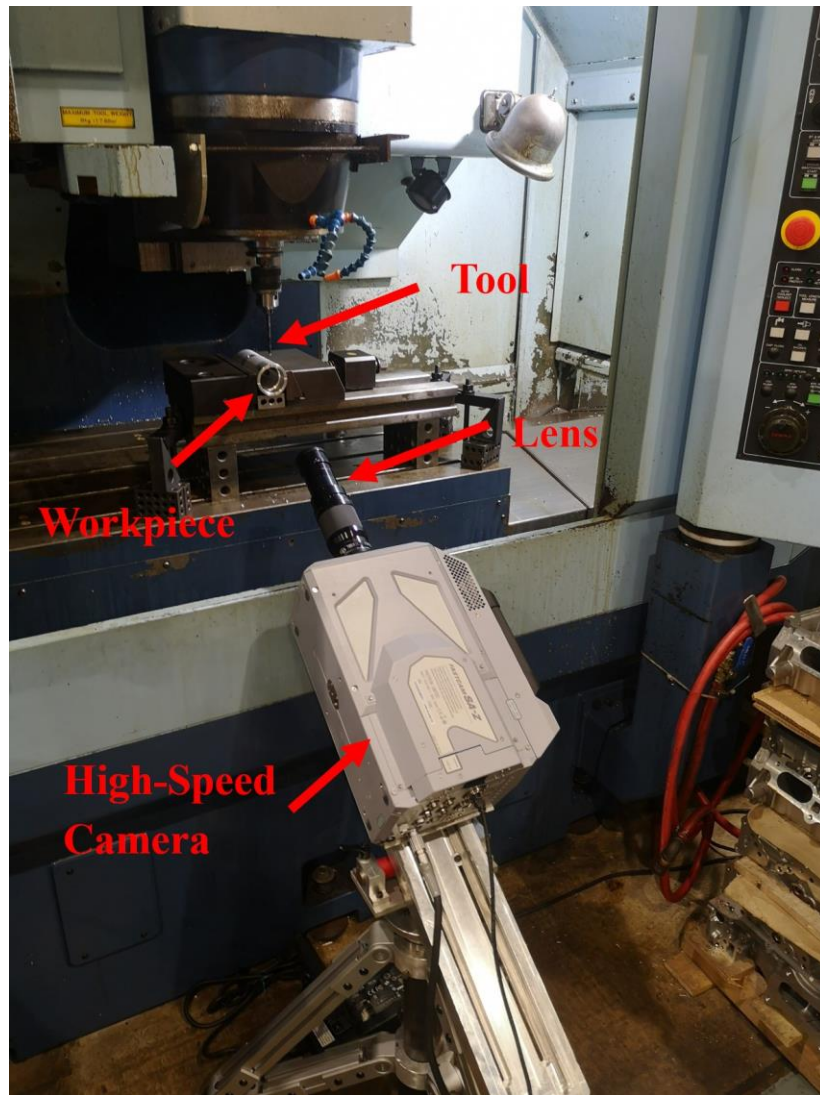
Figure 48: Experimental setup for drilling tests in a vertical CNC machine

4.2. Measurements

4.2.1. Burr size

Burr height measurements in this study were performed using an Alicona 3D optical microscope, as described in the burr size measurement description in section 3.2.3. Additionally, burr thickness was measured using 2D optical microscope (Keyence)

4.2.2. High-speed Camera:

The high-speed FASTCAM SA-Z camera can capture high-resolution digital images at an ultra-high speed up to 2 million frames per second and a shutter speed as short as 159 nanoseconds. A Model K1 CentriMax™ video microscope along with an MX-2 objective were used, as shown in Figure 49. The camera was connected to A Photron FASTCAM viewer software version .368 to control the camera as well as data saving and motion analysis. For all tests, the slow-motion videos of the exit burr formation were captured at a frame rate of 20,000 fps and a resolution of 1024*688 px.

Figure 49: High-speed camera

4.3. Results

4.3.1. Burr Height and Drill Cap

The graph in Figure 50 illustrates the measured burr height and the number of drilled caps observed out of three repetitions for each test. As seen in the chart, test # 5 showed the shortest burr height compared to all other tests and no drilled caps during all three trials. Test #5 was performed using two drills: drill #2, with a 6.4 mm diameter, and drill #7, which has a 1.4 mm corner radius. This combination made the step length equal to 0.3 mm and the step profile radius 1.4 mm.

	1	2	3	4	5	6	7	8	9	10	11	12	13	14	15
Mean	381.	416.	365.	429.	216.	496.	548.	591.	554.	638.	342.	723.	518.	493.	900
Drill caps observed	1	0	2	1	0	1	0	0	0	1	0	2	3	3	1
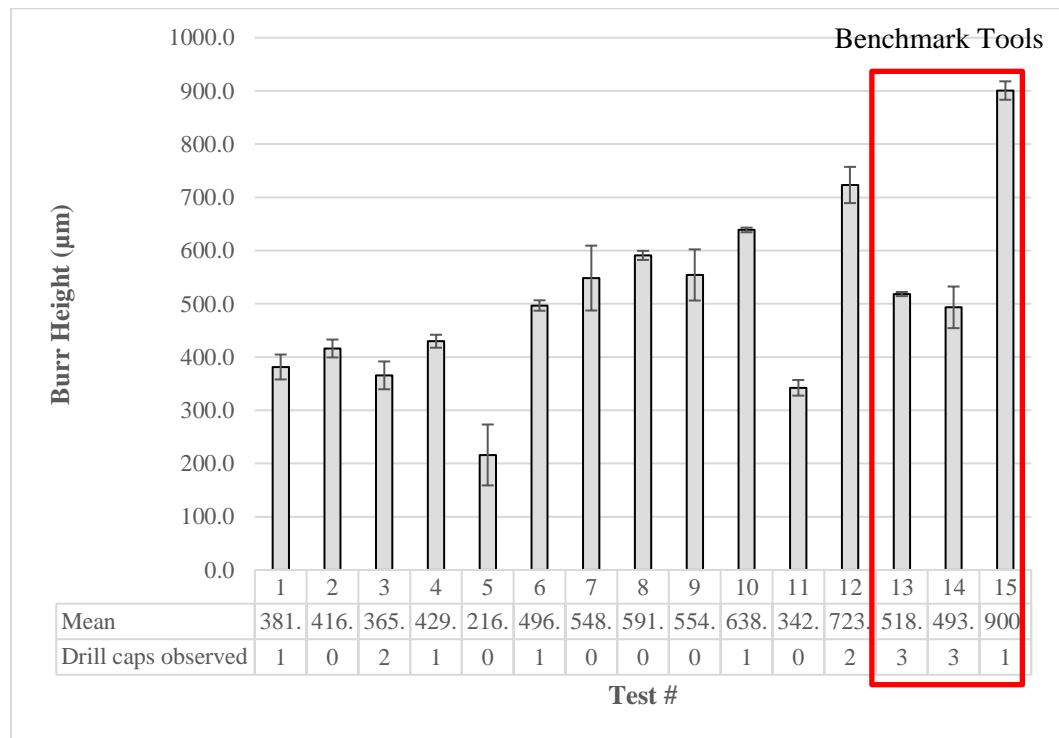
Figure 50:Burr size comparison and No. of observed caps for all tests

4.3.2. Influence of Step Size

Figure 51 shows the relationship between step size and burr height in addition to the number of drilled caps observed out of three repetitions. A trend can be observed from the chart that burr height increases in tandem with the step size when using a 180° step angle. The results revealed a 67% increase in burr height from step size 0.15 mm to 0.6 mm. The graph also showed no correlation between the number of drill caps observed and the step size.

	0.15	0.30	0.45	0.60
Mean	381.4	429.8	548.4	638.9
Drill cap observed	1	1	0	1
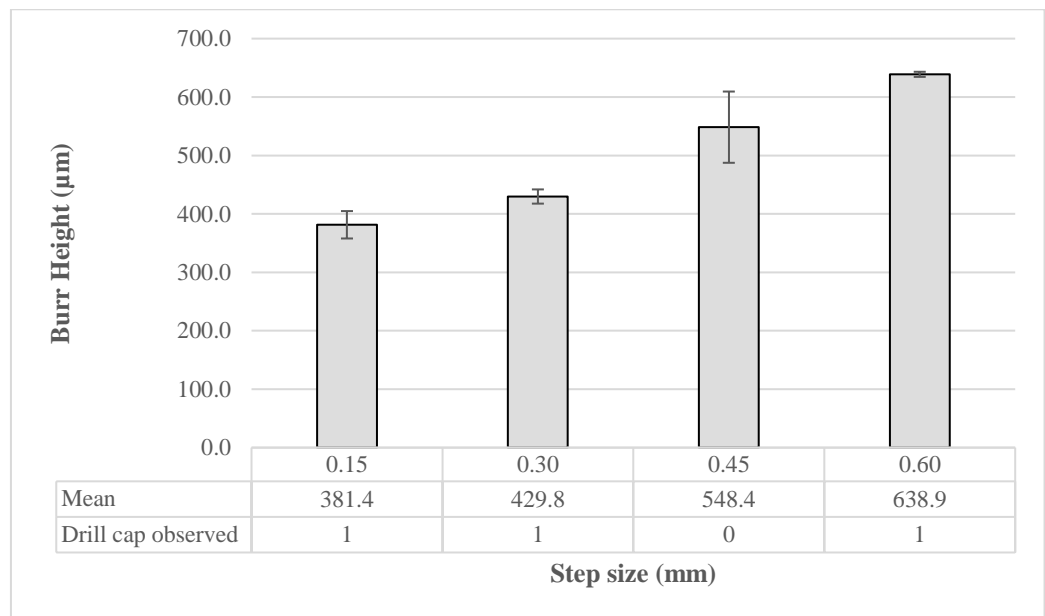
Figure 51: Burr height and No. of observed drill caps at different step sizes for 180° step angle

Burr formation images were extracted from the captured slow-motion videos at different step sizes when using a 180° step angle, as shown in Figure 52. It could be clearly seen that the burr height grew significantly as the step size increased.
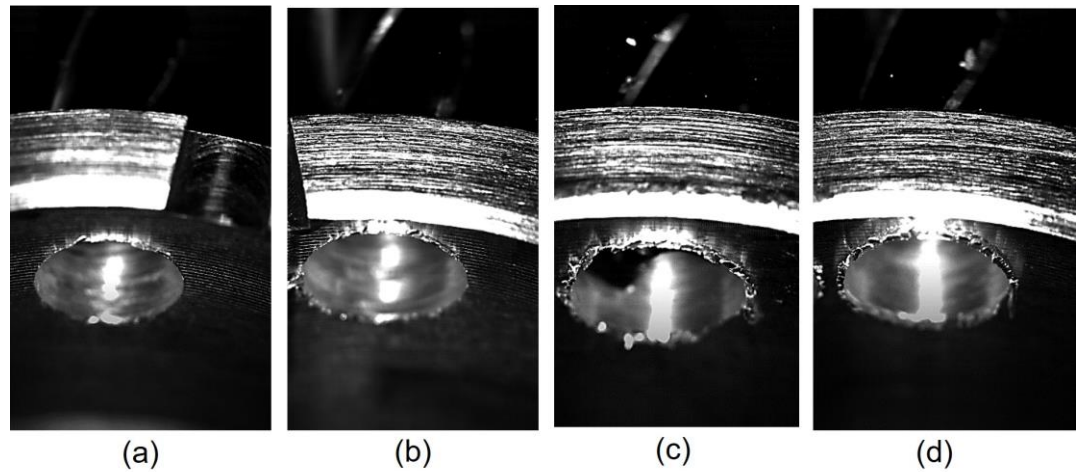
Figure 52: Exit burr images for different step sizes using 180° step angle, (a) 0.15 mm, (b) 0.3 mm, (c) 0.45 mm, and (d) 0.6 mm

Similar to the 180° step angle, it was noticed that increasing the step size when using a 130° step angle increases the burr height, as shown in Figure 53. Burr height grew by 83% when the step size increased from 0.15 mm to 0.6 mm. Besides that, the number of drill caps tended to change randomly with no relationship to the step size. Figure 54 compares the exit burr images for different step sizes when using a 130° step angle. The images show the same pattern of larger step sizes corresponding with taller burr heights.

	0.15	0.30	0.45	0.60
Mean	394.8	496.9	554.3	723.4
Drill cap observed	2	1	0	2

Step size (mm)

Figure 53:Burr height and No. of observed drill caps at different step sizes for 130° step angle
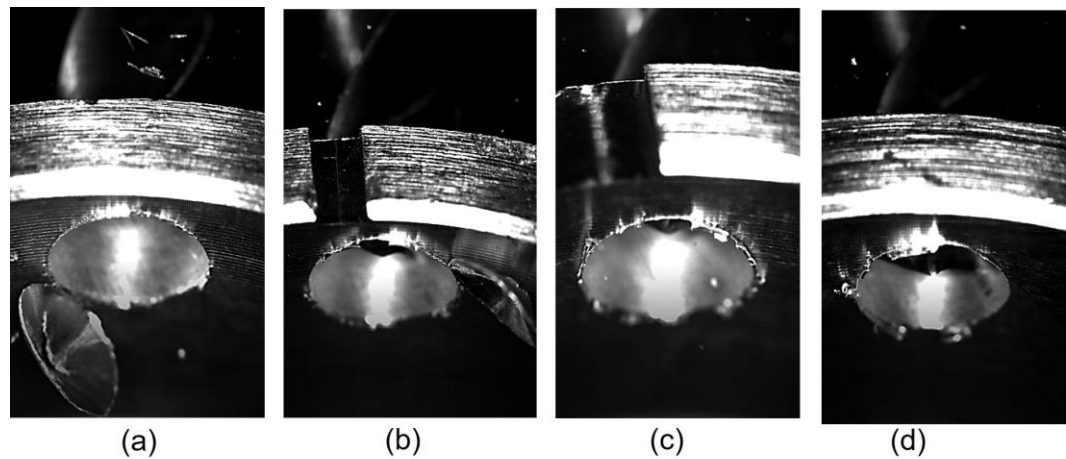
Figure 54: Exit burr images for different step sizes using 130° step angle, (a) at 0.15 mm, (b) 0.3 mm, (c) 0.45 mm, and (d) 0.6 mm

Unlike the linear correlation observed between burr height and step size in both 180° and 130° step angles, the R1.4 mm rounded step showed a nonlinear relation, as observed in Figure 55. The chart shows a minimum burr height of 216 microns at a 0.3

mm step size and a maximum burr height of 591 microns when a 0.45 mm step size was used. The chart also confirms that no drill caps were noticed at any of the step sizes tested during all the repetitions. Figure 56 compares the exit burr images at different step sizes side by side. As seen, the images show an irregular change in burr height when increasing the step size.

	0.15	0.30	0.45	0.60
Mean	416.1	216.1	591.0	342.3
Drill cap observed	0	0	0	0

Step size (mm)

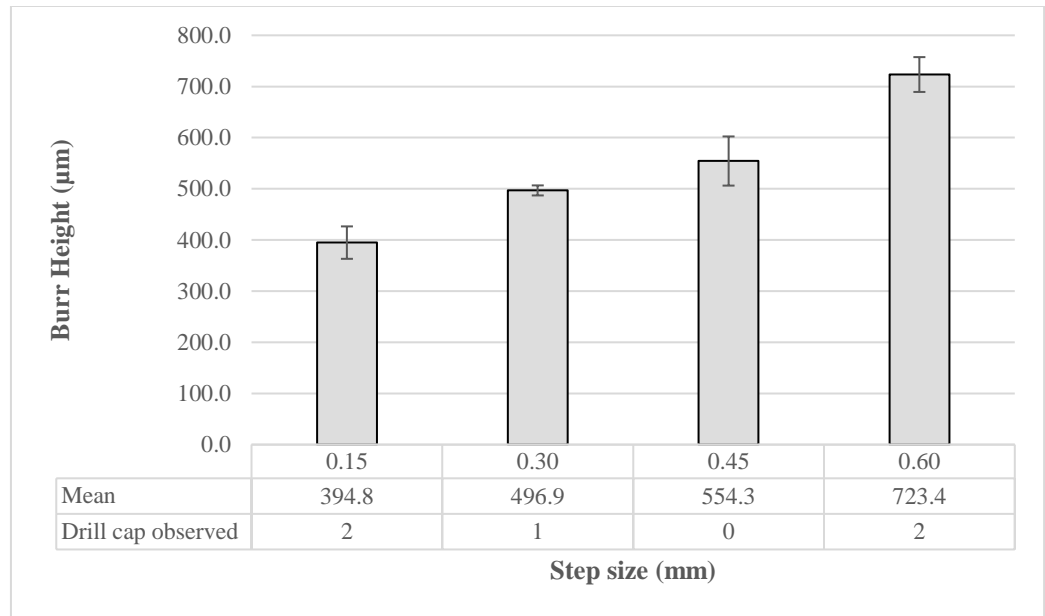**Figure 55: Burr height and No. of observed drill cap at different step sizes for the 1.4 mm radius step**
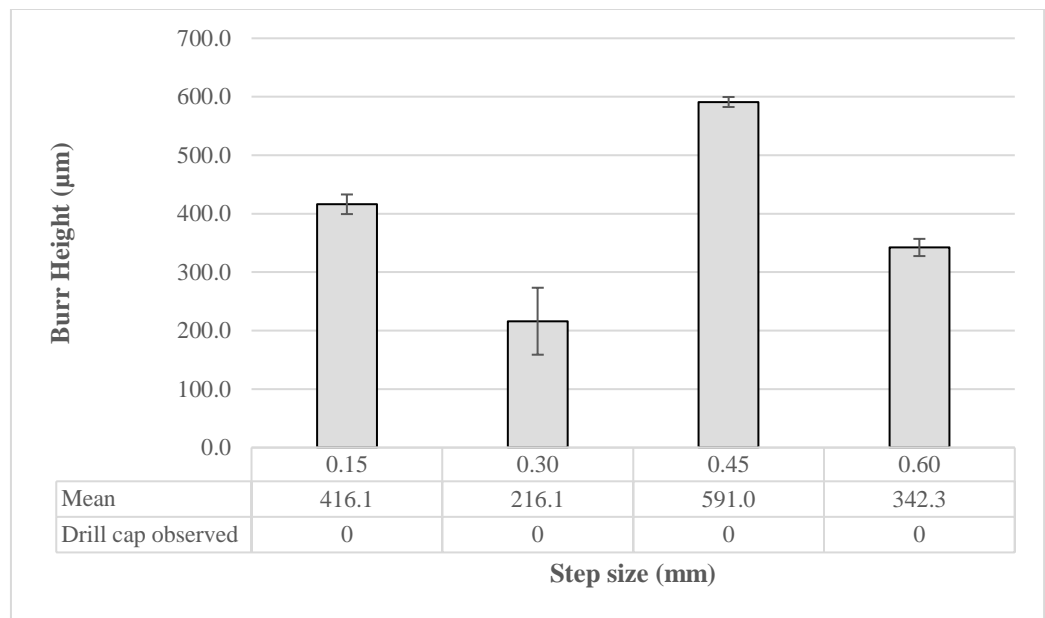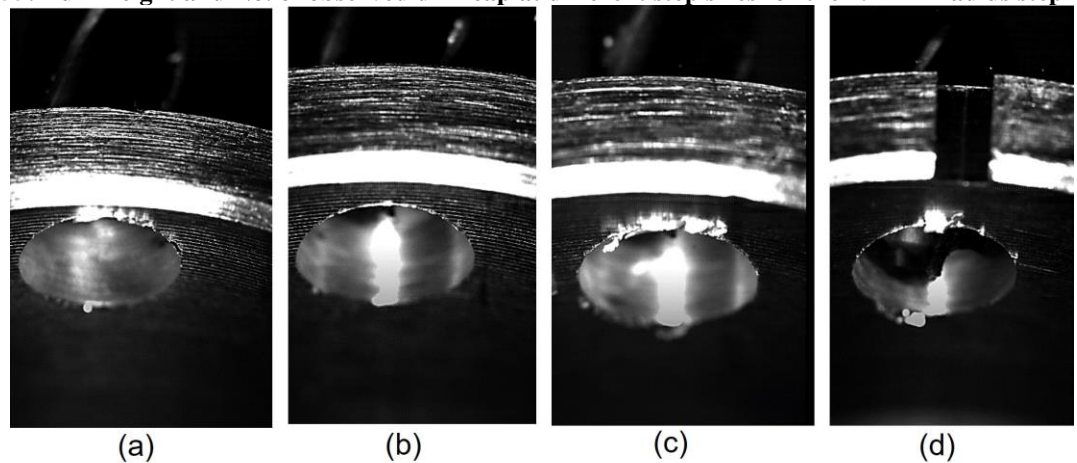

(a)　　　　(b)　　　　(c)　　　　(d)

Figure 56: Exit burr images for different step sizes using 1.4 mm rounded step, (a) at 0.15 mm, (b) 0.3 mm, (c) 0.45 mm, and (d) 0.6 mm

4.3.3. Influence of Step Profile:

The smaller step angle (130°) was found to produce relatively large burrs compared to the greater step angle (180°) in all step sizes. Figure 57 illustrates that the maximum burr height difference noticed was 13.5% at a step size of 0.6 mm. At step size 0.3 mm, the 1.4 mm radial step showed a large difference of 216.1 microns versus 496.9 and 429.8 microns in burr height for the 130° and 180° step angle profiles consecutively. Additionally, at step sizes 0.6 mm, the 1.4 mm radial drill produced a burr height of 342.3 microns compared to 723.4 microns for the 130° step angle and 638.9 microns for the 180° step angle. On the other hand, in step sizes 0.15 mm and 0.45 mm, no significant burr height differences between the three step profiles were observed.
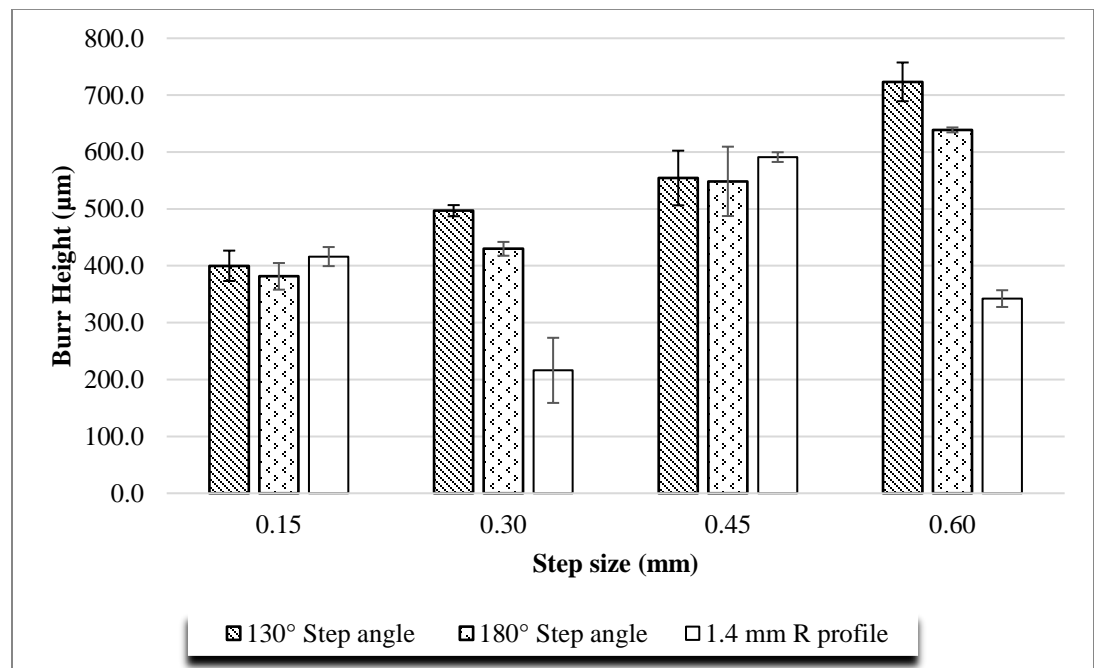

Figure 57: Burr height comparison with step size at different step profiles

4.3.4. Performance of the Step Drill

Based on the preliminary results from the previous tests that showed that test #5 had the shortest exit burr height compared to other tests, a step drill was designed to have a geometry similar to drill #2 and drill #7. The new step drill was tested, and Figure 58 illustrates the exit burr formation sequence while using the step drill.
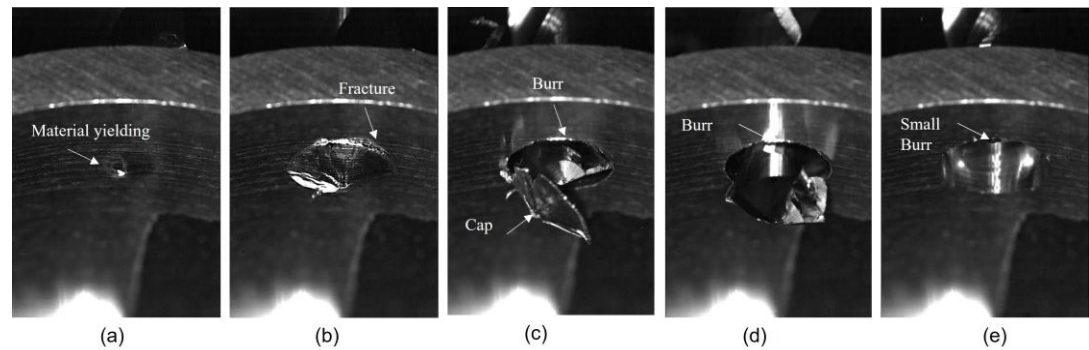
Figure 58: High-speed images of the step drill (a) burr initiation, (b) material plastic deformation and fracture, (c) burr and drilled cap, (d) step start cutting, (e) very small burr with no cap

The step drill successfully produced a very small exit burr with no observed cap during all the trials. It can be observed in the high-speed images in Figure 59 that the three tools used as a benchmark created larger burrs compared to the step drill. In order to further investigate the performance of the step drill, the burr height data of the step drill was plotted side by side with the values from the benchmark drills, as shown in Figure 60. As can be seen, the step drill produced a burr height of 58.7 microns, compared to 518.4 microns for drill #5, 493.5 microns for drill #7, and 900.8 microns for drill #6.
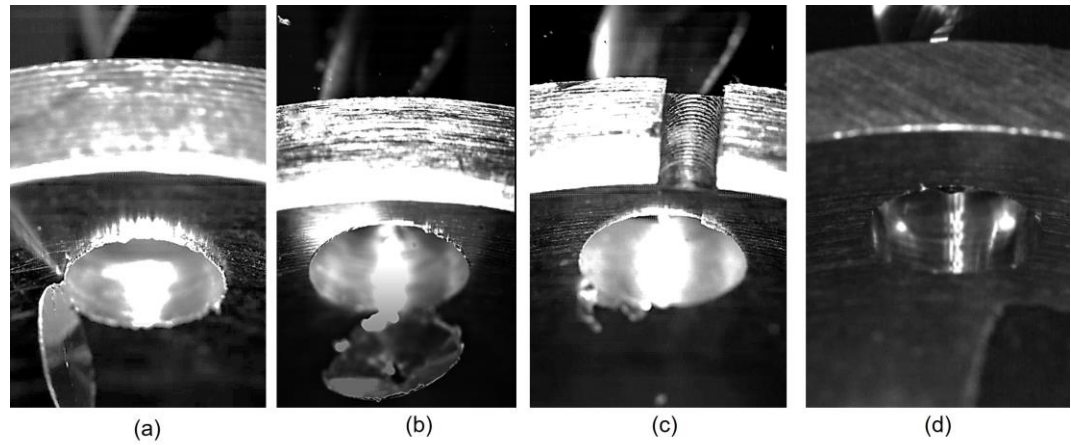
Figure 59: High-speed images of the exit burr, (a) drill #5 "benchmark", (b) drill #7 "benchmark", drill #6 "benchmark", (d) step drill

	Step drill	Drill #5	Drill #7	Drill #6
Mean	58.7	518.4	493.5	900.8
Cap observed	0	3	3	1
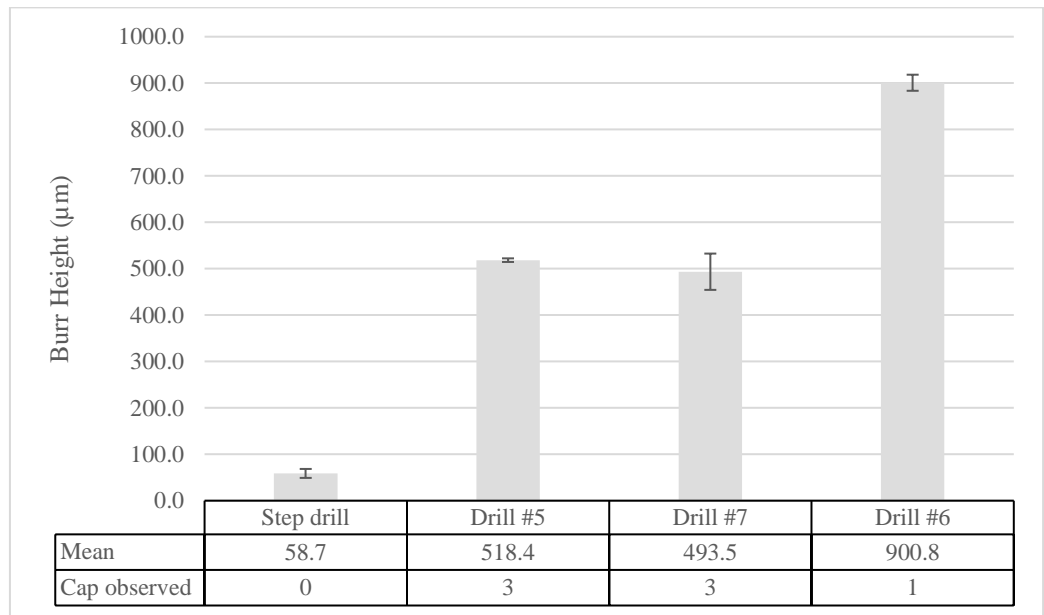
Figure 60: Burr height comparison between the step drill and the benchmark drills

4.4. Discussion

4.4.1. Influence of Step Size

When drilling with a step drill and the step starts to exit the hole, exit burrs could be described as a cantilever [48], as shown in Figure 61. The cantilever is supported from the workpiece end where it has its maximum thickness (h_0), and the thickness (h) varies as it tapers a constant gradient towards the hole center direction.
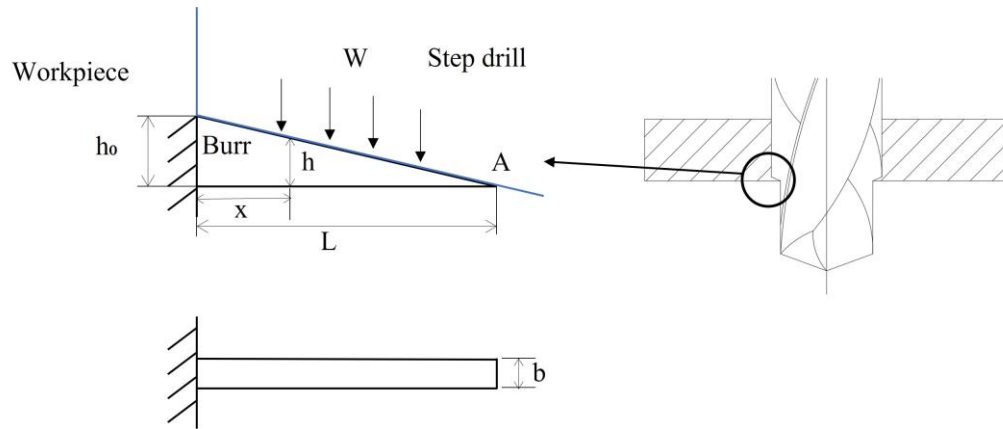
Figure 61: Burr explained as a cantilever under equiload W according to[48]**.**

As shown in Figure 61, when a uniform load W acts on this cantilever due to the thrust force, the deflection at point A when x=L could be calculated using Eq 6.

$$V_A = V_{x=L} = 6WL^4/Ebh_0{}^3 \qquad \text{Eq 6}$$

Where,

W = load acts on the cantilever

L = length of the cantilever

E = Modulus of Elasticity

b = width

h_o = maximum thickness

As described in the Results section, a linear correlation between burr height and step size was revealed for both the 180° and 130° step angles. The burr height increased in tandem with the step size. For the 180° step angle, the increase in burr height could be explained by increasing the step size, the length L in Eq 6 increases, resulting in a higher (L/h_o) ratio and higher deflection of the burr.

However, for the 130° step angle, increasing the step size will increases both L and h_o with the same ratio. Increasing the length L has more impact on the burr deflection than increasing the thickness h_o, according to Eq 6.

In the case of using a rounded corner step, as shown in Figure 62, the ratio L/h_o becomes smaller as the step proceeds to the hole exit, which causes lower deflection of the burr and, eventually, a smaller burr height.
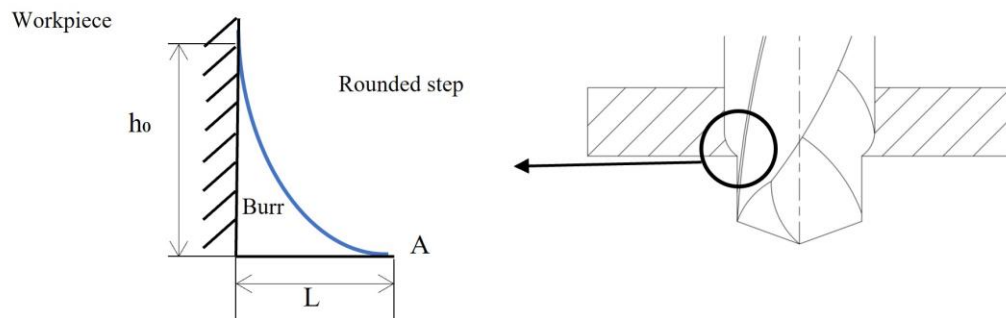
Figure 62: Burr explained as a cantilever in case of rounded step

However, minimizing the step size reduced the burr height, the burr thickness produced after drilling the first hole (D1) plays an important role in controlling the minimum step size. Step size needs to be larger than the burr thickness to completely cut the burr created from the first hole, as illustrated in Figure 63.
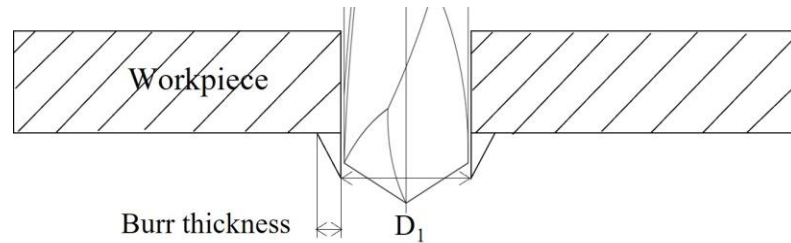
Figure 63: Burr thickness after the drilling the first hole

To determine the minimum step size, it was important to measure the burr thickness after drilling the first hole in each test. Figure 64 shows the measured burr thickness after drilling the first hole at different D_1 diameters. As seen, the burr thickness ranged between 175 microns to 204.9 microns for all the drill diameters. According to the burr thickness values, the step size needs to be larger than approximately 205 microns to completely remove the burr created after the first hole. This explains the reason why the 1.4 mm radial step profile with 0.15 mm step size produced burr height larger than 0.3 mm step size by approximately 92%. At 0.15 mm step size, the step was cutting inside the burr created from the first drill D_1, increasing the chances to plastically deform the burr out in the feed direction instead of steady cutting.
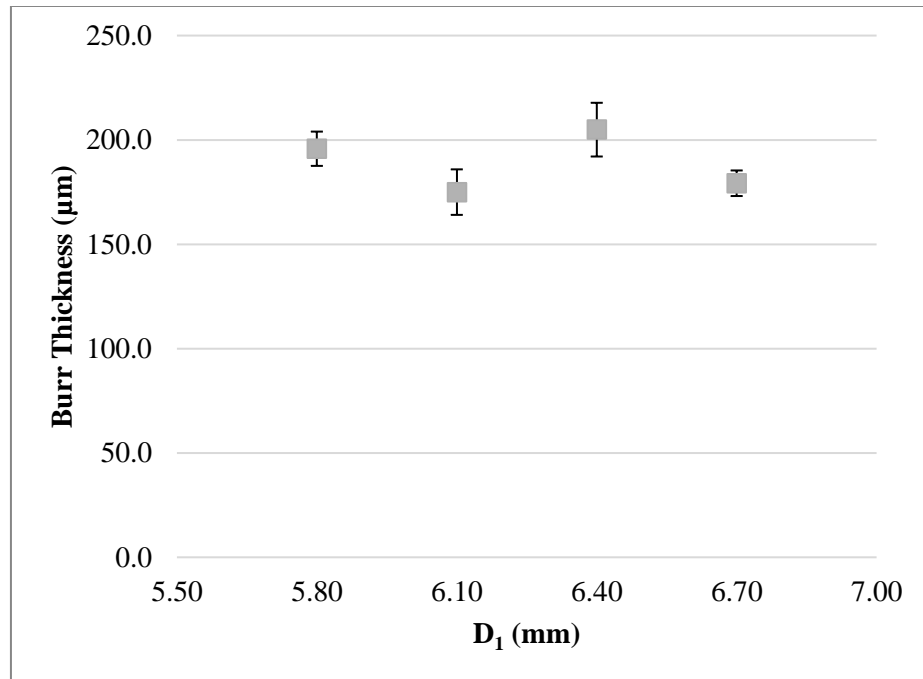
Figure 64: Burr thickness measurements after drilling the first hole at different D₁ diameters

4.4.2. Influence of Step Profile

In order to understand the effect of the step profile on the thrust force and burr height, an additional test was conducted using a table dynamometer to measure the thrust force. In this experiment, test #4, #5, and #6 was repeated to measure the thrust force for the $180°$ step profile, the $130°$ step profile, and the 1.4 mm radial step at a constant step size 0.3 mm. Figure 65 illustrates the measured thrust forces for the three step profiles. The force data was collected at the instant the step profile engages with material at the exit of the hole. As can be seen, the 1.4 mm R step profile generated the lowest thrust force with a mean value of 16.2 N compared to 27.19 N for the $180°$ step profile and 29.23 N for the $130°$ step profile. Thrust force was reported to have a relation with the burr height. The higher the thrust force, the larger the produced

burr[18]–[20]. The lower thrust force achieved by the 1.4 mm radial drill might be the reason for the lower burr height in comparison with the 180° step profile and the 130° step profile.
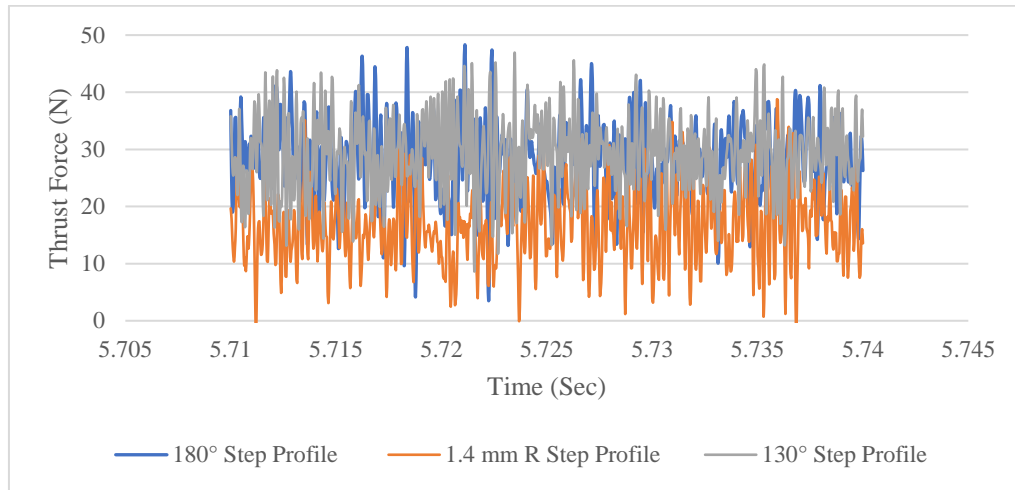
Figure 65: Thrust force measured at 0.3 mm step size for different step profiles

The lower thrust force generated by the 1.4 mm radial drill could be related to the forces distribution on the step profile. During the drilling operation, two major forces components are produced on the step edge, the cutting force F_c in the cutting direction, and the feed force F_q perpendicular on the cutting edge [9], as illustrated in Figure 66. The feed force could be analyzed into two components: F_r in a plan perpendicular on the drill axis and in the drill radius direction, and F_f in the drill feed direction. If the angle between the forces F_q and F_f is α, forces in the drill feed direction F_f can be calculated using the formula $F_f = F_q \cos\alpha$. In the case of the chamfer step profile, the angel α is constant along the chamfer edge, resulting in a constant force F_f on the step edge, as seen in Figure 66 (a). However, in the radial step profile, the forces F_f reduce

towards the final hole diameter as a function of increasing the angle α till it becomes almost zero at α= 90°.
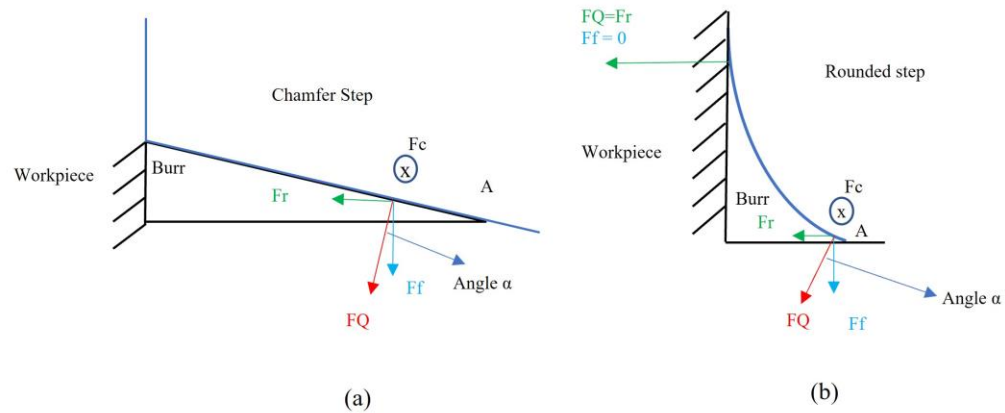
Figure 66: Cutting force components on (a) chamfer step, (b) radial step

4.4.3. Step Drill

Testing the step drill showed a significantly small burr height of 58.7 microns compared to 216.1 microns from test #5, approximately 73% lower burr height. To better understand the reasons behind the outperformance of the step drill, which exceeded the expectations from test #5, thrust forces were measured for both test #5 and the step drill, as shown in Figure 67. The step drill showed approximately 33 % lower thrust force with a mean value of 541.5 N compared to 807.7 N for test #5. To better understand the reason for the lower thrust force of the step drill, the two drills used in test #5 as well as the step drill were scanned using Alicona 3D optical microscope to identify the main geometry differences. Edge radius ($r_β$) at the front cutting lips and the step profile were measured for both cases. As seen in Figure 68, the step drill has a sharper edge radius compared to the tools used in test #5. On the front

cutting lips, the edge radius for the step drill was 12.1 microns compared to 48.6 microns for drill #2, which was used to drill the first hole in test #5. Similarly, on the step profile, the step drill has an edge radius of 7.8 microns compared to 41.4 microns for drill #7. Increasing the drill edge radius was related to an increase in the thrust force [49], resulting in a larger burr height
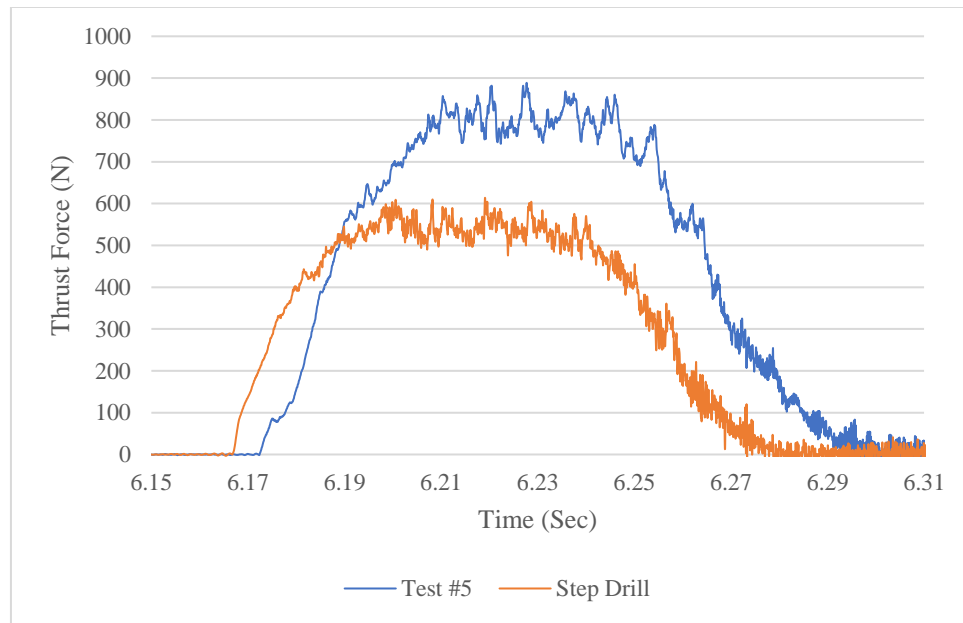
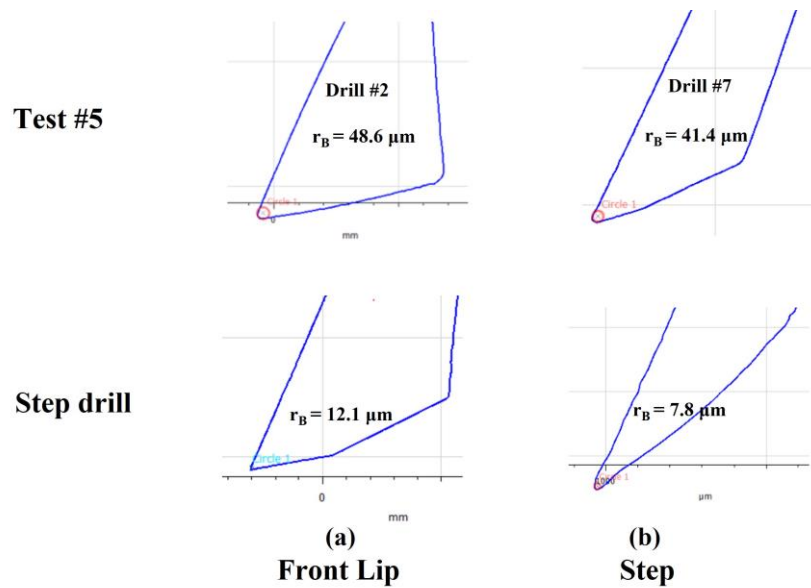**Figure 67: Thrust force comparison between test #5 and the step drill**

Figure 68: Drill edge radius measurements comparison between test #5 and the step drill (a) on the cutting lip, (b) on the step

4.5. Conclusions

A new approach for designing and testing application-based step drills was investigated. The study mainly focused on optimizing the two major parameters in step drill design, the step length (ℓ) and the step profile to minimize the drill exit burr height and produce high-quality holes with no caps. The experimental work included using two off-the-shelf drills to simulate the cutting action of a step drill. The first drill had different diameters (D_1) to simulate the change in step sizes. The second drill had the same final diameter (D_2) but with different point angles and corner shapes to mimic the change in the step profile. An industrial partner provided automotive parts to use as a workpiece and test the approach. The initial results revealed that a combination of a 0.3 mm step size and a rounded step with a 1.4 mm radius produced the minimum burr height, about 56% less compared to the benchmark with no drilled cap observed. Based

on the preliminary results, a step drill was designed to have the optimum step size and geometry. The step drill was tested, and the results showed an excellent performance and ability to reduce the burr height by 88% compared to the best benchmark drill with no drilled cap.

Chapter 5. Conclusions and Future work

5.1 Conclusions

5.1.1. Approach 1-Burr Control Using Pressurized Materials

The research conducted in this study focused on introducing a new technique for exit burr control and drill cap elimination into the drilling of ductile materials. The study examined the efficacy of injecting different materials underneath the hole exit at high pressures. Aluminum 6061-T6 flats were used as workpieces. A summary of major findings and conclusions drawn from this study is given below.

1. A special design was developed for injecting high-pressure coolant at the hole exit. Injecting a semi-synthetic coolant with 8-10% concentration had no effect on burr height compared to the benchmark.

2. The design was modified to deliver materials in the form of paste. The first material tested was a commercial anti-seize that was injected at a pressure of 7000 psi. The results showed an approximately 54% reduction in burr height, and no drill cap was observed. Despite the significant improvement in burr height, using anti-seize inside a CNC machine is not preferred because it can affect the machine and cause failures.

3. A new injecting material was developed to have similar results to the anti-seize and avoid its drawbacks. The material was an aluminum paste that had a mixture of aluminum micro powder and liquid machining coolant concentrate. Testing this material at a pressure of 7000 psi showed severe leakage at different locations.

4. A unique aluminum paste was developed especially for this study to avoid leakage at high pressures. The material was a mixture of aluminum microparticles and a high viscosity coolant concentrate. The mixture showed an excellent ability to generate a supporting load under the high injecting pressure without any leakage noticed.

5. Aluminum pastes with different aluminum powder to coolant ratios were tested to identify the minimum Al powder content needed to reduce the burr height the most. The aluminum paste with 20% Al content showed no difference in burr height compared to the benchmark. The aluminum paste containing 40% aluminum powder showed a burr reduction of 57% compared to the benchmark. By increasing the aluminum content in the mixture by more than 40%, no further burr height reduction was noticed.

6. Another set of experiments were conducted using aluminum paste with 40% Al powder and 60% high viscosity coolant at different injecting pressures. The minimum burr height achieved 202.6 microns at a pressure of 7000 psi. The burr height increased with reducing the injecting pressure to be 239.3 microns at a pressure of 4000 psi. Reducing the pressure to 3000 psi led to a significant increase in burr height to be 529.6.

7. Thrust forces were measured for all the experiments. As a result of using the same drill geometry and cutting conditions during all the tests, the force values were similar for all the tests at about 431N.

8. Forces under the hole exit were calculated using different pressure values, and the minimum effective force was found to be 1061 N.

9. The ratios between injecting forces acting under the drilled hole and thrust forces were also calculated. The minimum effective ratio to reduce the burr height was found to be approximately two and a half times the thrust force value.

To summarize, this study introduced a new effective technique for burr control. The research included developing a new setup to perform experiments, testing different injecting materials, developing a new injecting material, and studying the effect of injecting pressure on burr height.

5.1.2. Approach 2-Burr Control Using Step Drills

This research presented a new approach for designing highly effective step drills for a specific application. The study focused on two significant parameters in designing step drills: the step size and the step profile. The new technique involved using two off-the-shelf drills to drill one hole to simulate the cutting action of the step drill. The first drill's diameter acts as the small front diameter of the step drill (D_1). The second drill's diameter represents the final diameter of the step drill (D_2). The point angle and lip corner shape mimic the step profile. Various drills were tested to study different combinations of step sizes and step angles. Additionally, one drill with rounded corners was tested to analyze the performance of rounded step geometry. Finally, a step drill

was designed and tested according to the preliminary results. Based on the results, the following conclusions can be drawn.

1. Step size was found to have a significant impact on burr height. For both step angles, 180° and 130°, increasing the step size led to a larger burr height.

2. For the 1.4 mm rounded step, no apparent relationship was noticed between changing the step size and the burr height.

3. An increase in burr height was observed by reducing the step angle from 180° to 130°.

4. The minimum burr height was found by using the rounded step with a 1.4 mm radius and a step size of 0.3 mm. This combination successfully reduced the burr height by 56% compared to the benchmark with no cap observed.

5. The step drill was designed to have the optimum step size and shape found in the preliminary results. The step drill was tested, and the results showed a remarkable reduction in burr height of 88%.

To sum up, a new approach was developed for designing application-based step drills. The study included testing off-the-shelf drills to simulate various step lengths and step profiles on an automotive part. After testing, the optimum parameters were selected to design a step drill. The step drill was tested and showed excellent performance for controlling burr height and drilling cap.

5.2 Future Work

5.2.1. Approach 1-Burr Control Using Pressurized Materials

According to the major findings and challenges associated with this study, some recommendations for future work are provided as follows:

1. To understand the mechanism behind burr minimization better, injecting pressure changes over the course of the drilling operation need to be measured. A pressure sensor with a high measurement range, more than 7000 psi should be used.

2. The phases of burr formation need to be studied by enabling the feed to stop at different points during the burr formation, then cross sectioning the samples to see a better view of the burr mechanism.

3. Applying a continuous injecting material at a steady high-pressure needs to be studied as it could further reduce burr formation.

4. Developing other injecting materials that better support loads without deforming could further reduce burr height.

5. A progressive tool wear study needs to be conducted to understand the effect of using this technique on tool wear.

5.2.2. Approach 2-Burr Control Using Step Drills

1. A progressive study of the tool wear using the step drill needs to be conducted to understand the main wear mechanisms and the maximum tool life.

2. The effect of the tool wear on the exit burr height needs to be studied throughout the step drill's life to understand the progression of the burr height over time and identify the point when the tool should be changed based on the maximum acceptable burr height in the process.

3. Study the impact of microstructure changes due to cutting conditions on burr formation. Of particular note is the material that the second step drill engages with after the first step of the drill has past.

References

[1]   J. P. Davim, *Modern Machining Technology, A practical guide*. Woodhead Publishing Limited, Cambridge, UK, 2011.

[2]   D. Dornfeld and S. Min, "A Review of Burr Formation in Machining," *Burrs - Anal. Control Removal, Heidelberg, Ger. Springer*, pp. 3–11, 2010.

[3]   S. Kalpakjian and S. R. Schmid, *Manufacturing engineering and technology*, 6th edtion. USA: Prentice Hall, 2009.

[4]   M. Groover, *Fundementals of Modern Manufacturing Materials,Processes and Systems*, 4th Editio. USA: John Wiley & Sons, 2010.

[5]   H. K. Toenshoff and B. Denkena, *Basics of cutting and abrasive processes*. Springer-Verlag Berlin Heidelberg, 2013.

[6]   *DIN 1412: Twist drills made of high-speed steel—Shapes of points.* Berlin: German Institute for Standardization, 2001.

[7]   D. A. Stephenson and A. J. S., *Metal Cutting Theory and Practice*, 3rd Editio. USA: CRC Press, 2016.

[8]   M. Aamir, K. Giasin, M. Tolouei-Rad, and A. Vafadar, "A review: drilling performance and hole quality of aluminium alloys for aerospace applications," *J. Mater. Res. Technol.*, vol. 9, no. 6, pp. 12484–12500, 2020, doi: 10.1016/j.jmrt.2020.09.003.

[9]   P. Koshy, "Manufacturing Processes I , Lecture Notes," McMaster University, Hamilton, ON, Canada, 2021.

[10]   Ş. Yazman, U. Köklü, L. Urtekin, S. Morkavuk, and L. Gemi, "Experimental study

on the effects of cold chamber die casting parameters on high-speed drilling machinability of casted AZ91 alloy," *J. Manuf. Process.*, vol. 57, no. June, pp. 136–152, 2020, doi: 10.1016/j.jmapro.2020.05.050.

[11] J. C. Aurich, D. Dornfeld, P. J. Arrazola, V. Franke, L. Leitz, and S. Min, "Burrs-Analysis, control and removal," *CIRP Ann. - Manuf. Technol.*, vol. 58, no. 2, pp. 519–542, 2009, doi: 10.1016/j.cirp.2009.09.004.

[12] L. K. Gillespie and P. T. Blotter, "The formation and properties of machining burrs," *J. Manuf. Sci. Eng. Trans. ASME*, vol. 98, no. 1, pp. 66–74, 1976, doi: 10.1115/1.3438875.

[13] L. K. Gillespie, *Deburring and Edge Finishing Handbook*, 1st editio. Dearborn,Michigan, USA:Society of Manufacturing Engineers, 1999.

[14] X. Pang, J. Zhang, X. Yin, B. Zhang, and W. Deng, "Analytical and experimental investigation of improved burr morphology prediction at the top edge in metal machining," *Int. J. Adv. Manuf. Technol.*, vol. 108, no. 5–6, pp. 1343–1355, 2020, doi: 10.1007/s00170-020-05418-3.

[15] J. Kim, S. Min, and D. A. Dornfeld, "Optimization and control of drilling burr formation of AISI 304L and AISI 4118 based on drilling burr control charts," *Int. J. Mach. Tools Manuf.*, vol. 41, no. 7, pp. 923–936, 2001, doi: 10.1016/S0890-6955(00)00131-0.

[16] J. Kim and D. A. Dornfeld, "Development of an analytical model for drilling burr formation in ductile materials," *J. Eng. Mater. Technol. Trans. ASME*, vol. 124, no. 2, pp. 192–198, 2002, doi: 10.1115/1.1429937.

[17] M. Hashimura, Y. P. Chang, and D. Dornfeld, "Analysis of burr formation mechanism in orthogonal cutting," *J. Manuf. Sci. Eng. Trans. ASME*, vol. 121, no. 1, pp. 1–7, 1999, doi: 10.1115/1.2830569.

[18] S. S. Pande and H. P. Relekar, "Investigations on reducing burr formation in drilling," *Int. J. Mach. Tool Des. Res.*, vol. 26, no. 3, pp. 339–348, 1986, doi: 10.1016/0020-7357(86)90010-7.

[19] A. M. Abdelhafeez, S. L. Soo, D. K. Aspinwall, A. Dowson, and D. Arnold, "Burr formation and hole quality when drilling titanium and aluminium alloys," *Procedia CIRP*, vol. 37, pp. 230–235, 2015, doi: 10.1016/j.procir.2015.08.019.

[20] J. M. Stein and D. A. Dornfeld, "Burr formation in drilling miniature holes," *CIRP Ann. - Manuf. Technol.*, vol. 46, no. 1, pp. 63–66, 1997, doi: 10.1016/s0007-8506(07)60776-8.

[21] E. S. Costa, M. B. Da Silva, and A. R. Machado, "Burr produced on the drilling process as a function of tool wear and lubricant-coolant conditions," *J. Brazilian Soc. Mech. Sci. Eng.*, vol. 31, no. 1, pp. 57–63, 2009, doi: 10.1590/S1678-58782009000100009.

[22] D. Biermann and H. Hartmann, "Reduction of burr formation in drilling using cryogenic process cooling," *Procedia CIRP*, vol. 3, no. 1, pp. 85–90, 2012, doi: 10.1016/j.procir.2012.07.016.

[23] L. K. Gillespie, R. K. Albright, and B. J. Neal, "Effects of drilling variables on burr properties," *Bendix Kansas City:BDX-613-1502*, no. September, 1976.

[24] R. Neugebauer, G. Schmidt, and M. Dix, "Size Effects in Drilling Burr

Formation," *Burrs - Anal. Control Removal, Heidelberg, Ger. Springer*, pp. 117–127, 2010, doi: 10.1007/978-3-642-00568-8.

[25] A. Rivero, G. Aramendi, S. Herranz, and L. N. L. De Lacalle, "An experimental investigation of the effect of coatings and cutting parameters on the dry drilling performance of aluminium alloys," *Int. J. Adv. Manuf. Technol.*, vol. 28, no. 1–2, pp. 1–11, 2006, doi: 10.1007/s00170-004-2349-3.

[26] M. F. Huang and T. R. Lin, "Application of grey - Taguchi method to optimise drilling of aluminium alloy 6061 with multiple performance characteristics," *Mater. Sci. Technol.*, vol. 20, no. 4, pp. 528–532, 2004, doi: 10.1179/026708304225012369.

[27] I. Park, "Modeling of Burr Formation Processes in Metal Cutting, PhD Thesis," University of California at Berkeley, 1996.

[28] S. Min, D. A. Dornfeld, and Y. Nakao, "Influence of exit surface angle on drilling burr formation," *J. Manuf. Sci. Eng. Trans. ASME*, vol. 125, no. 4, pp. 637–644, 2003, doi: 10.1115/1.1596573.

[29] E. Bahçe and B. Özdemir, "Investigation of the burr formation during the drilling of free-form surfaces in al 7075 alloy," *J. Mater. Res. Technol.*, vol. 8, no. 5, pp. 4198–4208, 2019, doi: 10.1016/j.jmrt.2019.07.028.

[30] J. C. Aurich, H. Sudermann, and H. Bil, "Characterisation of burr formation in grinding and prospects for modelling," *CIRP Ann. - Manuf. Technol.*, vol. 54, no. 1, pp. 313–316, 2005, doi: 10.1016/S0007-8506(07)60111-5.

[31] V. Franke, L. Leitz, and J. C. Aurich, "Burr Measurement: A Round Robin Test

Comparing Different Methods," *Burrs - Anal. Control Removal, Heidelberg, Ger. Springer*, no. 2010, pp. 167–178.

[32]   A. Kienzler, M. Deuchert, and V. Schulze, "Burr Minimization and Removal by MicroMilling Strategies or Micro Peening Processes," *Burrs - Anal. Control Remov.*, pp. 237–243, 2010, doi: 10.1007/978-3-642-00568-8.

[33]   L. Leitz, V. Franke, and J. C. Aurich, "Burr Formation in Drilling Intersecting Holes," *Burrs - Anal. Control Removal, Heidelberg, Ger. Springer*, pp. 99–105, 2021.

[34]   D. Biermann and M. Heilmann, "Burr Minimization Strategies in Machining Operations," *Burrs - Anal. Control Removal, Heidelberg, Ger. Springer*, pp. 13–20, 2010.

[35]   E. Whinnem, G. Lipczynski, and I. Eriksson, "Development of orbital drilling for the Boeing 787," *SAE Int. J. Aerosp.*, vol. 1, no. 1, pp. 811–816, 2009, doi: 10.4271/2008-01-2317.

[36]   E. Brinksmeier and S. Fangmann, "Burr and cap formation by orbital drilling of aluminum," *Burrs - Anal. Control Removal, Heidelberg, Ger. Springer*, pp. 31–45, 2010.

[37]   S. Kundu, S. Das, and P. P. Saha, "Optimization of drilling parameters to minimize burr by providing back-up support on aluminium alloy," *Procedia Eng.*, vol. 97, pp. 230–240, 2014, doi: 10.1016/j.proeng.2014.12.246.

[38]   S. N. Melkote, T. R. Newton, C. Hellstern, J. B. Morehouse, and S. Turner, "Interfacial Burr Formation in Drilling of Stacked Aerospace Materials," *Burrs -

Anal. Control Removal, Heidelberg, Ger. Springer, pp. 89–98, 2010.

[39] W. Tian, J. Hu, W. Liao, Y. Bu, and L. Zhang, "Formation of interlayer gap and control of interlayer burr in dry drilling of stacked aluminum alloy plates," *Chinese J. Aeronaut.*, vol. 29, no. 1, pp. 283–291, 2016, doi: 10.1016/j.cja.2015.11.002.

[40] H. Takeyama and S. Kato, "Burrless Drilling by Means of Ultrasonic Vibration," *CIRP Ann. - Manuf. Technol.*, vol. 40, no. 1, pp. 83–86, 1991, doi: 10.1016/S0007-8506(07)61939-8.

[41] S. S. F. Chang and G. M. Bone, "Burr size reduction in drilling by ultrasonic assistance," *Robot. Comput. Integr. Manuf.*, vol. 21, no. 4–5, pp. 442–450, 2005, doi: 10.1016/j.rcim.2004.11.005.

[42] ASTM, "Standard Specification for Aluminum-Alloy 6061-T6 Standard Structural Profiles 1," *Standard*, vol. 03, no. C, pp. 1–6, 2010, doi: 10.1520/B0308.

[43] J. R. Davis and Committee, *ASM Specialty Handbook: Aluminum and Aluminum Alloys*. ASM International, 1993.

[44] Kistler, "Dynamometer Type 9255B Data Sheet, Document # 9255C_003-051e-07.18," 2012.

[45] *International Standard ISO 13715:2000, Technical drawings – Edges of undefined shape – Vocabulary and indications*. .

[46] S. L. Ko, J. E. Chang, and G. E. Yang, "Burr minimizing scheme in drilling," *J. Mater. Process. Technol.*, vol. 140, no. 1-3 SPEC., pp. 237–242, 2003, doi: 10.1016/S0924-0136(03)00719-2.

[47] R. S. Xia and S. M. Mahdavian, "Experimental studies of step drills and

establishment of empirical equations for the drilling process," *Int. J. Mach. Tools Manuf.*, vol. 45, no. 2, pp. 235–240, 2005, doi: 10.1016/j.ijmachtools.2004.07.002.

[48] H. Wada and K. Yoshida, "Burrless drilling of metals," *JSPE*, vol. 66, no. 7, pp. 1109–1114, 2000, doi: 10.2493/jjspe.66.1109.

[49] B. Luo, K. Zhang, Y. Li, H. Cheng, and S. Liu, "Modelling of thrust force for worn drill bits characterised by cutting edge radius in drilling carbon fibre–reinforced plastic/Ti-6Al-4V alloy stacks," *Proc. Inst. Mech. Eng. Part B J. Eng. Manuf.*, vol. 232, no. 11, pp. 1960–1972, 2018, doi: 10.1177/0954405416682791.

Appendix A: Burr formation images for approach 2
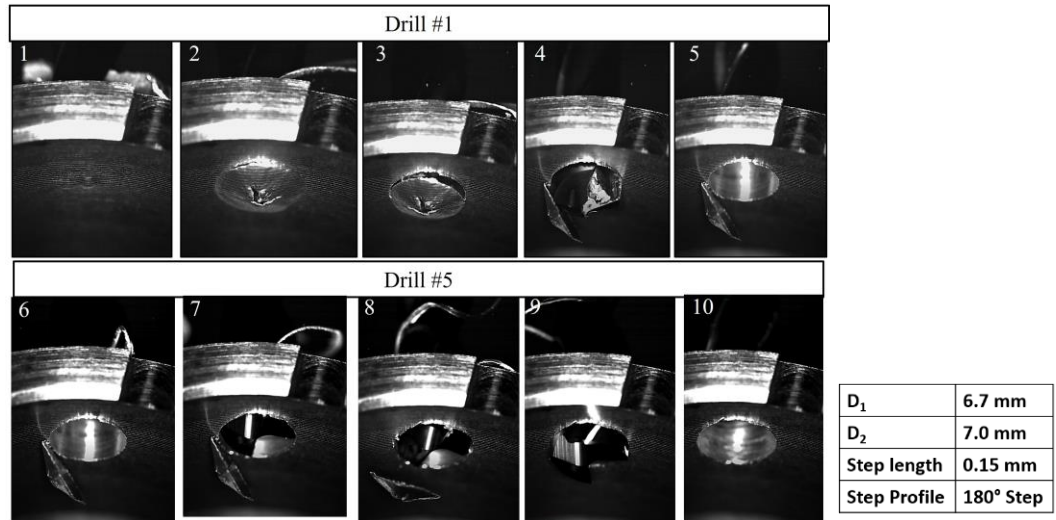
Figure 69: High-speed video images of the burr formation for test #1.
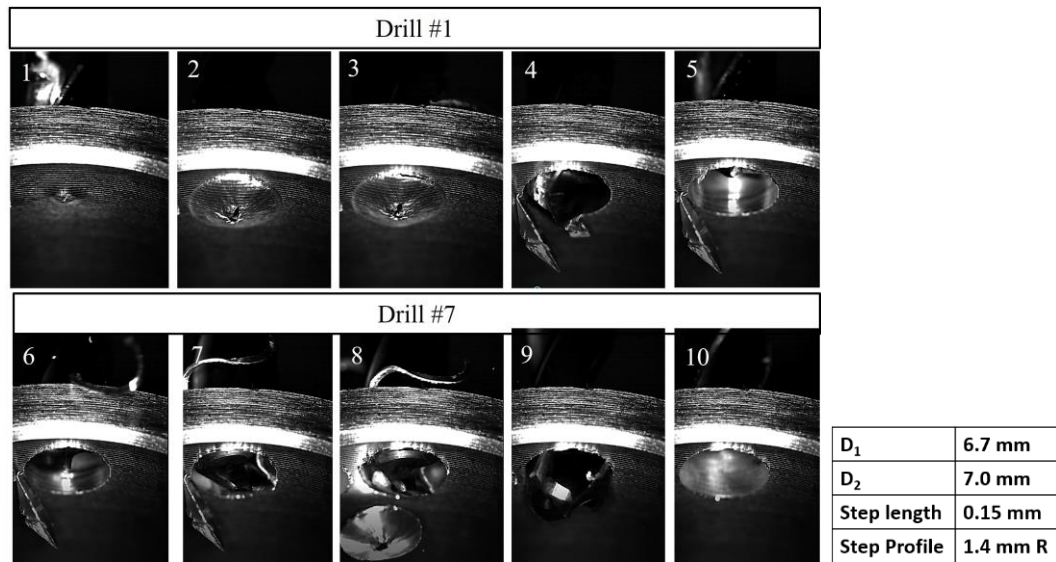
Figure 70 High-speed video images of the burr formation for test #2
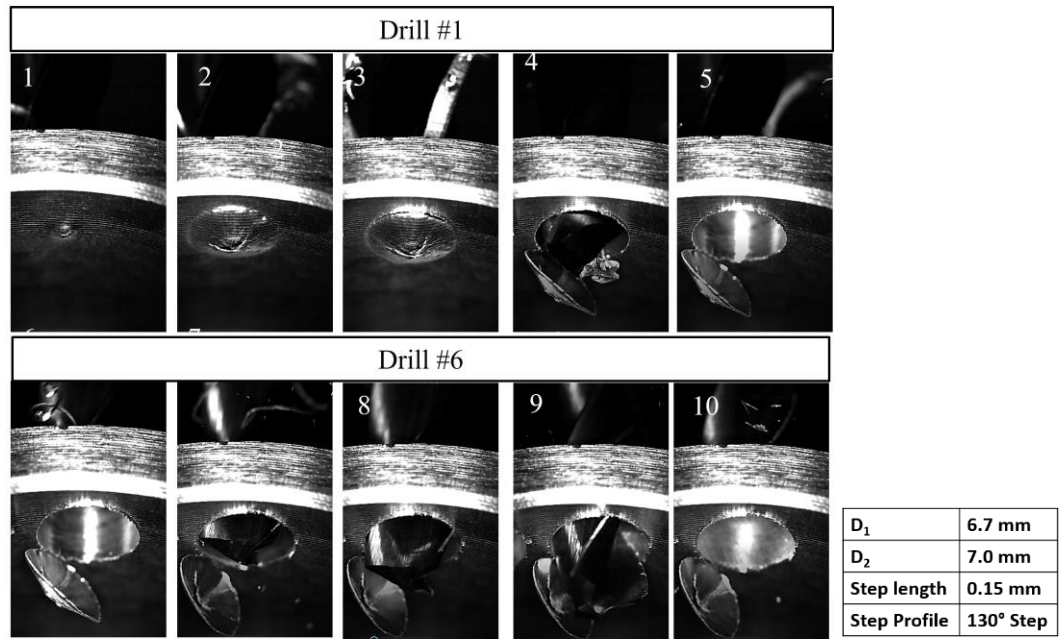
Figure 71: High-speed video images of the burr formation for test #3
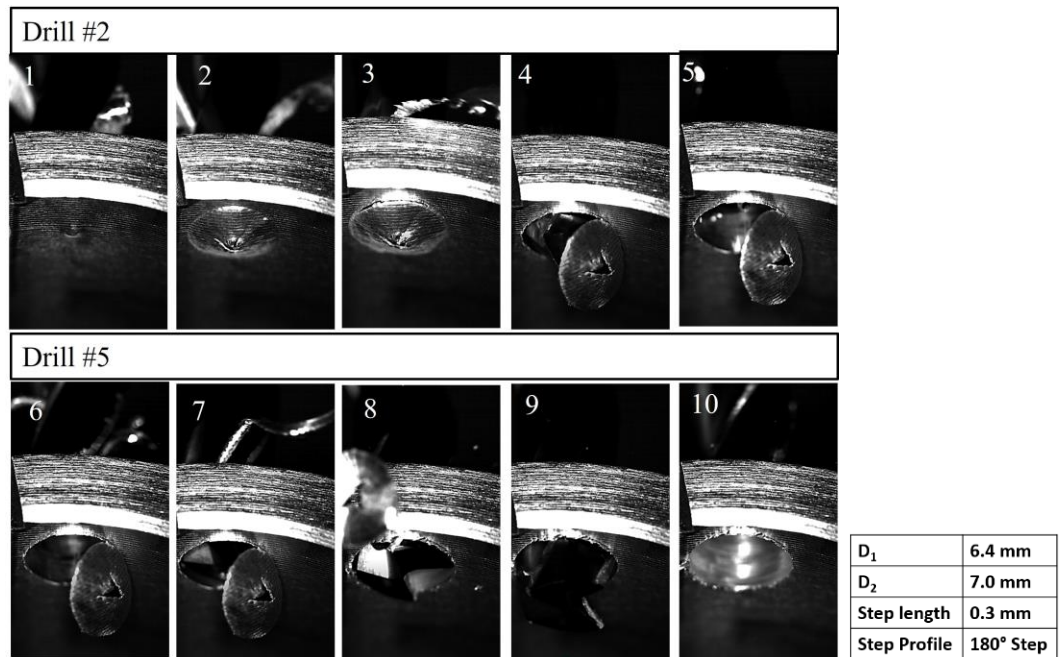
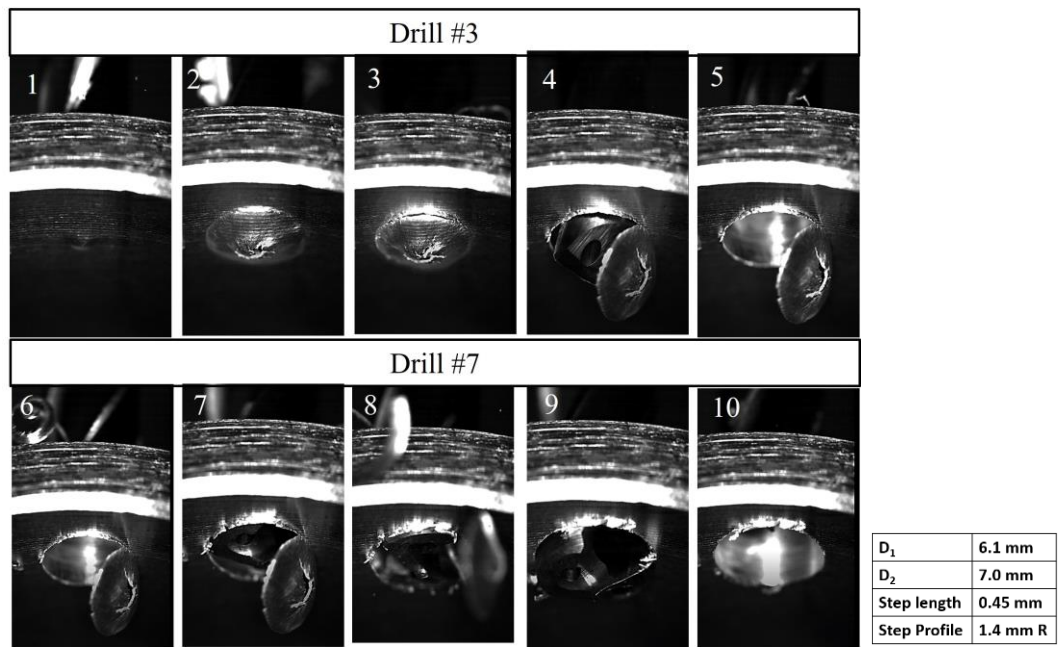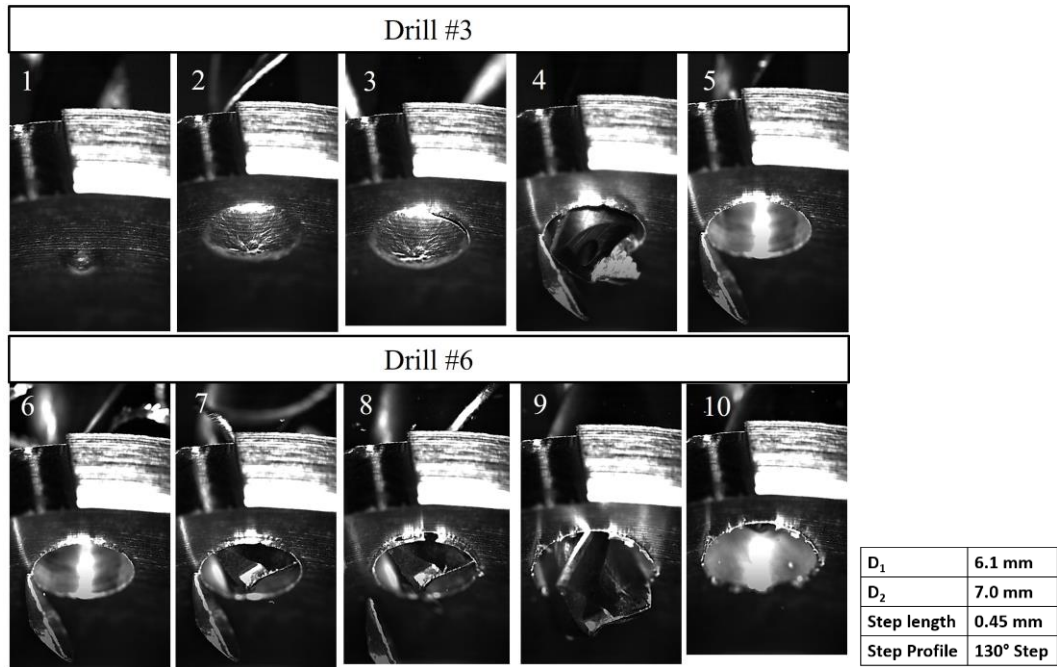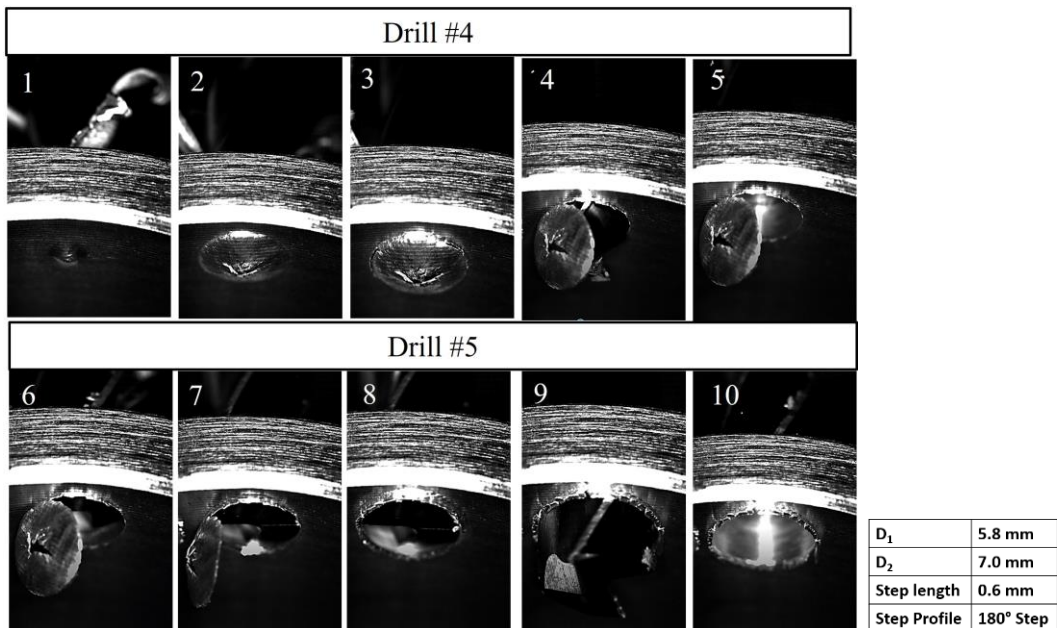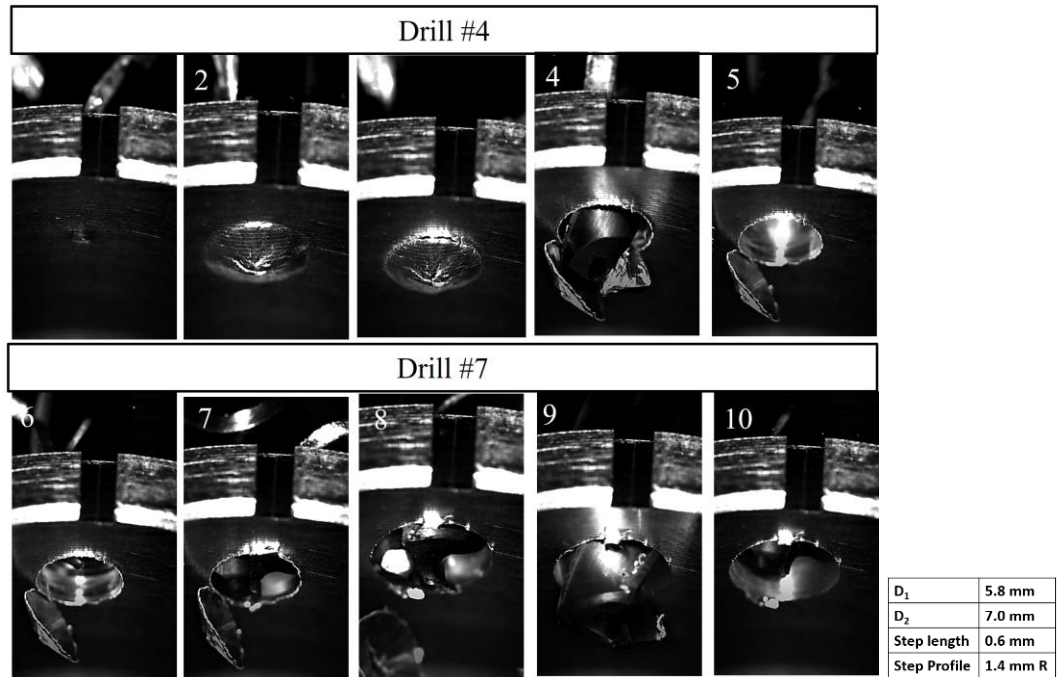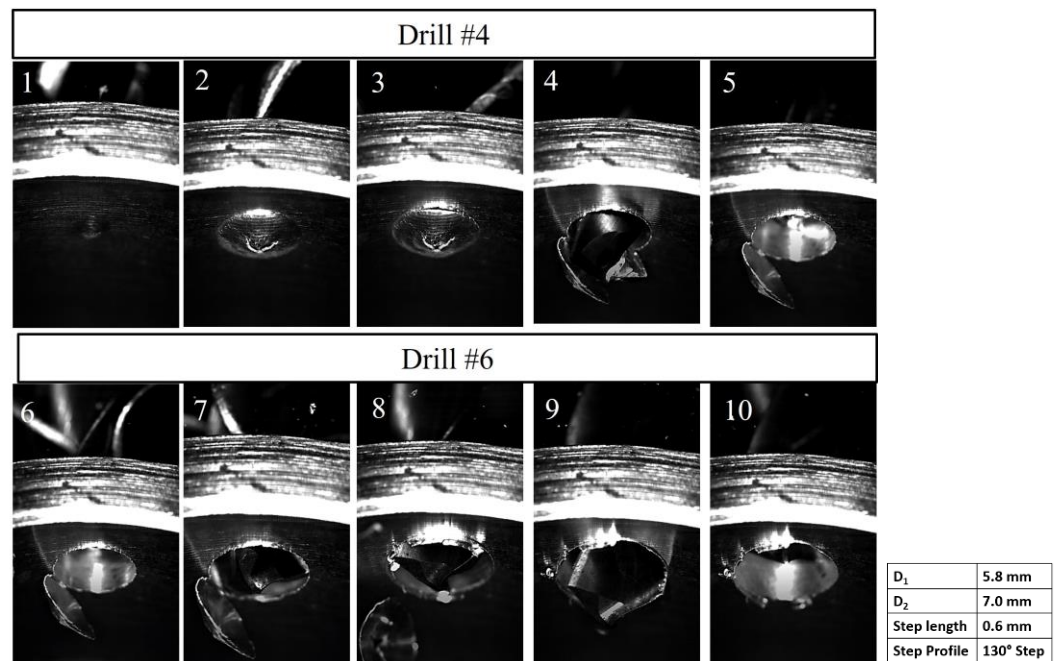**Figure 72: High-speed video images of the burr formation for test #4**
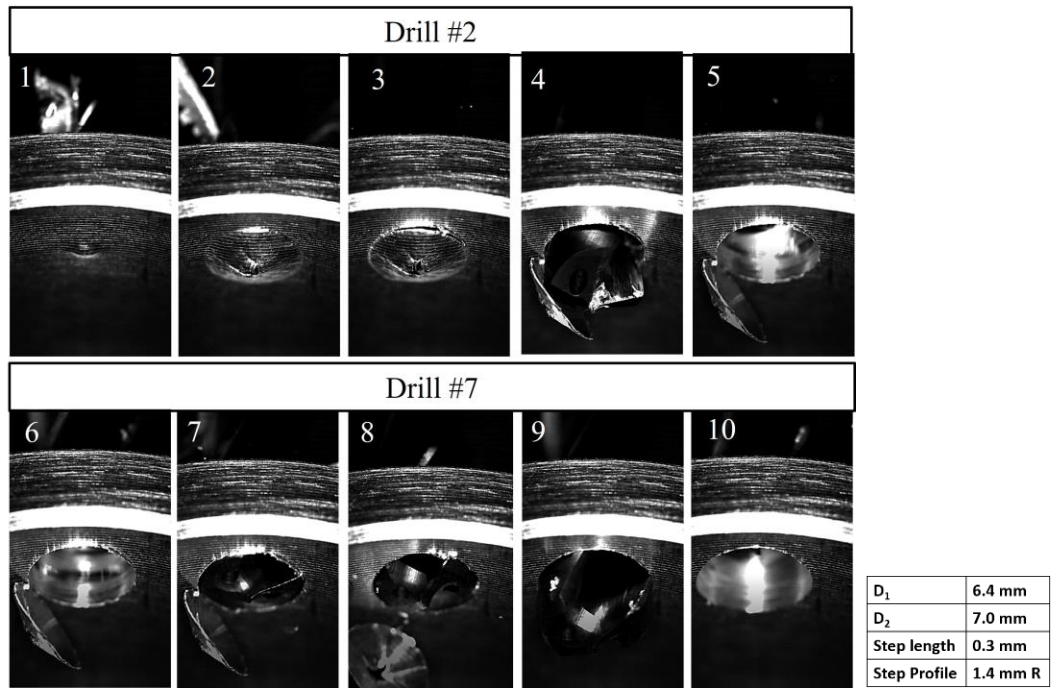
Figure 73: High-speed video images of the burr formation for test #5
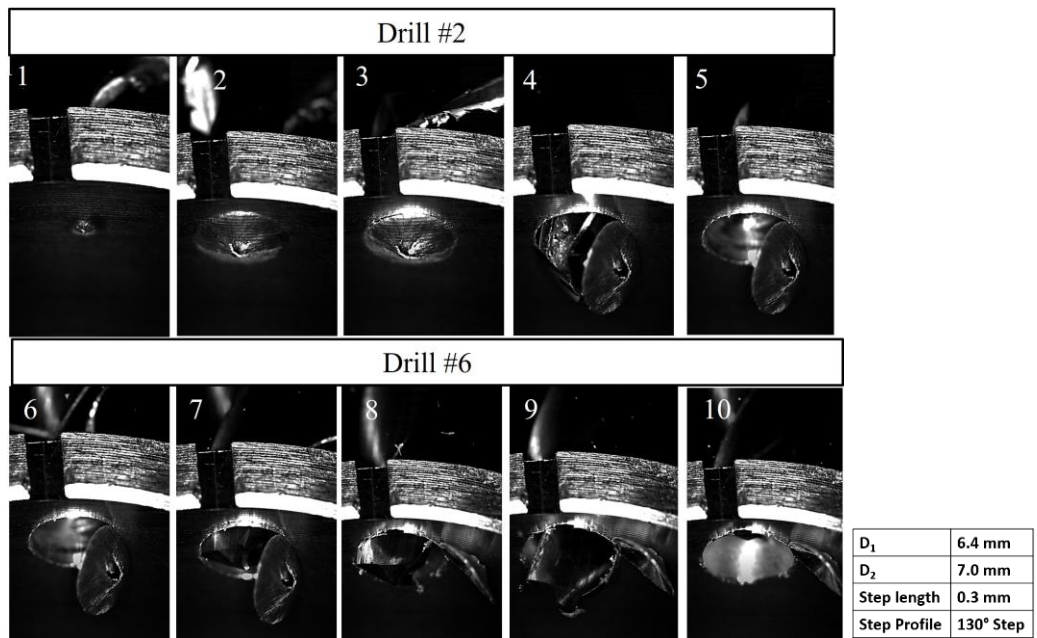
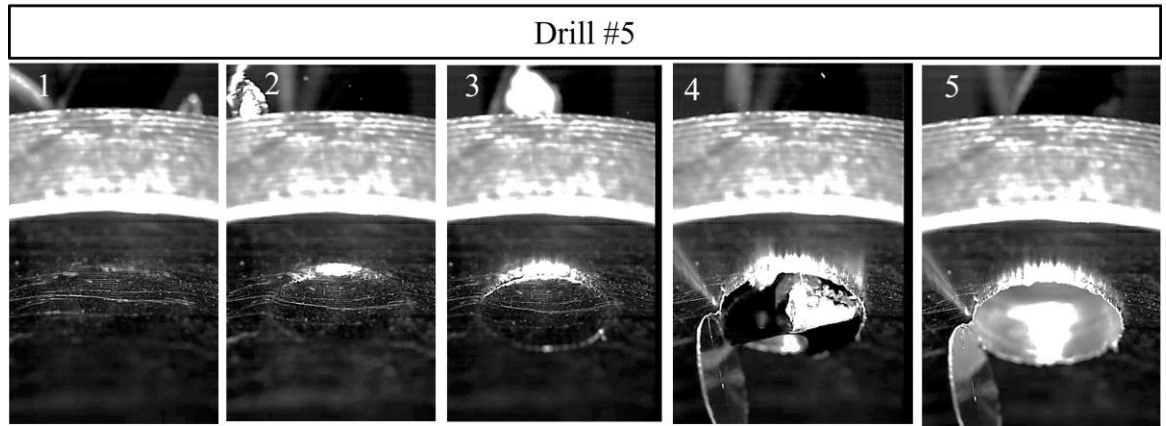**Figure 74: High-speed video images of the burr formation for test #6**
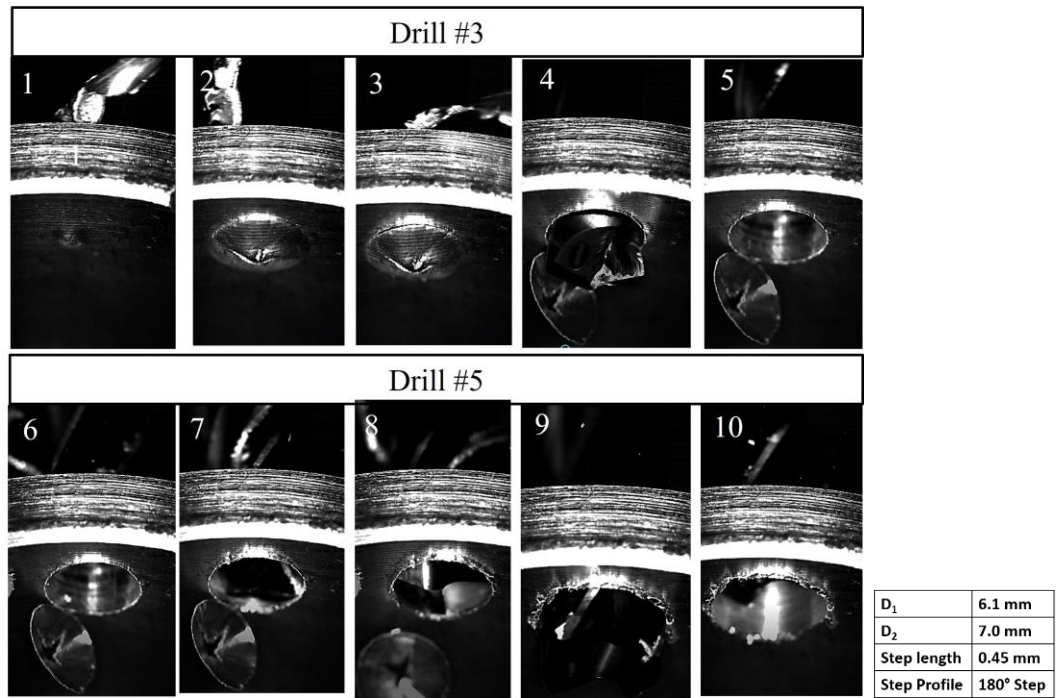
Figure 75: High-speed video images of the burr formation for test #7

Figure 76: High-speed video images of the burr formation for test #8

Figure 77: High-speed video images of the burr formation for test #9

Figure 78: High-speed video images of the burr formation for test #10

Figure 79: High-speed video images of the burr formation for test #11

Figure 80: High-speed video images of the burr formation for test #12

Figure 81: High-speed video images of the burr formation for test #13 (Drill #5- Benchmark)
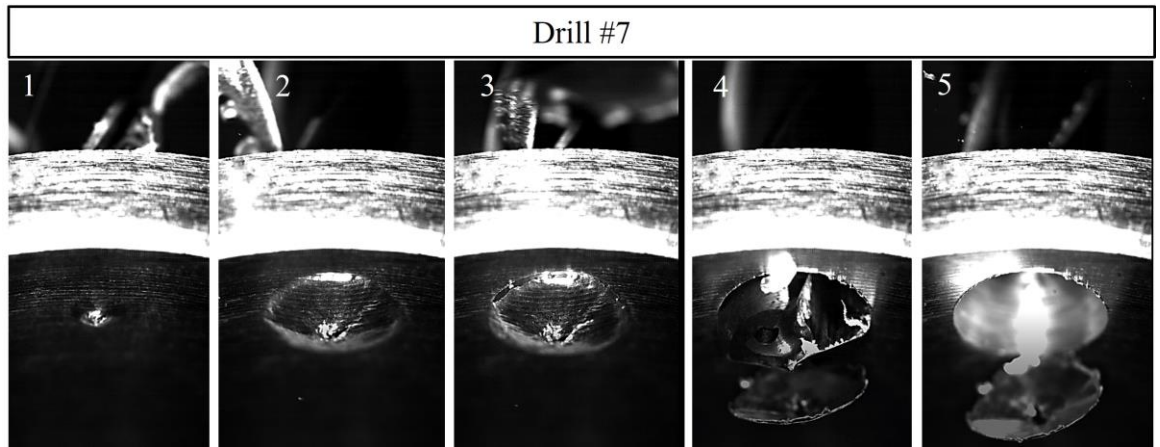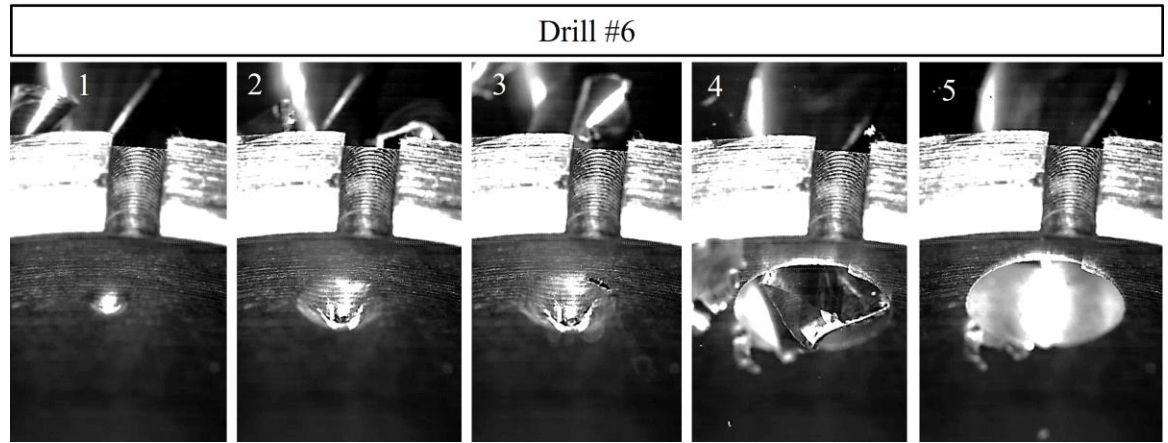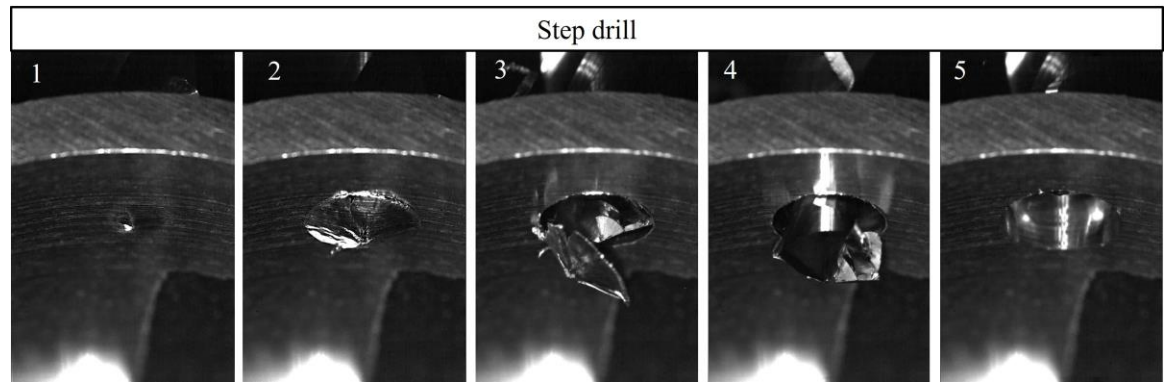

Figure 82: High-speed video images of the burr formation for test #14 (Drill #7-Benchmark)

Figure 83: High-speed video images of the burr formation for test #15 (Drill #6-Benchmark)

Figure 84: High-speed video images of the burr formation for the step drill